Meas. Sci. Technol. **11** (2000) R1–R36. Printed in the UK PII: S0957-0233(00)92099-X

REVIEW ARTICLE

A systematic approach to TV holography

Ángel F Doval

Departamento de Física Aplicada, ETS de Ingenieros Industriales y de Minas, Universidad de Vigo, E36 200 Vigo, Spain

E-mail: adoval@uvigo.es

Received 21 May 1999, in final form and accepted for publication 20 September 1999

Abstract. Television holography (TVH) can be defined as 'the family of optical measurement techniques based on the electronic recording and processing of holograms'. Image-plane TVH was introduced in the early 1970s with the name 'electronic speckle-pattern interferometry' (ESPI). Since then, TVH has undergone an impressive development and become one of the most promising optical techniques for non-destructive testing and industrial inspection. The aim of this review is to propose an original scheme for the systematic treatment of TVH and to review the existing techniques according to it. In this approach we split the measurement process into four highly independent stages (illumination and observation geometry, temporal treatment, secondary-correlogram generation and fringe-pattern analysis) and establish a common notation to formulate the corresponding techniques. Such a strategy allows the free combination of the techniques proposed for each stage as building blocks to obtain every particular variant of the whole TVH measurement process, whether it has already been reported or not, and also the incorporation of new techniques while retaining compatibility with the existing variants of the previous and following stages.

Keywords: displacement, shape, vibration, TV holography, electronic speckle-pattern interferometry, non-destructive testing

1. Introduction

Television holography (TVH) can be defined as the family of measurement techniques based on the recording of holograms with video cameras and their subsequent processing by electronic means, either analogue or digital. Classical holography and TVH differ both in recording media (photographic in the former and optoelectronic in the later) and in processing methods (a sequence of procedures of heterogeneous nature (chemical developing, optical reconstruction and processing and, possibly, optoelectronic recording and post-processing) for the first and purely electronic processing for the second).

TVH appeared during the early 1970s as a result of the efforts of several research groups trying to solve similar problems that had arisen in the field of classical holography. In the UK, Butters and Leendertz [1–4] conceived this technique as a natural extension of speckle interferometry, that they and other authors had developed to implement holographic measurement techniques using photographic film with less resolution and more sensitivity than the holographic plates. Almost at the same time, in the USA, Macovski *et al* [5] developed an analogous technique in the context of research on the recording and transmission of holograms by television. Also Schwomma [6] in Austria and Köpf [7] in Germany reached this technique from the field of holographic interferometry.

Of these four pioneering groups, the Austrian and the British matured the new technique to produce marketable prototypes, but only the British group continued the development of TVH and has remained in this field to date. The name that Butters and Leendertz coined, 'electronic speckle-pattern interferometry' (ESPI), which is closely related to the approach that led to their original technique, very soon became popular and has been the most usual name for it and also for all the variants that have appeared during the last few years.

During the 1970s and early 1980s, some other research groups, mainly based in European universities, developed their own prototypes and new techniques and the name 'TV holography' was introduced [8, 9]. All these systems had in common that the video signal was processed with analogue techniques and as a result they were expensive, bulky and not versatile enough.

The ultimate impulse for TVH came in the mid 1980s with the production of microcomputers and peripherals for the digitization and processing of images at affordable prices. The integration of these programmable, versatile and relatively inexpensive digital devices into the schemes for

processing the images generated with speckle interferometers was almost immediate [10–12] and encouraged many groups to become involved in the development of TVH. New names such as 'computer-aided speckle-pattern interferometry' [11], 'digital TV speckle interferometry' [13] and 'digital speckle-pattern interferometry' (DSPI) [14] were then proposed in order to distinguish between the digital and analogue implementations.

The numerical handling of speckle interferograms allowed a more comfortable implementation of the original analogue methods, the development of new fringe-formation techniques and the automatic analysis of the resulting fringe patterns. The introduction of digital methods into holographic interferometry (HI) and TVH was simultaneous and, since then, these two metrological disciplines have evolved in parallel; thus, almost any technique developed for HI is immediately adapted to TVH and vice versa. This parallelism led some authors to propose new names for the digital implementations of speckle-pattern interferometry, such as 'electro-optical holography' (EOH) [15] and 'electronic holography' [16] and, finally, to reconsider [17] the name 'TV holography', which had already been proposed by Gåsvik [8] for the original analogue techniques.

The continuous incrementations of the resolution of video cameras and of the power of computers have recently allowed the recording of Fresnel and Fourier holograms and their subsequent analysis and reconstruction by numerical methods [18, 19]. With the currently available devices, this is feasible only with small objects located far from the camera and small angles between the object and reference beams; for large objects it is necessary to use diverging lenses to get a virtual image with suitable dimensions and position [20] or to magnify a small portion of the hologram with a converging lens [21]. In spite of its being in its early development stages, the numerical reconstruction of holograms has already been used to implement methods for the measurement of displacements [22] and derivatives of displacement [23] and applied to the measurement of vibrations [24], surface contouring [25, 26] and the characterization of wavefronts [27]. This new measurement technique was initially named 'direct holography' [18] and 'digital holographic interferometry' [24], but it has finally been recognized as a variant of TVH [21, 25] thus establishing the final connection between classical holography and TVH.

Nowadays, the term 'television holography' covers a field wider than the original electronic speckle-pattern interferometry and its derivations, that can be regarded as image-plane TV-holography techniques, and is a well-established technique of optical metrology. TVH shares with classical HI many of its best characteristics, such as interferometric sensitivity, high precision and whole-field and non-contact operation, and inherits from speckle metrology such advantages as the possibility of adjusting both the direction and the magnitude of the sensitivity within a wide range of values, the availability of geometries that provide direct sensitivity to the derivatives of the measurand and that the fringes are always localized on the surface of the object.

However, the characteristics that make TVH one of the optical metrology techniques with higher potential for industrial application derive from the use of video cameras as recording media.

(i) Their sensitivity is much higher than that of holographic plates and thus allows one to use shorter exposure times than those in classical holography. This allows TVH measurements under low-stability conditions and with poor vibration isolation, which often happens in field applications.
(ii) The operating cost is insignificant since no consumables such as holographic plates, photographic film and developing chemicals are required. This allows its unrestricted use for interactive development processes and its application to massive quality control on production lines.
(iii) The electronic processing of the hologram information is very fast (compared with chemical developing) and is often performed in real time.
(iv) TVH systems are very easy to use since they can operate in the presence of ambient light, there is no need to develop or re-position the holograms and their components as well as the signal processing are usually computer controlled. Therefore, they can even be operated by staff not specifically trained in optical metrology.
(v) The results are usually displayed on a video monitor that allows comfortable observation even for several operators simultaneously. Since the information is in an electronic format, either analogue or digital, it can be printed and stored without excessive additional costs.
(vi) The small size achieved for modern video cameras allows the development of highly portable systems such as those needed for field applications and even miniaturization of the optical sensor by using microcameras to inspect remote areas.

Certainly, to get these benefits some of the features of classical holography must be sacrificed.

(i) The spatial resolution for video cameras is substantially lower than that for holographic plates. This not only means that part of the detail is lost but also reduces the measurement range insofar as its upper limit is basically set by the maximum fringe density that the recording medium admits.
(ii) In TVH the presence of speckle noise is much more noticeable than it is in HI, precisely because its size must be kept coarse enough to be resolved.
(iii) The presence of speckle implies a sensitivity to de-correlation induced by the movements of the object, that in HI lead to a de-localization of the fringes but in TVH can make them disappear.
(iv) The cost of a basic TVH system is comparable to or higher than that of an elementary HI set-up because the first must include a computer equipped with an image digitizer, that is not essential for the second; but the incorporation of automatic fringe-analysis and processing techniques into the basic TVH system involves a minimal extra cost.

Fresnel and Fourier TVH techniques are already in their first stages of development. Just a few of their potential

variants have been investigated and, in our opinion, it is perhaps too early to analyse them from a global point of view. On the other hand, image-plane TVH has evolved from the original ESPI techniques during the last three decades and has reached a considerable degree of development.

Many reviews on image-plane TVH have been published and cover virtually all the existing methods and techniques from various points of view. Among them we may highlight those of Butters *et al* [28], Løkberg [29–31], Løkberg and Slettemoen [32], Jones and Wykes [33] and Davies and Buckberry [34].

In this review we propose a new systematic treatment for TVH techniques. We split the measurement process into four mutually independent stages, extract the different variants for each of them from the techniques reported by many authors and establish a common notation for all of them. These stages are conceived as building blocks with standard inputs and outputs that allow one, on the one hand, to combine with almost total freedom the techniques proposed for each stage to obtain every particular version, whether it has already been reported or not, of the whole TVH measurement process and, on the other, to incorporate new variants for a given stage, while retaining compatibility with the techniques already established for the preceding and following stages so that a whole new set of combinations can be established.

2. A systematic approach to TVH

A TVH system (figure 1) comprises two clearly different groups of elements: the optical part, a speckle interferometer with electronic recording (ESPI), wherein the holograms (speckle interferograms) are generated, and the electronic part, wherein correlation fringes are eventually generated and analysed.

The ESPI is usually a two-beam interferometer, although it may also be a multiple-beam one. A beam splitter (BS) divides the light of a coherent source, typically a laser, among the two arms of the interferometer, one or both of them interact, either by reflection or transmission, with a diffusing object (OBJ) (or with two different objects to perform comparative measurements) and, finally, they pass through a beam combiner (BC) (that for some designs is the same beam splitter (BS)) to interfere on the sensitive element of a video camera (TVC). The instantaneous value of the measurand X at every point of the object is encoded in the resulting interferogram. The output of the video camera results from the integration of the irradiance incident during the exposure of a video frame and, consequently, reflects the temporal evolution of the measurand during that time. The ESPI may incorporate additional elements used for the implementation of certain techniques; the most usual are speckle de-correlating devices (SDD), amplitude modulators (AM) and phase modulators (PM).

The role of the electronic part of the TVH system is to reveal the information related to the measurand that is present in the holograms recorded by the video camera. Its most elementary function is the generation of secondary correlation fringes; this corresponds, up to a point, to the reconstruction of a double- or multiple-exposure hologram in HI, although they are processes of different natures: in HI

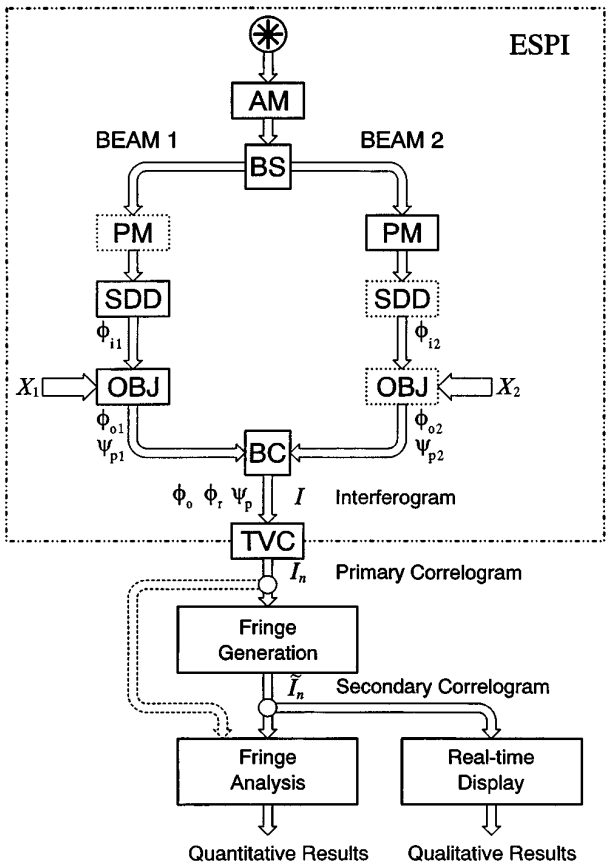

Figure 1. The scheme of a generic TVH system.

the secondary fringes are generated by the interference of true reconstructed wavefronts whereas in TVH they are obtained by electronic processing of the video signal that represents the hologram itself. The secondary fringe pattern is usually displayed on a video monitor, very often in real time. Its observation provides essentially qualitative information about the value of the measurand. A further fringe-analysis process, also committed to the electronic subsystem and similar to those used with other interferometric techniques although adapted to the characteristic omnipresence of speckle noise, must be applied either to the secondary fringes or directly to the output of the video camera to yield quantitative measurements.

In our systematic approach to TVH we consider four stages in the measurement process, the first two related to the electronic speckle-pattern interferometer (ESPI) and the last to the image-processing subsystem, shown in figure 2. These stages are highly independent and the techniques corresponding to any of them can be combined with the others' almost without restrictions.

The first stage (section 3) is the generation of a *speckle interferogram* with a given illumination and observation geometry. The technique implemented for this stage determines the nature of the measurand as well as the magnitude and direction of the sensitivity, i.e. how the measurand $X(\boldsymbol{x})$ is related to the optical phase difference associated with the object $\phi_o(\boldsymbol{x})$ in the interferometer and, ultimately, to the instantaneous value of the intensity of the resulting interferogram.

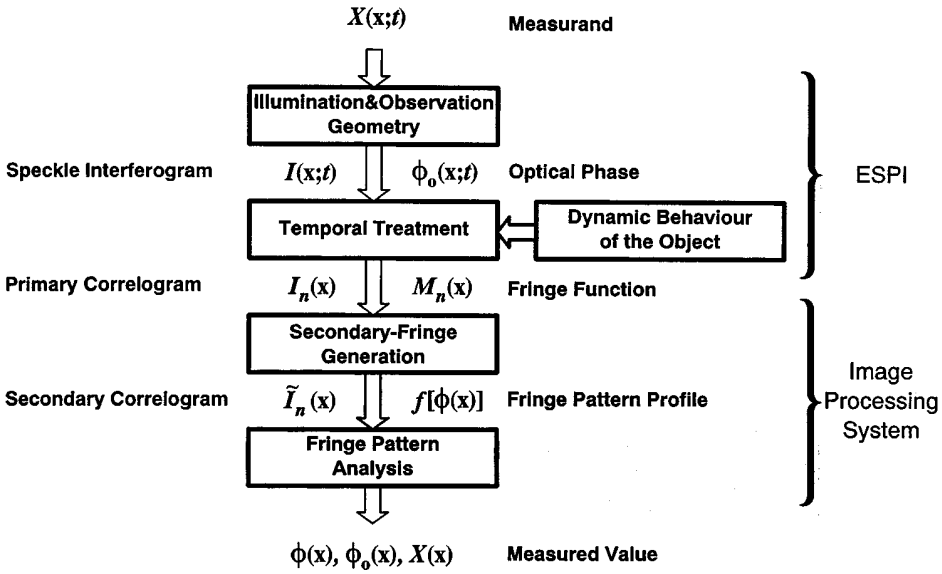

Figure 2. A block diagram of the TVH measurement process.

The second (section 4) is connected with the integration of the irradiance of the interferograms at the video camera during the exposure period. Both the temporal treatment applied to the optical signal (i.e. amplitude and phase modulation) and the dynamic behaviour of the object during the integration period determine how the measurand-related optical phase difference $\phi_o(\boldsymbol{x})$ is encoded in the electronic images provided by the camera, that we call *primary correlograms*; this relationship is formalized through the fringe function $M_n(\boldsymbol{x})$.

In primary correlograms the information is embedded in the random speckle field. A third stage (section 5), the generation of a *secondary correlogram*, must be applied if one needs a fringe pattern with visible changes of the average intensity is to be either displayed or quantitatively analysed. The phase $\phi(\boldsymbol{x})$ and the profile of the secondary correlograms are related both to the fringe function $M_n(\boldsymbol{x})$ and to the technique used to generate them.

The fourth and last of the stages (section 6) in the TVH measuring process is fringe analysis to ultimately obtain the value of the measurand $X(\boldsymbol{x})$, its associated optical phase difference $\phi_o(\boldsymbol{x})$ or the phase of the fringe pattern $\phi(\boldsymbol{x})$. Most current fringe-analysis techniques are used in TVH, with some particularities arising from the presence of the speckle noise.

3. Illumination and observation geometry

The sensitivity of speckle phase. Although the optical phase of speckle patterns follows a random distribution in space, its increments due to the displacement of the diffuser, the modification of the illumination and observation geometry and the changes either in the wavelength or in the refractive index are deterministic and can be used to make measurements. Throughout this review we will use a model inherited from holographic interferometry [32, p 465; 33, p 81ff] to quantify these increments. As shown in figure 3,

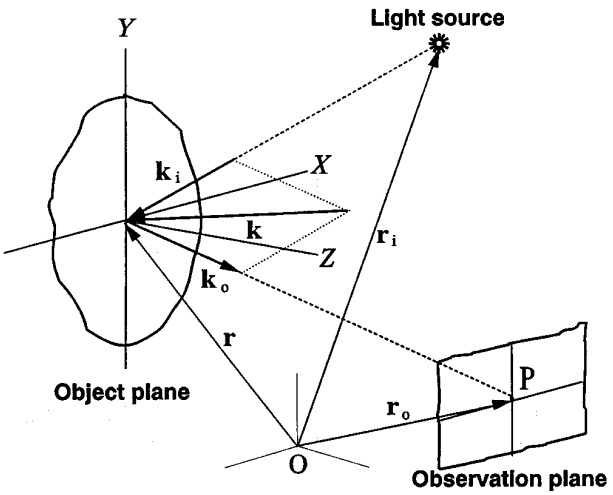

Figure 3. The geometry used to analyse the sensitivity of the speckle phase.

the optical phase of a speckle pattern at each point of the observation plane can be written as

$$\psi = \psi_p + \phi = \psi_p + \phi_i + \boldsymbol{k}_i \cdot (\boldsymbol{r} - \boldsymbol{r}_i) + \boldsymbol{k}_o \cdot (\boldsymbol{r}_o - \boldsymbol{r}). \quad (3.1)$$

According to this expression, the phase of the speckle ψ results from the sum of a random component ψ_p, whose value depends on the particular distribution of roughness across the surface of the diffuser, and a deterministic component ϕ. The latter comprises the initial optical phase of the light source ϕ_i as well as the phase delays due to the propagation from the source to the object $\boldsymbol{k}_i \cdot (\boldsymbol{r} - \boldsymbol{r}_i)$ and from this to the observation plane $\boldsymbol{k}_o \cdot (\boldsymbol{r}_o - \boldsymbol{r})$.

Both phase delays are functions of the position vectors of the considered point of the diffuser $\boldsymbol{r}$, the centre of curvature of the illuminating wavefront $\boldsymbol{r}_i$ (typically representing the position of a point light source) and the observation point $\boldsymbol{r}_o$. Finally, $\boldsymbol{k}_i$ and $\boldsymbol{k}_o$ are the wavevectors of the illumination and

observation directions (figure 3)

$$\boldsymbol{k}_i = \frac{2\pi}{\lambda}\hat{\boldsymbol{n}}_i \qquad \boldsymbol{k}_o = \frac{2\pi}{\lambda}\hat{\boldsymbol{n}}_o \tag{3.2}$$

$\hat{\boldsymbol{n}}_i$ and $\hat{\boldsymbol{n}}_o$ being the corresponding unit vectors.

By use of the *sensitivity vector* (figure 3), defined as

$$\boldsymbol{k} = \boldsymbol{k}_i - \boldsymbol{k}_o = \frac{2\pi}{\lambda}(\hat{\boldsymbol{n}}_i - \hat{\boldsymbol{n}}_o) \tag{3.3}$$

the expression (3.1) can be written

$$\psi = \psi_p + \phi' + \boldsymbol{k}\cdot\boldsymbol{r} \tag{3.4}$$

with

$$\phi' = \phi_i + \boldsymbol{k}_o\cdot\boldsymbol{r}_o - \boldsymbol{k}_i\cdot\boldsymbol{r}_i. \tag{3.5}$$

Any displacement of the diffuser or change of illumination and observation conditions yields an increment of the phase of the speckle, given by

$$\Delta\psi = \Delta\psi_p + \Delta\phi' + \Delta(\boldsymbol{k}\cdot\boldsymbol{r}) \tag{3.6}$$

where

$$\Delta\phi' = \Delta\phi_i + \Delta(\boldsymbol{k}_o\cdot\boldsymbol{r}_o) - \Delta(\boldsymbol{k}_i\cdot\boldsymbol{r}_i) \tag{3.7}$$

$$\begin{aligned}\Delta(\boldsymbol{k}\cdot\boldsymbol{r}) &= [(\boldsymbol{k}+\Delta\boldsymbol{k})\cdot(\boldsymbol{r}+\Delta\boldsymbol{r})] - (\boldsymbol{k}\cdot\boldsymbol{r})\\ &= \Delta\boldsymbol{k}\cdot\boldsymbol{r} + \boldsymbol{k}\cdot\Delta\boldsymbol{r} + \Delta\boldsymbol{k}\cdot\Delta\boldsymbol{r}.\end{aligned} \tag{3.8}$$

$\boldsymbol{k}\cdot\Delta\boldsymbol{r}$ is the phase increment due to the displacement of the object, $\Delta\phi' + \Delta\boldsymbol{k}\cdot\boldsymbol{r}$ is due to the changes in illumination and observation geometries, refractive index, wavelength and initial phase of the source and $\Delta\boldsymbol{k}\cdot\Delta\boldsymbol{r}$ is the combined effect of the simultaneous changes in both types of parameters.

Whenever changes neither affect the microstructure of the diffuser nor are large enough to produce significant global displacements of the speckle pattern, the random component of its optical phase remains virtually constant (i.e. $\Delta\psi_p \approx 0$) and all of the observed increment is due to the deterministic component. Furthermore, in most practical situations it can be assumed that the object is displaced without changing illumination and observation conditions and vice versa, so that $\Delta\boldsymbol{k}\cdot\Delta\boldsymbol{r} \approx 0$.

The interference of speckle patterns. To exploit the sensitivity of the speckle phase it is necessary to transform its changes into variations of intensity. This is achieved through the interference of the original speckle pattern with either a smooth reference beam or another speckle pattern. Practically all the classical interferometers (Michelson, Mach–Zehnder, Fizeau etc.) have been or can be adapted to operate with speckle patterns instead of smooth beams.

The interference of two perfectly coherent light fields yields an interference pattern following the well-known expression

$$I = I_1 + I_2 + 2(I_1 I_2)^{1/2}\cos(\psi_1 - \psi_2) \tag{3.9}$$

where I_1 and I_2 are the local irradiances and ψ_1 and ψ_2 are the optical phases of the interfering beams.

Equation (3.9) can be written in the more convenient form

$$I = \mathcal{I}_0[1 + \mathcal{V}\cos(\psi_1 - \psi_2)] \tag{3.10}$$

with the local *average irradiance* $\mathcal{I}_0$ and the *visibility* $\mathcal{V}$ of the interferogram defined as

$$\mathcal{I}_0 = I_1 + I_2 \tag{3.11}$$

$$\mathcal{V} = \frac{2(I_1 I_2)^{1/2}}{I_1 + I_2}. \tag{3.12}$$

Expression (3.10) is also valid for partially coherent light, but the visibility is lower according to the more general definition

$$\mathcal{V} = \frac{2(I_1 I_2)^{1/2}}{I_1 + I_2}|\gamma(\tau)| \tag{3.13}$$

where $0 \leqslant |\gamma(\tau)| \leqslant 1$ is the modulus of the *complex degree of coherence* [35].

These expressions can be applied both in classical and in speckle interferometry; in classical interferometry the spatial distributions of $\mathcal{I}_0$, $\mathcal{V}$, ψ_1 and ψ_2 are essentially smooth and fully deterministic whereas in speckle interferometry they are random and, therefore, noisy.

In the latter case, the one with which we are concerned here, two basic situations are apparent. The first arises when both interfering fields are speckle patterns; then, the statistical properties of the resulting speckle interferogram are similar to those of the original patterns [36, pp 19–29]. The second is the interference of a speckle pattern with a smooth reference beam; the resulting interferogram is also speckled, but with statistical properties departing from those of the original pattern [36, pp 29–34; 37].

Regardless of the nature of the interfering beams, in TVH the information related to the measurand is encoded in the difference between their optical phases $\psi_1 - \psi_2$. To give a uniform treatment for both types of techniques (those using two speckle patterns and those with a smooth reference beam) we shall write this *phase difference*, using expression (3.4), as

$$\begin{aligned}\psi_1 - \psi_2 &= (\psi_{p1} - \psi_{p2}) + (\phi_1' - \phi_2') + (\boldsymbol{k}_1\cdot\boldsymbol{r}_1 - \boldsymbol{k}_2\cdot\boldsymbol{r}_2)\\ &= \psi_p - \phi_r + \phi_o\end{aligned} \tag{3.14}$$

where $\psi_p = \psi_{p1} - \psi_{p2}$ is the difference between the random components of the phases of the interfering speckle patterns and, therefore, has a random spatial distribution and behaves as *phase noise*; $\phi_r = \phi_2' - \phi_1'$ is the *reference phase difference* that, in general, is deliberately introduced either by changing the initial phases of the beams or by modifying illumination and observation conditions (i.e. distance, direction, wavelength, etc.); and, finally, $\phi_o = \boldsymbol{k}_1\cdot\boldsymbol{r}_1 - \boldsymbol{k}_2\cdot\boldsymbol{r}_2$ is the *object phase difference*, related to the instantaneous position of each point of the surface of the diffusing object. The last term is the one that contains the usable information of the *speckle interferogram*, whose expression (3.10) results in

$$I = \mathcal{I}_0[1 + \mathcal{V}\cos(\psi_p - \phi_r + \phi_o)]. \tag{3.15}$$

In the most general case, all the terms in expression (3.15) are functions both of time t and of position $\boldsymbol{x} = (x, y)$ on the image plane. However, the following simplifying hypotheses can be assumed valid for most practical speckle interferometers.

(i) The speckle pattern experiences neither significant decorrelation nor transversal displacement during the measuring interval and consequently $\mathcal{I}_0$, $\mathcal{V}$ and ψ_p are independent of t.
(ii) The illumination and observation directions for each beam are the same at all points of the interferogram and therefore $\boldsymbol{k}_1$, $\boldsymbol{k}_2$ and ϕ_r do not depend on $\boldsymbol{x}$.

The first of these hypotheses sets an upper limit for the measurement range as well as stability requirements for the interferometric arrangement. The second assumes the use of collimated illumination beams and telecentric observation. In practice, this is feasible only with relatively small objects; medium-sized and large objects are illuminated with slightly diverging beams (generally obtained with spatial filters or monomode optical fibres) and observed with long focal objectives; condition (ii) is then satisfied with a good degree of approximation by placing their foci far enough from the object.

Using both hypotheses together with expression (3.15), the instantaneous value of the local intensity of the speckle interferogram corresponding to a given state of the object can be written as

$$I(\boldsymbol{x};t) = \mathcal{I}_0(\boldsymbol{x})\{1 + \mathcal{V}(\boldsymbol{x})\cos[\psi_p(\boldsymbol{x}) - \phi_r(t) + \phi_o(\boldsymbol{x};t)]\} \tag{3.16}$$

with

$$\phi_o(\boldsymbol{x};t) = \boldsymbol{k}_1(t)\cdot\boldsymbol{r}_1(\boldsymbol{x};t) - \boldsymbol{k}_2(t)\cdot\boldsymbol{r}_2(\boldsymbol{x};t). \tag{3.17}$$

In TVH, measurements are performed on the basis of a temporal change in intensity that, under these hypotheses, is exclusively determined by the changes in the deterministic component of the optical phase difference $\Delta(\phi_o - \phi_r)$ and, considering that changes in the reference phase difference $\Delta\phi_r$ are usually known, it ultimately reflects the changes in the object phase difference $\Delta\phi_o$.

The techniques connected to the illumination- and observation-geometry techniques can be classified into families characterized by the object-related parameter that $\Delta\phi_o$ represents. From expressions (3.16) and (3.17), it is apparent that

(i) keeping the sensitivity vectors constant, the object-phase-difference changes are due solely to the components of the *displacement* vector $\boldsymbol{u}(\boldsymbol{x};t) = \Delta\boldsymbol{r}(\boldsymbol{x};t)$;
(ii) on imposing a known change to the sensitivity vectors while the object is kept undeformed, the object-phase-difference increment is related to the *shape* of the object $\boldsymbol{r}(\boldsymbol{x})$; and
(iii) when the refractive index of the medium surrounding a diffuser of known shape experiences changes, the magnitudes of the sensitivity vectors change accordingly: hypothesis (ii) is then violated and the increments of the object phase difference reveal the local variations of the *refractive index*.

3.1. Displacement-sensitive interferometers.

Displacement is measured in TVH by using interferometers with fixed sensitivity vectors; thus, the object-phase-difference increment is related solely to the local displacement of the object. The directions of the sensitivity vectors, given by the illumination and observation geometries, determine to which component of $\Delta\boldsymbol{r}$ the interferometer is sensitive, as well as how large the sensitivity is.

3.1.1. Out-of-plane (axial) displacements. The sensitivity to displacements along the observation direction (out of the object plane of the image forming system and, with 'ideal' (telecentric) observation, along the optical axis) is achieved with parallel illumination and observation directions (figure 4) that very often are also perpendicular to the surface of the object.

Only one beam, the *object beam*, illuminates the object while the other, the *reference beam* (that can be either smooth ($\psi_{p2} = 0$) or speckled ($\psi_{p2} \neq 0$)), does not interact with it. The main difference between using a smooth and a speckled reference beam lies in the statistical properties of the resulting speckle interferograms. Those obtained with smooth reference beams have lower speckle contrast and are intrinsically less noisy; they have also a larger average speckle size, which is a valuable feature when low-resolution imaging devices such as video cameras are used.

For both cases it is $\hat{\boldsymbol{n}}_o = -\hat{\boldsymbol{n}}_i$, following (3.3), the sensitivity vector of the object beam is

$$\boldsymbol{k}_1 = \frac{4\pi}{\lambda}\hat{\boldsymbol{n}}_i \tag{3.18}$$

while the sensitivity can be assumed zero in the reference beam ($\boldsymbol{k}_2 = 0$) as long as the state of the object does not affect its optical phase. The increment of the object phase difference is, consequently, proportional to the axial displacement $w(\boldsymbol{x};t)$ of the diffuser; after substituting (3.18) into expression (3.17) and using the reference system shown in figure 4, it can be expressed as

$$\Delta\phi_o(\boldsymbol{x};t) = \boldsymbol{k}_1\cdot\Delta\boldsymbol{r}_1(\boldsymbol{x};t) = \frac{4\pi}{\lambda}\hat{\boldsymbol{n}}_i\cdot\Delta\boldsymbol{r}_i(\boldsymbol{x};t)$$
$$= \frac{4\pi}{\lambda}\Delta z(\boldsymbol{x};t) = \frac{4\pi}{\lambda}w(\boldsymbol{x};t). \tag{3.19}$$

This geometry has been by far the most usual ever since the first steps of TVH; hence, there is a host of different implementations for it. They can be classified according to the type of reference beam (smooth or speckled), to the type of classical interferometer from which they are derived and the way that the beams are combined.

Out-of-plane-sensitive interferometers with smooth reference beams are very popular devices and many configurations have been proposed. Most of them derive from the Mach–Zehnder interferometer and use separated optical elements to split and combine again the object and reference beams. Generally, the reference beam is made to diverge (either really or virtually) from the centre of the output pupil of the objective (i.e. an *in-line reference beam*) to keep the average grain size of the speckle interferograms as large as possible. This is achieved by placing beam splitters (wedges [2], cubes [38], etc.) between the objective lens and the image plane, using mirrors with a hole through which the reference beam is passed [39], placing tiny mirror balls behind the objective [34], carving concave mirrors onto the rear surface

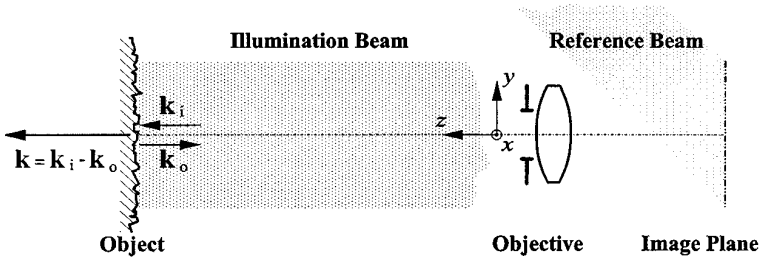

Figure 4. The typical illumination and observation geometry used to get sensitivity to out-of-plane displacements.

of the objective lens [40] and placing optical fibres behind the objective [14, 41] or passing them through a hole in the centre of the imaging lens [42]. Sometimes, the reference beam is made to diverge from a point placed outside the output pupil in order to separate the spectra of interference and additive speckle noise. This can be implemented either using an *off-axis reference beam* [5, 43] or with the aid of special lens apertures such as the double slit [44].

Some authors have proposed arrangements based on other classical types of interferometers, for example, replacing one of the mirrors in a Michelson interferometer by a diffusing object [45] or building quasi-common-path speckle interferometers based on Fizeau interferometers by use of an optical flat [46] or a plano-concave lens [47] placed just in front of the diffuser to obtain a smooth reference beam. Even shearing interferometers with abnormally large shears [48] have been used to get the reference beam from a mirror placed side by side with the object.

Out-of-plane-sensitive interferometers with speckle reference beams are not so widespread because they make less efficient use of the available power (the aperture of the objective must be smaller than that in smooth-reference-beam interferometers to obtain the same average speckle size) and the contrast of speckle noise is higher; on the other hand, they have the merits of ruggedness and simplicity of alignment. Several implementations have been proposed: modified Mach–Zehnder interferometers with the reference beam passed through a piece of ground glass interposed in its path [49], reflected from a diffuser placed at the rim of the objective lens [50] or passed through a diffuser that covers one half of the aperture of the objective [51]; other variants consist of forming an image of the object on a ground-glass screen obliquely illuminated by the reference beam and imaging the resulting speckle interferogram on the video camera [52] or placing a reference diffuser side by side with the object and overlapping their images by means of a sort of shearing interferometer with a striped beam splitter that also plays the role of a special aperture stop [50]. Finally, the generation of a speckled reference beam through the reconstruction of the hologram of a diffuser [53] has recently been proposed.

Strictly speaking, and with independence of the type of reference beam, the illumination and observation directions must be parallel if one is to get sensitivity only to out-of-plane displacements. Several authors have proposed solutions to satisfy this condition: illuminating and observing the object through a beam splitter, observing the object reflected on a plane mirror with a tiny hole through which to pass the illumination beam [39] or illuminating the object with an optical fibre passing through a hole in the centre of the objective lens [42]. Nevertheless, when the object is conveniently far away, the aforementioned condition is very often accomplished to a good approximation by illuminating and observing from very close proximity.

It is worth remarking, finally, that out-of-plane-sensitive interferometers can be used to measure displacements with components essentially parallel to the surface of the object. This is achieved with very oblique illumination and observation [54] that, with the aid of prisms [55], can be made almost parallel to the surface of the object.

3.1.2. In-plane (transversal) displacements. To get sensitivity to displacements of the diffuser in a direction contained in the object plane (i.e. transverse to the observation direction), two speckle patterns originating from the same object and obtained with conveniently chosen sensitivity vectors $\boldsymbol{k}_1$ and $\boldsymbol{k}_2$ are made to interfere point to point, namely $\boldsymbol{r}_1(\boldsymbol{x};t) = \boldsymbol{r}_2(\boldsymbol{x};t) = \boldsymbol{r}(\boldsymbol{x};t)$, on the image plane of the video camera.

Following expression (3.17), the resulting object phase difference is

$$\phi_o(\boldsymbol{x};t) = (\boldsymbol{k}_1 - \boldsymbol{k}_2)\cdot\boldsymbol{r}(\boldsymbol{x};t) = \boldsymbol{K}\cdot\boldsymbol{r}(\boldsymbol{x};t). \qquad (3.20)$$

The vector $\boldsymbol{K} = \boldsymbol{k}_1 - \boldsymbol{k}_2$ represents the global sensitivity of the interferometer. It is perpendicular to the observation direction whenever $\boldsymbol{k}_1$ and $\boldsymbol{k}_2$ have identical components along that direction. Then, the changes in object phase difference can be expressed as

$$\Delta\phi_o(\boldsymbol{x};t) = \boldsymbol{K}\cdot\Delta\boldsymbol{r}(\boldsymbol{x};t) = K_x u(\boldsymbol{x};t) + K_y v(\boldsymbol{x};t). \qquad (3.21)$$

The geometry most often used in practice, which was developed by the pioneers of TVH [4], involves illumination of the object with two beams symmetrically tilted with respect to the observation direction as shown in figure 5. The magnitude of the resulting sensitivity is related to the tilt angle θ

$$K = |\boldsymbol{K}| = \frac{4\pi}{\lambda}\sin\theta \qquad (3.22)$$

and, therefore, the sensitivity can be controlled to have values between zero and $4\pi/\lambda$.

Double illumination can be obtained either through use of a beam splitter [56] or by dividing the wavefront of a single illumination beam with a plane mirror placed near the object parallel to the observation direction [38]. Other geometries that are not so widespread are the double observation with symmetrical direction [57], the combination

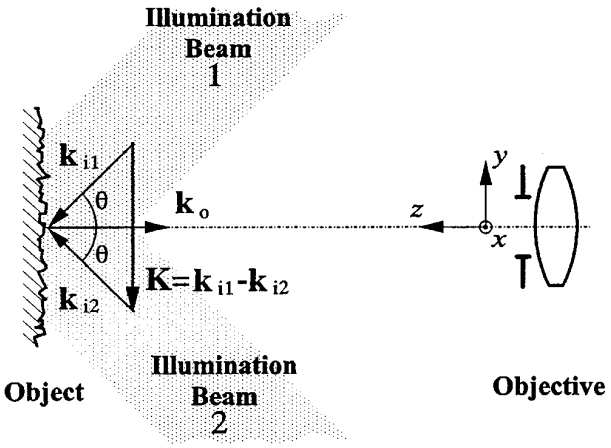

Figure 5. The typical illumination and observation geometry used to get sensitivity to in-plane displacements.

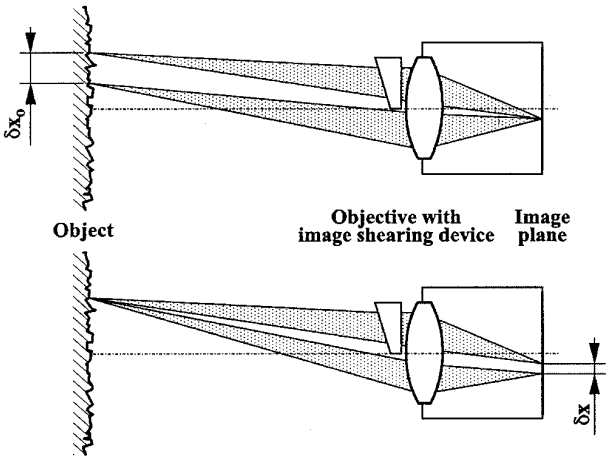

Figure 6. The geometry of an image-shearing speckle interferometer. Two points of the object are imaged together at each point of the sensor and, reciprocally, each object point has two images.

of double illumination and double observation to get twofold sensitivity [58, 59], and double illumination with directions lying in perpendicular planes [28, p 135].

3.1.3. Displacements in general directions. Speckle interferometers with sensitivity to displacement in general directions, with in-plane and out-of-plane components, are built by combining convenient illumination and observation directions, either with object and reference beams or with double illumination. Configurations of this type are used to get sensitivity with a particular direction (e.g. perpendicular to the surface of the object [60]), to control the magnitude of the sensitivity (e.g. to reduce it [61]) and to obtain different components of the displacement vector, which are needed if one is to perform multi-dimensional measurements.

3.1.4. Two- and three-dimensional displacements. The changes in the object phase difference provide only the component of the displacement along the direction of the sensitivity vector. The full calculation of the displacement vector requires three measurements of object phase differences to be made with independent sensitivity vectors $\boldsymbol{k}_1$, $\boldsymbol{k}_2$ and $\boldsymbol{k}_3$; the displacement vector is then obtained as the solution of the following system of linear equations [62]:

$$\left.\begin{aligned}\Delta\phi_{o1} &= \boldsymbol{k}_1 \cdot \boldsymbol{u}\\ \Delta\phi_{o2} &= \boldsymbol{k}_2 \cdot \boldsymbol{u}\\ \Delta\phi_{o3} &= \boldsymbol{k}_3 \cdot \boldsymbol{u}\end{aligned}\right\}$$

$$\Leftrightarrow \begin{pmatrix}\Delta\phi_{o1}\\ \Delta\phi_{o2}\\ \Delta\phi_{o3}\end{pmatrix} = \begin{pmatrix}k_{1x} & k_{1y} & k_{1z}\\ k_{2x} & k_{2y} & k_{2z}\\ k_{3x} & k_{3y} & k_{3z}\end{pmatrix}\begin{pmatrix}u\\ v\\ w\end{pmatrix}$$

$$\Leftrightarrow \Delta\Phi_o = \mathbf{K}\cdot\boldsymbol{u} \tag{3.23}$$

$$\boldsymbol{u} = \mathbf{K}^{-1}\cdot\Delta\Phi_o. \tag{3.24}$$

In-plane displacements are two-dimensional and, therefore, only two components are needed for their complete description. Their measurement is usually performed with in-plane-sensitive interferometers (section 3.1.2) either sequentially, rotating the object [63] or the interferometer [64], or simultaneously, with crossed polarization [65].

Three-dimensional measurement techniques use three or more sensitivity vectors. This is achieved by combining two in-plane-sensitive interferometers and one out-of-plane-sensitive interferometer [66], using a smooth-reference beam interferometer with three [62, 67] or four [68] independent illumination directions in sequence or even with simultaneous multiple observation directions [69] and, finally, with a double-illumination interferometer [70], keeping constant one of the illuminating directions and changing sequentially the other.

3.1.5. The difference of displacements. In the interference of two speckle patterns produced by two macroscopically identical objects illuminated and observed with the same geometry (i.e. $\boldsymbol{k}_1 = \boldsymbol{k}_2 = \boldsymbol{k}$) the object phase difference is, according to expression (3.17),

$$\phi_o(\boldsymbol{x};t) = \boldsymbol{k}\cdot[\boldsymbol{r}_1(\boldsymbol{x};t) - \boldsymbol{r}_2(\boldsymbol{x};t)] \tag{3.25}$$

and its changes measure the difference between the displacements experienced by the objects

$$\begin{aligned}\Delta\phi_o(\boldsymbol{x};t) &= \boldsymbol{k}\cdot[\Delta\boldsymbol{r}_1(\boldsymbol{x};t) - \Delta\boldsymbol{r}_2(\boldsymbol{x};t)]\\ &= \boldsymbol{k}\cdot[\boldsymbol{u}_1(\boldsymbol{x};t) - \boldsymbol{u}_2(\boldsymbol{x};t)].\end{aligned} \tag{3.26}$$

The superposition of these speckle patterns is achieved by means of modified Twyman–Green interferometers with the objects instead of mirrors [71, 72] or using shearing interferometers (section 3.2) with an abnormal lateral shear large enough to superimpose the images of the two objects placed side by side [73]. The main use of these configurations is to compare the behaviour of production items with that of a standard prototype.

3.2. Interferometers sensitive to the spatial derivative of the displacement (shearing interferometers)

Sensitivity to the spatial derivatives of displacement is obtained with image-shearing interferometers, that can be regarded as a special class of difference-of-displacement-sensitive interferometers for which only one object is used.

Two images of the object, obtained with the same illumination and observation directions (i.e. with the same sensitivity vector $\boldsymbol{k}_1 = \boldsymbol{k}_2 = \boldsymbol{k}$) are superposed slightly out of record. As shown in figure 6, at each point of the sensor one has the interference of light coming from two different points of the object for which the separation $\delta\boldsymbol{x}_o = (\delta x_o, \delta y_o)$ is the object shearing and its conjugate $\delta\boldsymbol{x} = (\delta x, \delta y) = M\delta\boldsymbol{x}_o$ is the image shearing.

Therefore

$$\boldsymbol{r}_2(\boldsymbol{x}; t) = \boldsymbol{r}(\boldsymbol{x}; t) \tag{3.27}$$

$$\boldsymbol{r}_1(\boldsymbol{x}; t) = \boldsymbol{r}_2(\boldsymbol{x} + \delta\boldsymbol{x}; t) = \boldsymbol{r}(\boldsymbol{x} + \delta\boldsymbol{x}; t) \tag{3.28}$$

according to expression (3.17), the object phase difference is

$$\phi_o(\boldsymbol{x}; t) = (\boldsymbol{k} \cdot \boldsymbol{r})(\boldsymbol{x} + \delta\boldsymbol{x}; t) - (\boldsymbol{k} \cdot \boldsymbol{r})(\boldsymbol{x}; t) \tag{3.29}$$

and, for small values of the shearing, it becomes approximately proportional to the spatial derivatives of $\boldsymbol{k} \cdot \boldsymbol{r}$

$$\begin{aligned}\delta\boldsymbol{x} \to 0 \Rightarrow \phi_o(\boldsymbol{x}; t) &\approx \delta x \frac{\partial}{\partial x}(\boldsymbol{k} \cdot \boldsymbol{r})(\boldsymbol{x}; t) \\ &+\delta y \frac{\partial}{\partial y}(\boldsymbol{k} \cdot \boldsymbol{r})(\boldsymbol{x}; t) = (\delta\boldsymbol{x}\nabla)(\boldsymbol{k} \cdot \boldsymbol{r})(\boldsymbol{x}; t).\end{aligned} \tag{3.30}$$

Assuming that $\boldsymbol{k}$ is constant, (3.29) shows that the changes in the object phase difference measure the difference in displacement between the points of the object that have been imaged together

$$\begin{aligned}\Delta\phi_o(\boldsymbol{x}; t) &= \boldsymbol{k} \cdot [\Delta\boldsymbol{r}(\boldsymbol{x} + \delta\boldsymbol{x}; t) - \Delta\boldsymbol{r}(\boldsymbol{x}; t)] \\ &= \boldsymbol{k} \cdot [\boldsymbol{u}(\boldsymbol{x} + \delta\boldsymbol{x}; t) - \boldsymbol{u}(\boldsymbol{x}; t)]\end{aligned} \tag{3.31}$$

that, with the approximation (3.30), is proportional to the spatial derivatives of displacement

$$\begin{aligned}\Delta\phi_o(\boldsymbol{x}; t) &\approx (\delta\boldsymbol{x}\nabla)(\boldsymbol{k} \cdot \boldsymbol{u})(\boldsymbol{x}; t) \\ &= \delta x \frac{\partial}{\partial x}(\boldsymbol{k} \cdot \boldsymbol{u})(\boldsymbol{x}; t) + \delta y \frac{\partial}{\partial y}(\boldsymbol{k} \cdot \boldsymbol{u})(\boldsymbol{x}; t).\end{aligned} \tag{3.32}$$

Just like with displacement-sensitive interferometers, the direction of the sensitivity vector $\boldsymbol{k}$ establishes which components of the displacement are present in $\Delta\phi_o$. Out-of-plane sensitivity is the most usual, but in-plane [74, 75] and three-dimensional [45] sensitivities can also be achieved.

The direction of the shearing vector $\delta\boldsymbol{x}$ sets the direction of the spatial derivative. The overall sensitivity is proportional to the magnitude of the shearing as well as to that of the sensitivity vector.

The direction and magnitude of $\delta\boldsymbol{x}$ may be either the same or different at every point of the interferogram. According to this, several types of shearing are defined.

Lateral shearing is the most widely used variant. One of the images is transversally displaced and all its points experience the same shearing regardless of their positions. Typically $\delta\boldsymbol{x} = (\delta x, 0)$ or $\delta\boldsymbol{x} = (0, \delta y)$ is taken to get derivatives along the coordinate axes. Many techniques for obtaining this kind of shearing have been described [76]; among the most popular are use of modified Michelson interferometers with the object as the light source and one of the mirrors tilted to introduce the shearing [33, p 156; 77]; placing wedge prisms [78], Fresnel biprisms [79] or diffraction gratings [80, 81] in front of the objective; use of split lenses [82, 83] or special diffractive optical elements [84] as objectives; and combination of Wollaston prisms with circularly polarized light [85, 86].

Other types of shearing are radial [87], rotational, inversion and folding [88]. They can be implemented either with specific or with general shearing devices [89]. Shearing and displacement-sensitive interferometers can be combined in a single instrument [48, 90] to get simultaneous sensitivity to the displacement and to its derivatives in the same interferogram.

One of the main benefits of shearing interferometry is that the two beams follow almost the same path. This allows one to use light sources with lower coherence than is required for other TVH techniques; it is even possible to illuminate several areas on the object with different light sources [91] and get good interferograms.

3.3. Shape-sensitive interferometers

Unlike displacement-sensitive interferometers, in shape-sensitive ones the position of the points of the object $\boldsymbol{r}$ is constant and the sensitivity vector is changed by a known amount $\Delta\boldsymbol{k}$ to get an object-phase-difference increment that follows an expression of the type

$$\Delta\phi_o = \Delta\boldsymbol{k} \cdot \boldsymbol{r} \tag{3.33}$$

where the sensitivity to the object shape is given by $\Delta\boldsymbol{k}$.

All the points with a given value of $\Delta\phi_o$ are placed on the intersection of the object with a set of surfaces (the *contouring surfaces*) that are perpendicular to the vector $\Delta\boldsymbol{k}$ and separated by a distance $2\pi/|\Delta\boldsymbol{k}|$ (the *contouring interval*). Contouring surfaces may have any shape and orientation, although the interpretation of the resulting fringes is easier when they are planes perpendicular to the observation direction.

Contouring techniques can be classified into three groups according to the shape of the illuminating wavefront [92, pp 180–91].

(i) *Absolute contouring*. Using collimated illumination, the sensitivity vector is the same at every point, the contouring surfaces are planes and object-phase-difference increments reveal the shape of the object. This is the most usual variant and its use will be assumed henceforth unless some other is specified.

(ii) *Relative contouring*. Illuminating wavefronts are shaped with optical elements to be spherical or cylindrical [93]. Contouring surfaces became more general and $\Delta\phi_o$ measures the difference between these and the shape of the object.

(iii) *Comparative contouring*. The illuminating beam is generated, either directly [94] or holographically [95], from a standard nominally identical to the object being tested, in order to contour their differences.

The change $\Delta\boldsymbol{k}$ induced in the sensitivity vector must be small in order to avoid speckle de-correlation [96]. Care must also be taken to avoid unwanted changes in the reference phase difference ϕ_r. These two restrictions impose a limit on the range of sensitivities that can be achieved with TVH contouring techniques.

Because the sensitivity vector is (3.3)

$$\boldsymbol{k} = \boldsymbol{k}_i - \boldsymbol{k}_o = \frac{2\pi}{\lambda}(\hat{\boldsymbol{n}}_i - \hat{\boldsymbol{n}}_o) = \frac{2\pi n}{\lambda_0}(\hat{\boldsymbol{n}}_i - \hat{\boldsymbol{n}}_o) \quad (3.34)$$

its increments $\Delta\boldsymbol{k}$ can be induced by changing the wavelength in vacuum λ_0 of the light source, the index of refraction n or the directions of illumination $\hat{\boldsymbol{n}}_i$ and observation $\hat{\boldsymbol{n}}_o$. Each of these three options gives rise to a different family of contouring techniques.

3.3.1. Two-wavelength contouring. This technique derives from an earlier method developed for holographic interferometry and was one of the first contouring techniques used with TVH. It is often implemented with out-of-plane-sensitive interferometers (section 3.1.1), wherein the wavelength of the light source is changed from λ_a to λ_b while the object remains undeformed. The sensitivity vector thus experiences an increment [33, pp 204–33; 92]

$$\Delta\boldsymbol{k} = \frac{2\pi}{\Lambda}(\hat{\boldsymbol{n}}_i - \hat{\boldsymbol{n}}_o) \quad (3.35)$$

where

$$\Lambda = \frac{\lambda_a\lambda_b}{\lambda_a - \lambda_b} \quad (3.36)$$

is the *equivalent contouring wavelength*.

The contouring surfaces are perpendicular to the sensitivity vector ($\Delta\boldsymbol{k}$ is parallel to $\boldsymbol{k}$) and the contouring interval is proportional to Λ. The sensitivity of contouring increases with the change in wavelength up to a limit imposed by speckle de-correlation [96]. Wavelength changes can be attained by switching among emission lines of argon-ion [92], dye or pulsed ruby lasers [25] and also by means of current [97] or temperature [98] modulation of laser diodes.

3.3.2. Double-refraction-index contouring. This technique also derives from holographic interferometry. It consists of changing the refractive index surrounding the object between exposures, generally by inmersion in a liquid [99, p 86]. Assuming that the refractive index is uniform, the sensitivity of contouring is

$$\Delta\boldsymbol{k} = \frac{2\pi}{\lambda_0}\Delta n(\hat{\boldsymbol{n}}_i - \hat{\boldsymbol{n}}_o). \quad (3.37)$$

In practice submerging the object to be contoured is very seldom possible and, therefore, this technique is rarely used.

3.3.3. Contouring by changing the geometry. In this family of techniques, the increment of the sensitivity vector is induced by a change in the illumination $\hat{\boldsymbol{n}}_i$ or the observation direction $\hat{\boldsymbol{n}}_o$. Two groups of techniques can be considered, according to the number of illumination beams used.

3.3.3.1. Single illumination. This is implemented with modified Mach–Zehnder interferometers with sensitivity in general directions (section 3.1.3), wherein $\Delta\boldsymbol{k}$ is induced by slightly tilting the illumination direction [100–102]:

$$\Delta\boldsymbol{k} = \frac{2\pi}{\lambda}\Delta(\hat{\boldsymbol{n}}_i - \hat{\boldsymbol{n}}_o) = \frac{2\pi}{\lambda}\Delta\hat{\boldsymbol{n}}_i. \quad (3.38)$$

If the tilt angle $\delta\beta$ is small, $\Delta\hat{\boldsymbol{n}}_i \perp \hat{\boldsymbol{n}}_i \Rightarrow \Delta\boldsymbol{k} \perp \boldsymbol{k}_i$ and, consequently, the contouring surfaces are parallel to the illumination direction and the contouring interval is

$$\frac{2\pi}{|\Delta\boldsymbol{k}|} \approx \frac{\lambda}{\delta\beta}. \quad (3.39)$$

3.3.3.2. Double illumination. Although it is possible to design contouring techniques with general geometries [103, 104], it is usual to employ interferometers with double illumination symmetrical with respect to the observation direction, such as those dedicated to the measurement of in-plane displacements (section 3.1.2). The global sensitivity vector of the interferometer $\boldsymbol{K}$ is modified by a relative tilt between the object and the illumination directions

$$\Delta\boldsymbol{K} = \Delta(\boldsymbol{k}_1 - \boldsymbol{k}_2) = \frac{2\pi}{\lambda}\Delta(\hat{\boldsymbol{n}}_{i1} - \hat{\boldsymbol{n}}_{i2}). \quad (3.40)$$

The orientation of the contouring surfaces and the value of the contouring interval are determined by how the tilting is performed.

(i) *Tilting the object.* If the object is rotated by a small angle $\delta\beta$ [105] the magnitude of $\boldsymbol{K}$ does not change and therefore $\Delta\boldsymbol{K} \perp \boldsymbol{K}$ and the contouring surfaces are perpendicular to the observation direction. The contouring interval depends on the illumination angle θ and tilt angle $\delta\beta$ and on the tilt axis [106]; for a tilt axis in the object plane and perpendicular to the sensitivity vector $\boldsymbol{K}$ its value is

$$\frac{2\pi}{|\Delta\boldsymbol{K}|} \approx \frac{\lambda}{2\delta\beta\sin\theta}. \quad (3.41)$$

(ii) *Tilting the illumination.* The observation direction is kept constant while one or both illuminating beams are slightly tilted by $\delta\beta$ around an axis perpendicular to the plane that contains the illumination and observation directions. Three variants have been proposed [103, 107]. First, *only one illumination beam is tilted*. As for single illumination (section 3.3.3.1) the contouring surfaces are perpendicular to this beam and the contouring interval follows expression (3.39). Second, *both beams are tilted by the same angle in the same direction*. This is equivalent to tilting the object ((i) above). The contouring surfaces are perpendicular to the observation direction and the contouring interval is given by expression (3.41). Third, *both beams are tilted by the same angle in opposite directions*. The contouring surfaces are parallel to the observation direction and the contouring interval once again follows expression (3.41). The tilting of the illumination directions, which is common to all these techniques, can be implemented by use of tilting mirrors or translating lenses [107, 108], by switching two sets of fixed illumination beams [109] or by use of tilting diffraction gratings [110]. Large objects have to be illuminated with diverging beams; in that case the tilting can be performed by translating their foci [101], but the effect of the curved wavefront must be corrected [111] for absolute contouring.

3.3.4. Contouring by limited coherence. This last group of techniques is also called *single-fringe contouring* [112]. Low-coherence sources and balanced interferometers are used to get non-zero visibility in the speckle interferogram, $\mathcal{V}(\boldsymbol{x}) \neq 0$, just for the points of the object where the optical path difference is almost zero. This single fringe of contrasted speckle is used to scan the contour of the object as the length of one of the arms of the interferometer is changed.

3.4. Refractive-index-sensitive interferometers

The measurement range of TVH has recently been extended to the measurement of spatial distributions of refractive index (*phase objects*) such as those due to pressure or temperature fields in liquids and gases. The techniques proposed to date use interferometers with parallel illumination and observation directions, generally with a uniform reference beam, and the phase object is placed in front of a diffusing background. The object phase difference is related, aside from to the shape of the diffuser $\boldsymbol{r}(\boldsymbol{x})$, to the *optical thickness* of the phase object along the observation direction (the z axis) by

$$\phi_o(\boldsymbol{x}; t) = \boldsymbol{k} \cdot \boldsymbol{r}(\boldsymbol{x}) + q\frac{2\pi}{\lambda_0}\int_{Object}[n_o(x, y, z; t) - n]\,\mathrm{d}z \tag{3.42}$$

q being the number of times the illumination beam passes through the object, λ_0 the wavelength in vacuum of the light source, n the refractive index of the medium surrounding the set-up and $n_o(x, y, z; t)$ that of the phase object at a given position and time.

With a static background, the increment of ϕ_o measure the changes in optical thickness. The spatial distribution of the refractive index $n_o(x, y, z; t)$ can be obtained by measuring the optical thicknesses along various directions and applying tomographic reconstruction techniques [113–116].

Two variants of the basic geometry can be considered [117]: reflection and transmission.

3.4.1. Reflection geometry. The diffuser is illuminated from the same side as that from which the object is observed (figure 7(*a*)) so that illumination and observation have opposite directions and light passes twice through the phase object. The object phase difference is then given by

$$\phi_o(\boldsymbol{x}; t) = \frac{4\pi}{\lambda_0}\left(\hat{\boldsymbol{n}}_i \cdot \boldsymbol{r}(\boldsymbol{x}) + \int_{Object}[n_o(x, y, z; t) - n]\,\mathrm{d}z\right). \tag{3.43}$$

3.4.2. Transmission geometry. The diffuser is illuminated and observed in the same direction [113] and light passes just once through the object. The sensitivity vector is

$$\boldsymbol{k}_i = \boldsymbol{k}_o \Rightarrow \boldsymbol{k} = \boldsymbol{k}_i - \boldsymbol{k}_o = 0 \tag{3.44}$$

and the object phase difference becomes

$$\phi_o(\boldsymbol{x}; t) = \frac{2\pi}{\lambda_0}\int_{Object}[n_o(x, y, z; t) - n]\,\mathrm{d}z. \tag{3.45}$$

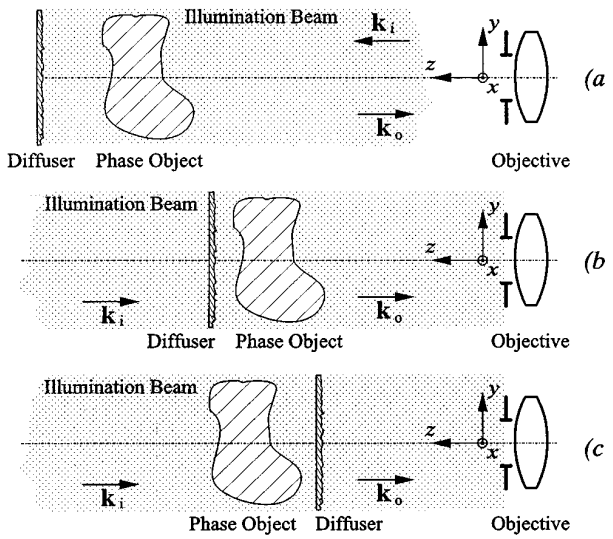

Figure 7. Illumination and observation geometries for the measurement of phase objects: (*a*) reflection, (*b*) transmission with the object in front of the diffuser and (*c*) transmission with the diffuser in front of the object.

This implies that, although it is one half as sensitive to the optical thickness, this variant is much less sensitive to the instabilities of the diffuser than is the previous one.

The object may be placed either in front of or behind the diffuser (figures 7(*b*) and (*c*)). The last of these configurations avoids the de-correlation of speckle by the changes of direction that light may experience as it passes through the phase object [118].

4. The temporal treatment

The description of the temporal treatment of speckle interferograms in TVH is greatly simplified by using the concept of the *fringe function*, which was introduced by Stetson [119] for holographic interferometry and later developed by other authors. According to the expression (3.16), the instantaneous irradiance at each point $\boldsymbol{x} = (x, y)$ of the sensor of the camera is

$$I(\boldsymbol{x}; t) = \mathcal{I}_0(\boldsymbol{x})\{1 + \mathcal{V}(\boldsymbol{x})\cos[\psi_p(\boldsymbol{x}) - \phi_r(t) + \phi_o(\boldsymbol{x}; t)]\}. \tag{4.1}$$

Video cameras integrate this irradiance both in space (over a pixel) and in time (during a period equal to or shorter than their frame period T_F). As a result, the measured irradiance in the nth video frame can be expressed [32, p 464] as

$$\begin{aligned} I_n(\boldsymbol{x}) &= I_n(x, y) \\ &= g\int_{-\infty}^{\infty}\int_{-\infty}^{\infty}\left(\int_{-\infty}^{\infty} I(x', y'; t')s_n(t')m_n(t_n - t')\,\mathrm{d}t'\right) \\ &\quad \times h_n(x - x', y - y')\,\mathrm{d}x'\,\mathrm{d}y'. \end{aligned} \tag{4.2}$$

This expression corresponds to an optoelectronically generated additive correlation pattern that from now on we will call a *primary correlogram*. Its parameters are the following.

(i) $g = g(\lambda)$, the *spectral sensitivity* of the camera for the wavelength λ.

(ii) $t_n = t_n(x, y)$, the *reading instant*, corresponding to the end of the integration period for the pixel placed at the position $\boldsymbol{x} = (x, y)$. Its expression depends on the integration mode of the camera [120].

(iii) $m_n(\Delta t)$, the *normalized exposure weighting function* of the camera [32, 120] that establishes the relative contribution of the instantaneous irradiance, within as well as outside the integration period, to the measured irradiance, taking into account such effects as persistence, electronic shuttering and ghost images. Løkberg [32] includes in this function the effect of intensity modulation of the light source, but we find it more convenient to consider this separately (as $s_n(t)$) because its time dependence need not be referred to the reading instant as $m_n(\Delta t)$ is.

(iv) $s_n(t)$, the *intensity modulation* or '*shutter' function* of the light source. The definition of this function characterizes each type of temporal treatment.

(v) $h_n(\Delta x, \Delta y)$, the *spatial impulse response* of the camera, that describes its resolving power. It can be generalized to comprise such factors as the temporal transfer function of the amplifiers and filters of the camera [37] and the spatial resolution of the image-storage systems.

Combining expressions (4.1) and (4.2) results in

$$\begin{aligned} I_n(x, y) = g \int_{-\infty}^{\infty} \int_{-\infty}^{\infty} & \mathcal{I}_0(x', y') \\ & \times \left(1 + \mathcal{V}(x', y') \int_{-\infty}^{\infty} \cos[\psi_p(x', y') - \phi_r(t') \right. \\ & \left. + \phi_o(x', y'; t')] s_n(t') m_n(t_n - t') \, \mathrm{d}t' \right) \\ & \times h_n(x - x', y - y') \, \mathrm{d}x' \, \mathrm{d}y' \end{aligned} \tag{4.3}$$

where

$$\begin{aligned} & \cos[\psi_p(x', y') - \phi_r(t') + \phi_o(x', y'; t')] \\ & \quad = \mathrm{Re}\{\exp\{\mathrm{i}[\psi_p(x', y') - \phi_r(t') + \phi_o(x', y'; t')]\}\} \end{aligned} \tag{4.4}$$

The *fringe function* is defined [119] as

$$\begin{aligned} M_n(\boldsymbol{x}) = M_n(x, y) = \int_{-\infty}^{\infty} & \exp\{\mathrm{i}[\phi_o(x', y'; t') - \phi_r(t')]\} \\ & \times s_n(t') m_n(t_n - t') \, \mathrm{d}t'. \end{aligned} \tag{4.5}$$

If the speckle does not experience de-correlation during the exposure period, ψ_{p1} and ψ_{p2} become constants and (4.3) can be written as

$$\begin{aligned} I_n(x, y) = g \int_{-\infty}^{\infty} \int_{-\infty}^{\infty} & \mathcal{I}_0(x', y')[1 + \mathcal{V}(x', y') \\ & \times \mathrm{Re}\{\exp[\mathrm{i}\psi_p(x', y')] M_n(x', y')\}] \\ & \times h_n(x - x', y - y') \, \mathrm{d}x' \, \mathrm{d}y'. \end{aligned} \tag{4.6}$$

The fringe function $M_n(\boldsymbol{x})$ gives an explicit description of the secondary fringes that can be extracted from the primary correlogram by fringe-generation techniques. That is the importance of its role: it quantifies the output of the TVH system. The expression of $M_n(\boldsymbol{x})$ as a function of ϕ_o and ϕ_r is characteristic of each temporal treatment technique.

When the average size of the speckle is greater than or equal to a pixel and secondary fringes are wide (i.e. $\mathcal{I}_0$, ψ_p, $\mathcal{V}$ and ϕ_o are locally uniform in every pixel) expression (4.6) becomes simpler:

$$I_n(\boldsymbol{x}) = g\mathcal{I}_0(\boldsymbol{x})[1 + \mathcal{V}(\boldsymbol{x}) \, \mathrm{Re}\{\exp[\mathrm{i}\psi_p(\boldsymbol{x})] M_n(\boldsymbol{x})\}]. \tag{4.7}$$

Moreover, if the integration of the irradiance in the camera is uniform throughout the integration period and neither persistence nor ghost images are present, then

$$m_n(\Delta t) = \begin{cases} \dfrac{1}{T_{e,n}} & 0 \leqslant \Delta t \leqslant T_F \\ 0 & \text{otherwise} \end{cases} \tag{4.8}$$

where $T_{e,n}$ is the *effective exposure time*, that can be calculated from the intensity modulation function

$$T_{e,n} = \int_{t_n - T_F}^{t_n} s_n(t') \, \mathrm{d}t'. \tag{4.9}$$

In this case, the fringe function is

$$M_n(\boldsymbol{x}) = \frac{1}{T_{e,n}} \int_{t_n - T_F}^{t_n} \exp\{\mathrm{i}[\phi_o(\boldsymbol{x}; t') - \phi_r(t')]\} s_n(t') \, \mathrm{d}t'. \tag{4.10}$$

Expressions (4.7) and (4.10), although they correspond to the most favourable conditions, are a good approximation for many real situations. We will use them to describe the main temporal treatment techniques used in TVH.

4.1. Time averaging

The object is illuminated during a given *exposure interval* $[t_{1,n}, t_{2,n}]$ with a duration $T_{e,n} = t_{2,n} - t_{1,n}$ shorter than or equal to the frame period T_F. Continuous-emission lasers are suitable light sources for this temporal treatment mode. The exposure time can be controlled either with intensity modulators (acousto-optical, electro-optical and mechanical choppers) or with the electronic shutters of some cameras.

The intensity modulation function is (figure 8)

$$s_n(t) = \begin{cases} 1 & t_{1,n} \leqslant t \leqslant t_{2,n} \\ 0 & \text{otherwise} \end{cases} \tag{4.11}$$

and the fringe function

$$M_n(\boldsymbol{x}) = \frac{1}{T_{e,n}} \int_{t_{1,n}}^{t_{2,n}} \exp\{\mathrm{i}[\phi_o(\boldsymbol{x}; t') - \phi_r(t')]\} \, \mathrm{d}t'. \tag{4.12}$$

4.1.1. Static measurands. When the changes in the measurand are slow enough to allow one to assume that the object phase difference ϕ_o is constant during the exposure period and the reference phase difference ϕ_r also is kept constant, the fringe function becomes

$$M_n(\boldsymbol{x}) = \exp\{\mathrm{i}[\phi_o(\boldsymbol{x}) - \phi_r]\} \tag{4.13}$$

and, according to (4.7), the primary correlograms are

$$I_n(\boldsymbol{x}) = g\mathcal{I}_0(\boldsymbol{x})\{1 + \mathcal{V}(\boldsymbol{x}) \cos[\psi_p(\boldsymbol{x}) - \phi_r + \phi_o(\boldsymbol{x})]\}. \tag{4.14}$$

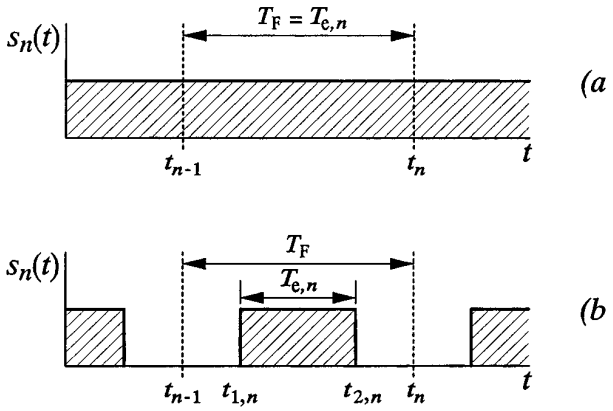

Figure 8. Shutter functions for time-average techniques: (*a*) continuous illumination and (*b*) illumination during a limited interval.

4.1.2. Harmonic oscillation. When the object phase difference experiences a sinusoidal oscillation one can write

$$\phi_o(\boldsymbol{x}; t) = \phi_{om}(\boldsymbol{x}) \sin[\omega_o t + \varphi_o(\boldsymbol{x})] \tag{4.15}$$

where $\phi_{om}(\boldsymbol{x}; t)$ is the amplitude in terms of the optical phase, ω_o is the angular frequency of oscillation and $\varphi_o(\boldsymbol{x})$ is the mechanical phase. Several variants are defined according to the relationship between the exposure interval $T_{e,n}$ and the mechanical oscillation period T_o and to the type of modulation of the reference phase difference ϕ_r.

4.1.2.1. Standard time averaging. The exposure interval is much longer than the oscillation period ($T_{e,n} \gg T_o = 2\pi/\omega_o$) and ϕ_r is kept constant during each exposure. The fringe function takes then the approximate value [33, pp 107–9]

$$M_n(\boldsymbol{x}) \approx \exp(-\mathrm{i}\phi_r) J_0[\phi_{om}(\boldsymbol{x})] \tag{4.16}$$

and therefore

$$I_n(\boldsymbol{x}) = g\mathcal{T}_0(\boldsymbol{x})\{1 + \mathcal{V}(\boldsymbol{x}) \cos[\psi_p(\boldsymbol{x}) - \phi_r] J_0[\phi_{om}(\boldsymbol{x})]\}. \tag{4.17}$$

The fringe function does not depend on the mechanical phase $\varphi_o(\boldsymbol{x})$; this information is lost. The reference phase difference ϕ_r can be used to modify the phase noise of the speckle, but has no effect on the argument of the Bessel function $J_0(\cdot)$ that contains the usable information. These two drawbacks can be overcome by using phase-modulation techniques [121]; the most widely used in TVH are described in sections 4.1.2.4 and 4.1.2.5.

The exposure interval is usually the whole frame ($T_{e,n} = T_F$) or field ($T_{e,n} = T_f = T_F/2$) period of the video camera. However, if the oscillation frequency is high enough, it is possible to reduce it to make measurements on unstable objects or in noisy environments.

4.1.2.2. Reduced-exposure time averaging. The exposure interval $T_{e,n}$ is comparable to or shorter than the oscillation period T_o. This situation is typically reached when the oscillation frequency is close to the frame frequency of the camera, or when the exposure interval is reduced to a minimum in order to gain stability.

If the reference phase difference is kept constant during each exposure, the fringe function [122, 123] becomes

$$M_n(\boldsymbol{x}) = \exp(-\mathrm{i}\phi_r) \sum_{q=-\infty}^{\infty} \left[J_q[\phi_{om}(\boldsymbol{x})] \times \exp\{\mathrm{i}q[\varphi_{m,n} + \varphi_o(\boldsymbol{x})]\} \operatorname{sinc}\left(q \frac{T_{e,n}}{T_o}\right) \right] \tag{4.18}$$

where

$$\varphi_{m,n} = \frac{2\pi}{T_o} \frac{t_{1,n} + t_{2,n}}{2} \tag{4.19}$$

is the average mechanical phase during the exposure interval.

4.1.2.3. Extended-exposure time averaging. For very-low-frequency oscillations (comparable to or lower than the frame frequency of the camera), several images corresponding to primary correlograms $I_n(\boldsymbol{x})$ obtained with the maximum exposure interval (typically $T_{e,n} = T_F$) and randomly distributed average mechanical phase $\varphi_{m,n}$ can be averaged to get

$$\hat{I}_n(\boldsymbol{x}) = \frac{1}{N} \sum_{i=0}^{N} I_{n-i}(\boldsymbol{x}) \tag{4.20}$$

whose fringe function [123] is

$$M_n(\boldsymbol{x}) = \exp(-\mathrm{i}\phi_r) \sum_{q=-\infty}^{\infty} \left[J_q[\phi_{om}(\boldsymbol{x})] \operatorname{sinc}\left(q \frac{T_{e,n}}{T_o}\right) \right]. \tag{4.21}$$

4.1.2.4. Time averaging with homodyne phase modulation. The reference phase difference $\phi_r(t)$ is sinusoidally modulated during the exposure interval with the same frequency as that of the object according to the expression

$$\phi_r(t) = \phi_{rA} + \phi_{rm} \cos(\omega_r t + \varphi_r) \tag{4.22}$$

where ϕ_{rA} is a phase offset that is kept constant during the exposure period, ϕ_{rm} is the amplitude of the modulation in terms of the optical phase, $\omega_r = \omega_o$ is its angular frequency and φ_r is its mechanical phase. The resulting fringe function is [121, 124]

$$M_n(\boldsymbol{x}) \approx \exp(-\mathrm{i}\phi_{rA}) J_0\{\{\phi_{om}^2(\boldsymbol{x}) + \phi_{rm}^2 - 2\phi_{om}(\boldsymbol{x})\phi_{rm} \cos[\varphi_o(\boldsymbol{x}) - \varphi_r]\}^{1/2}\}. \tag{4.23}$$

A particularly interesting case arises when the modulation is in phase with the oscillation of the object ($\varphi_r = \varphi_o(\boldsymbol{x})$, $\forall \boldsymbol{x}$). The fringe function is then simplified to

$$M_n(\boldsymbol{x}) \approx \exp(-\mathrm{i}\phi_{rA}) J_0[\phi_{om}(\boldsymbol{x}) - \phi_{rm}]. \tag{4.24}$$

Homodyne modulation makes it possible to do the following.

(i) To get fringes with sensitivity both to the amplitude and to the phase of the oscillation of the object and to shift them by means of the modulation parameters ϕ_{rm} and φ_r [125].

(ii) To control the sensitivity of the fringe function to the amplitude of oscillation. This is achieved by shifting the zeroth-order fringe with an appropriate value of ϕ_{rm} in expression (4.24) and can be used to detect oscillations with either very small [124] or very large [126, 127] amplitudes.

(iii) To implement phase-shifting evaluation techniques [128] on time-average correlograms.

The modulation of the reference phase difference is usually derived from the signal used to excite the oscillation of the object. It is also possible to generate it from the measurand itself by optical [129] or optoelectronic [130, 131] means.

Homodyne modulation has been combined with reduced exposure (section 4.1.2.2) to increase the immunity to object and environment instabilities. The fringe function [129, 132] then becomes more complicated than (4.23).

4.1.2.5. Time averaging with heterodyne phase modulation. The reference phase difference $\phi_r(t)$ is sinusoidally modulated with an angular frequency $\omega_r = \omega_o + \delta\omega$ slightly different from the object's. Expression (4.22) is then

$$\omega_r = \omega_o + \delta\omega \Rightarrow \phi_r(t) = \phi_{rA} + \phi_{rm}\sin[\omega_r t + (\varphi_r + \delta\omega t)]. \tag{4.25}$$

The practical interest of such modulation arises when the difference between these frequencies $\delta\omega$ is so small that the term $\varphi_r + \delta\omega t$ can be considered constant during each exposure period and the fringe function becomes

$$M_n(\boldsymbol{x}) \approx \exp(-\mathrm{i}\phi_{rA}) J_0\{\{\phi_{om}^2(\boldsymbol{x}) + \phi_{rm}^2 - 2\phi_{om}(\boldsymbol{x})\phi_{rm}\cos[\varphi_o(\boldsymbol{x}) - (\varphi_r + \delta\omega t_n)]\}^{1/2}\}. \tag{4.26}$$

Even if all the parameters of the object oscillation and of the phase modulation are constant, the value of the fringe function changes periodically with a frequency $\delta f = \delta\omega/(2\pi)$ wherever the amplitude of oscillation is not zero ($\phi_{om} \neq 0$). This allows the detection and measurement of extremely low-amplitude oscillations. Sensitivity limits of 20 Å with visual observation and 0.1 Å with lock-in detection have been reported [120, 133].

4.1.3. General periodic measurands. General periodic oscillations can be expressed as Fourier series and the corresponding object phase difference is

$$\phi_o(\boldsymbol{x}; t) = \sum_{k=1}^{\infty} \phi_{om,k}(\boldsymbol{x})\cos[k\omega_o t + \varphi_{o,k}(\boldsymbol{x})]. \tag{4.27}$$

4.1.3.1. Standard time averaging. Substituting expression (4.27) into (4.12) and considering an exposure interval much longer than the oscillation period ($T_{e,n} \gg T_o = 2\pi/\omega_o$) results in the following fringe function [134]:

$$M_n(\boldsymbol{x}) \approx \mathrm{e}^{-\mathrm{i}\phi_r} \prod_{k=1}^{\infty} J_0[\phi_{om,k}(\boldsymbol{x})]. \tag{4.28}$$

4.1.3.2. Time averaging with phase modulation. When the reference phase difference ϕ_r is sinusoidally modulated according to expression (4.22) with the frequency of the jth harmonic $\omega_r = j\omega_o$ the resulting fringe function is [134]

$$M_n(\boldsymbol{x}) \approx \exp(-\mathrm{i}\phi_{rA}) J_0\{\{\phi_{om,j}^2(\boldsymbol{x}) + \phi_{rm}^2 - 2\phi_{om,j}(\boldsymbol{x})\phi_{rm}\cos[\varphi_{o,j}(\boldsymbol{x}) - \varphi_r]\}^{1/2}\} \times \frac{\prod_{k=1}^{\infty} J_0[\phi_{om,k}(\boldsymbol{x})]}{J_0[\phi_{om,j}(\boldsymbol{x})]} \tag{4.29}$$

that reveals the amplitude and mechanical phase of that harmonic as well as the amplitudes of all the remaining harmonics. The information about the harmonic of interest can be extracted by dividing expression (4.29) by (4.28). This allows one to analyse general oscillations on a harmonic basis, to apply sensitivity-control techniques to them and to evaluate the resulting fringes with phase-shifting techniques [135].

4.1.4. Non-periodic dynamic measurands. The applicability of time-average TVH to the measurement of non-periodic measurands is highly limited, although it is possible to analyse transient phenomena with such slow evolutions that they can be considered static (section 4.1.1) during the exposure interval and oscillations with a damping factor low enough to allow one to assume that their amplitudes, phases and frequencies are constant during the exposure [10].

It is also possible to measure movements with constant speed during the exposure interval. As suggested in [122], the fringe function for this case is similar to its holographic-interferometry counterpart [136, pp 93–4]. It can be found that

$$M_n(\boldsymbol{x}) = \exp(-\mathrm{i}\phi_r)\exp\left(\mathrm{i}\frac{\phi_o(\boldsymbol{x}; t_{1,n}) + \phi_o(\boldsymbol{x}; t_{2,n})}{2}\right) \times \frac{\sin\left(\frac{T_{e,n}}{2}\dot{\phi}_o(\boldsymbol{x})\right)}{\frac{T_{e,n}}{2}\dot{\phi}_o(\boldsymbol{x})} \tag{4.30}$$

with

$$\dot{\phi}_o(\boldsymbol{x}) = \frac{\mathrm{d}\phi_o}{\mathrm{d}t}(\boldsymbol{x}). \tag{4.31}$$

4.2. Stroboscopic illumination

The nature of stroboscopic techniques make them only useful for periodic or repetitive measurands. The object is illuminated with a train of light pulses synchronized to its oscillation (the width of these pulses T_p is shorter than the oscillation period ($T_p < T_o$)) resulting in a synchronous temporal sampling of the oscillation.

One of the main advantages of these techniques is that the instantaneous value of the measurand appears 'frozen' as if it were static; this means that the fringe function is sinusoidal and, therefore, easier to interpret and evaluate than is the Bessel function that arises from time averaging. Furthermore, the mechanical phase of the pulses can be controlled, thus providing temporal resolution to scan the vibration cycle. The price for these benefits is a higher complexity of the interferometer and a lower economy of the available light power.

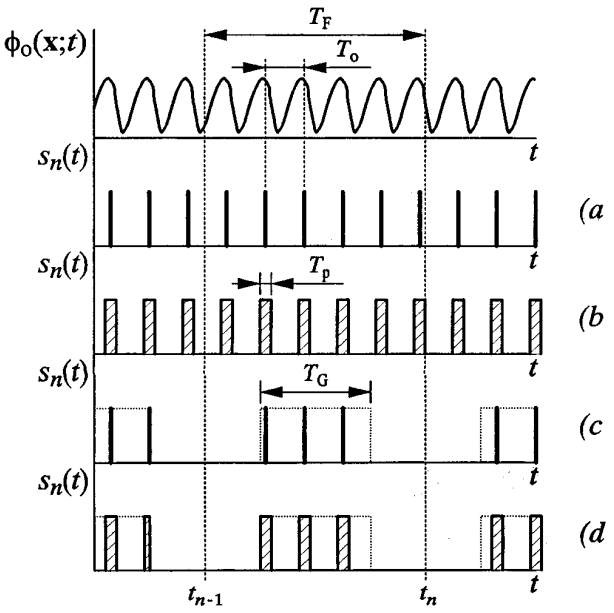

Figure 9. Shutter functions for stroboscopic illumination: (*a*) ideal pulses (from a pulsed laser), (*b*) finite-length pulses (from a chopped laser) and gated illumination with (*c*) ideal and (*d*) finite-length pulses.

Pulsed lasers would seem ideal for providing this kind of illumination (figure 9(*a*)), but in their current state of development they are able only to operate in very limited frequency ranges and they are too expensive for most applications. It is more usual to modulate the intensity of continuous-emission lasers with mechanical light choppers, or acousto-optical and electro-optical modulators, to generate finite-width pulses (figure 9(*b*)).

If the width of the pulses T_p is comparable to the oscillation period T_o, the stroboscopic method is equivalent to the superposition of multiple reduced-exposure time-average correlograms (section 4.1.2.2) with the same average mechanical phase φ_m. The fringe function is then (4.18).

The width of the pulses must be sufficiently short that one can consider that the object phase difference is constant during it. Most authors [30, 34, 137] assume that, for $T_p \leqslant T_o/10$ and moderate amplitudes, the oscillation is effectively 'frozen' in the mean instant of the pulses t_p and they can be reasonably represented as Dirac delta functions

$$I(t) = \mathcal{I}_0 \delta(t - t_p). \tag{4.32}$$

The length of the stroboscopic pulse trains is usually the whole frame period of the video camera T_F. However, illumination gates of shorter duration $T_G < T_F$ (figures 9(*c*) and (*d*)) may be used for the measurement of unstable objects or in hostile environments, albeit with an even lower light economy.

4.2.1. General periodic measurands. When the measurand experiences a general oscillation with period T_o, the object phase difference satisfies

$$\phi_o(\boldsymbol{x}; t + kT_o) = \phi_o(\boldsymbol{x}; t). \tag{4.33}$$

Since $T_o < T_F$, in every primary correlogram a given number N of oscillation cycles is recorded and in each of them q light pulses are fired. When expression (4.32) is applicable, the intensity-modulation function is

$$s_n(t) = \sum_{j=1}^{q} \mathrm{comb}\left(\frac{t - t_{pj,n}}{T_o}\right) \tag{4.34}$$

with [138]

$$\mathrm{comb}(x) = \sum_{k=-\infty}^{+\infty} \delta(x - k) \tag{4.35}$$

the function 'train of pulses' and $0 \leqslant t_{pj,n} \leqslant T_o$ the delays of the q light pulses with respect to the beginning of each oscillation cycle ($t = kT_o$).

The effective exposure time is, according to expression (4.9), $T_{e,n} = qN$. Considering expression (4.33) and assuming that the reference phase difference ϕ_r and the oscillation are stable during each frame period, the fringe function becomes

$$M_n(\boldsymbol{x}) = \exp(-\mathrm{i}\phi_r)\frac{1}{q}\sum_{j=1}^{q} \exp[\mathrm{i}\phi_o(\boldsymbol{x}; t_{pj,n})]. \tag{4.36}$$

To the best of our knowledge, only techniques with one or two pulses per oscillation cycle have been implemented in TVH, although the use of multiple pulses has been suggested [42] and its theoretical background is well known [121].

4.2.1.1. Single exposure. Only one light pulse with a delay $t_{p,n}$ (figure 10(*a*)) is fired in each oscillation cycle. The fringe function is

$$M_n(\boldsymbol{x}) = \exp\{\mathrm{i}[\phi_o(\boldsymbol{x}; t_{p,n}) - \phi_r]\} \tag{4.37}$$

and the intensity of the primary correlogram, according to expression (4.7), is

$$I_n(\boldsymbol{x}) = g\mathcal{I}_0(\boldsymbol{x})\{1 + \mathcal{V}(\boldsymbol{x})\cos[\psi_p(\boldsymbol{x}) - \phi_r + \phi_o(\boldsymbol{x}; t_{p,n})]\} \tag{4.38}$$

that is equivalent to an static displacement (4.14) corresponding to the state of the object at the sampling instants $t = t_{p,n} + kT_o$.

4.2.1.2. Double exposure

Standard double exposure. Two pulses with different delays $t_{p1,n}$ and $t_{p2,n}$ are fired within each oscillation cycle (figure 10(*b*)) or two bursts, with the same number of single light pulses but different delays, are fired alternately within the integration period of the camera [139]. The resulting fringe function is

$$M_n(\boldsymbol{x}) = \exp(-\mathrm{i}\phi_r)\tfrac{1}{2}\{\exp[\mathrm{i}\phi_o(\boldsymbol{x}; t_{p1,n})] + \exp[\mathrm{i}\phi_o(\boldsymbol{x}; t_{p2,n})]\} \tag{4.39}$$

that can be also written as

$$M_n(\boldsymbol{x}) = \exp(-\mathrm{i}\phi_r)\exp\left(\mathrm{i}\frac{\phi_o(\boldsymbol{x}; t_{p1,n}) + \phi_o(\boldsymbol{x}; t_{p2,n})}{2}\right) \times \cos\left(\frac{\phi_o(\boldsymbol{x}; t_{p1,n}) - \phi_o(\boldsymbol{x}; t_{p2,n})}{2}\right) \tag{4.40}$$

Therefore, the intensity of the primary correlograms depends sinusoidally on the change experienced by the object phase difference between light pulses $\Delta\phi_o(\boldsymbol{x}) = \phi_o(\boldsymbol{x}; t_{p1,n}) - \phi_o(\boldsymbol{x}; t_{p2,n})$.

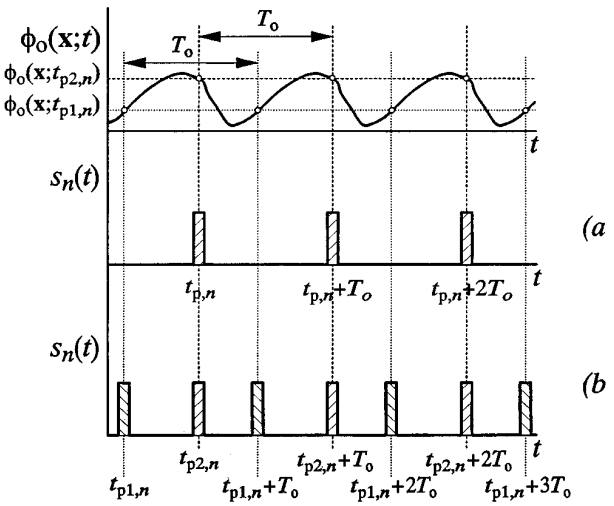

Figure 10. Shutter functions for (*a*) single-exposure and (*b*) double-exposure stroboscopic illumination.

Double exposure with synchronous phase modulation. The reference phase difference is alternately changed on going from one pulse to the next of each pair. The shape of the modulation is not as relevant as the value of the phase when the pulses are fired. The resulting fringe function is then [140, 141]

$$M_n(\boldsymbol{x}) = \cos\left(\frac{\Delta\phi_{o,n}(\boldsymbol{x})}{2} - \phi_{rS,n}\right)\exp\{\mathrm{i}[\bar{\phi}_{o,n}(\boldsymbol{x}) - \phi_{rA,n}]\} \tag{4.41}$$

where $\Delta\phi_{o,n}(\boldsymbol{x})$ and $\bar{\phi}_{o,n}(\boldsymbol{x})$ are, respectively, the change between pulses and the average value of the object phase difference, $\phi_{rS,n}$ is the amplitude of the phase modulation between pulses and $\phi_{rA,n}$ its mean value. A pseudo-heterodyne effect [142] can be also achieved if the amplitude of the modulation is slightly increased between consecutive correlograms.

4.2.2. Harmonic oscillation. When the object phase difference follows a sinusoidal expression such as (4.15), it is more convenient to speak in terms of the mechanical phase φ_p rather than in terms of pulse delays t_p; the relation between these two parameters is trivial:

$$\varphi_p = \frac{2\pi}{T_o}t_p = \omega_o t_p \tag{4.42}$$

and, therefore, at the sampling instant

$$\phi_o(\boldsymbol{x};\, t_p) = \phi_{om}(\boldsymbol{x})\sin[\varphi_p + \varphi_o(\boldsymbol{x})]. \tag{4.43}$$

4.2.2.1. Single exposure The expression for the primary correlograms is obtained by combining (4.43) and (4.38). When the light pulses are synchronized to the maxima ($\varphi_{p,n} = -\varphi_o(\boldsymbol{x})$) or minima ($\varphi_{p,n} = \pi - \varphi_o(\boldsymbol{x})$) the correlogram measures the amplitude of oscillation ϕ_{om}:

$$I_n(\boldsymbol{x}) = g\mathcal{I}_0(\boldsymbol{x})\{1 + \mathcal{V}(\boldsymbol{x})\cos[\psi_p(\boldsymbol{x}) - \phi_r \pm \phi_{om}(\boldsymbol{x})]\}. \tag{4.44}$$

4.2.2.2. Double exposure The combination of (4.43), (4.40) and (4.7) gives the expression for the primary correlograms. The case of equally spaced light pulses is especially interesting: $t_{p2,n} = t_{p1,n} + T_o/2 \Leftrightarrow \varphi_{p2,n} = \varphi_{p1,n} + \pi \Leftrightarrow \phi_o(\boldsymbol{x};\, t_{p2,n}) = -\phi_o(\boldsymbol{x};\, t_{p1,n})$, thence

$$I_n(\boldsymbol{x}) = g\mathcal{I}_m(\boldsymbol{x})\{1 + \mathcal{V}(\boldsymbol{x})\cos[\psi_p(\boldsymbol{x}) - \phi_r] \times \cos\{\phi_{om}(\boldsymbol{x})\cos[\varphi_{p1,n} + \varphi_o(\boldsymbol{x})]\}\}. \tag{4.45}$$

Just like in single exposure, when the pulses are matched to the extrema of the oscillation [49] ($\varphi_{p1},\, n = -\varphi_o(\boldsymbol{x})$) the primary correlogram reflects the amplitude of oscillation

$$I_n(\boldsymbol{x}) = g\mathcal{I}_0(\boldsymbol{x})\{1 + \mathcal{V}(\boldsymbol{x})\cos[\psi_p(\boldsymbol{x}) - \phi_r]\cos[\phi_{om}(\boldsymbol{x})]\} \tag{4.46}$$

but with ϕ_{om} made independent of the speckle phase noise just like in time-average techniques (4.17).

4.2.3. General measurands. Stroboscopic techniques have been applied [143] to the measurement of transient events that are shorter than the frame period of the camera and can be accurately repeated. The transient is re-excited after its extinction at regular intervals, thus converting it into a periodic measurand (section 4.2.1).

4.3. Pulsed illumination

The exposure of each video frame is achieved with a reduced number of high-energy light pulses, typically one or two. The measurement time is very short and, therefore, these techniques are highly immune to object instability and environmental disturbance, as is required for industrial applications. Furthermore, since it allows recording of the state of the object at just one or two instants, this is the only TVH technique suitable for the analysis of transient events that, in general, are not repeatable as is required for stroboscopic techniques (section 4.2.3).

Light pulses with the required properties for TVH (i.e. coherence, very small width (tens of nanoseconds) and high energy (several millijoules)) can be obtained only with pulsed lasers. Nevertheless, some authors [42] have used continuous-emission lasers with acousto-optical or electro-optical intensity modulators, although with serious restrictions imposed by the lack of energy (small objects) and the length of the pulses (relatively slow measurands).

Ruby lasers have traditionally been used in TVH [62, 144, 145], but the current trend is to use Nd:YAG lasers optimized for operation at video frame rates [13, 146, 147] (25 Hz in Europe and 30 Hz in America) and also at field rates [148, 149] (50 or 60 Hz). A few research groups have even used double cavity lasers to get very small pulse separations [150–152].

Very short light pulses can be represented by Dirac delta functions and therefore

$$s_n(t) = \sum_{j=1}^{q}\delta(t - t_{pj,n}) \tag{4.47}$$

where q is the number of pulses fired during the integration period of the video camera (T_F for frame-integration cameras or T_f for field integration [153, 154]) and $t_{pj,n}$ are the

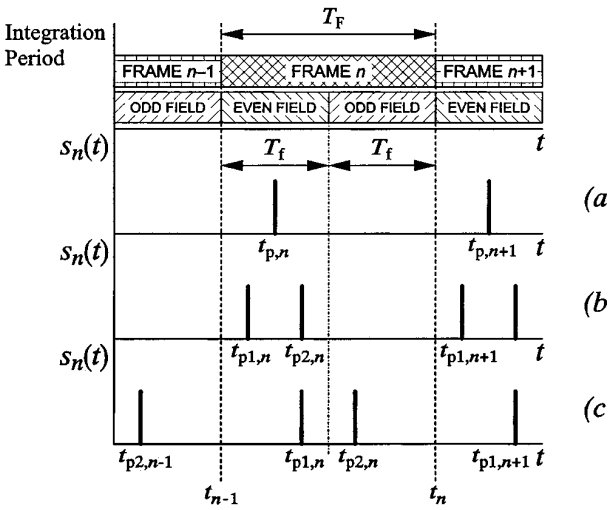

Figure 11. Shutter functions for pulsed TVH: (*a*) single exposure, (*b*) double exposure and (*c*) double single exposure.

respective pulse delays. The effective exposure time is, according to (4.9), $T_{e,n} = q$ and the fringe function becomes

$$M_n(\boldsymbol{x}) = \exp(-\mathrm{i}\phi_r)\frac{1}{q}\sum_{j=1}^{q}\exp[\mathrm{i}\phi_o(\boldsymbol{x};\, t_{pj,n})]. \qquad (4.48)$$

This is the same expression as that found for stroboscopic illumination (4.36), but in this case no assumptions about the dynamics of the measurand or its stability are needed. Several operating variants may be established according to the number of pulses fired during the integration period and their distribution with respect to the video fields for interlaced scanning cameras [155].

4.3.1. Single exposure. The laser is fired at the video frame rate, thus yielding a single pulse for each image (figure 11(*a*)). The state of the measurand at the exposure time $t_{p,n}$ is recorded. The expressions for the fringe function and the primary correlograms are the same as those for stroboscopic single exposure: (4.37) and (4.38).

4.3.2. Double exposure. Two pulses are fired at different instants $t_{p1,n}$ and $t_{p2,n}$ during the exposure interval (figure 11(*b*)); therefore, the pulse frequency must be twice the frame frequency. The expressions for the fringe function (4.39) and the primary correlograms are the same as those for stroboscopic double exposure.

4.3.3. Combined exposure

4.3.3.1. Double single exposure. Field-integration interline-transfer CCD cameras with interlaced scanning [153, 154] have non-overlapping integration periods for both image fields. Therefore, when they are illuminated with a single light pulse the image is present in just one half of the lines, even or odd ones. Some authors [156, 157] have used this operating particularity to get two single-exposure primary correlograms corresponding to different instants $t_{p1,n}$ and $t_{p2,n}$ within a single image, one in each field (figure 11(*c*)); this requires a pulsed laser operating at the video field frequency.

4.3.3.2. Double exposure plus double single exposure. Frame-integration interline-transfer CCD cameras with interlaced scanning [153, 154] have overlapping integration periods for both image fields. Cameras of this kind have been used to get, with only two light pulses, a double-exposure correlogram and the single-exposure ones corresponding to both pulses in three consecutive video fields [155].

5. Secondary-fringe generation

One of the most noticeable characteristics of primary correlograms is their random appearance, due to the distinctive spatial distribution of the irradiance and phase of the speckle patterns. The information related to the measurand (i.e. the object phase difference $\phi_o(\boldsymbol{x}; t)$) is contained in the fringe function $M_n(\boldsymbol{x})$ that modulates the speckle.

The fringe function can be expressed in terms of its modulus and argument

$$M_n(\boldsymbol{x}) = \mathrm{mod}[M_n(\boldsymbol{x})]\exp\{\mathrm{i}\arg[M_n(\boldsymbol{x})]\} \qquad (5.1)$$

and the primary correlograms (4.7) become

$$I_n(\boldsymbol{x}) = g\mathcal{I}_0(\boldsymbol{x})\{1 + \mathcal{V}(\boldsymbol{x})\,\mathrm{mod}[M_n(\boldsymbol{x})]\,\mathrm{Re}(\exp[\mathrm{i}\psi_p(\boldsymbol{x})] \times \exp\{\mathrm{i}\arg[M_n(\boldsymbol{x})]\})\} \qquad (5.2)$$

$$I_n(\boldsymbol{x}) = g\mathcal{I}_0(\boldsymbol{x})\{1 + \mathcal{V}(\boldsymbol{x})\,\mathrm{mod}[M_n(\boldsymbol{x})]\cos\{\psi_p(\boldsymbol{x}) + \arg[M_n(\boldsymbol{x})]\}\}. \qquad (5.3)$$

Speckle is present in two ways, with radically different behaviours: *intensity noise* and *phase noise*. Intensity noise is caused by the original irradiance distributions of the interfering speckle patterns and appears both in the average local intensity $\mathcal{I}_0(\boldsymbol{x})$ and in the visibility $\mathcal{V}(\boldsymbol{x})$ that are random variables with positive values and, consequently, non-zero spatial mean values. The phase noise $\psi_p(\boldsymbol{x})$, already defined in section 3, appears added to the argument of the fringe function; it is related to the random component of the phase in the interfering patterns and its spatial mean is zero, because its value is uniformly distributed between $-\pi$ and π.

The last fact implies that the mean value of $\cos\{\psi_p(\boldsymbol{x}) + \arg[M_n(\boldsymbol{x})]\}$ is also zero and, hence, the *mean brightness* (i.e. the local spatial mean of the intensity) of the primary correlograms is independent of the fringe function and, consequently, of the measurand. When one of these correlograms is observed, no intensity fringes can be seen but random fluctuations of the speckle pattern are noticed.

To get a *secondary fringe pattern* revealing the changes in ϕ_o it is necessary to remove, as far as possible, the speckle carrier and extract the fringe function. The procedure for generating such a secondary pattern can be understood as a spatial demodulation and allows several variants with different degrees of compromise among the resulting fringe quality, processing time, simplicity of implementation, etc.

Table 1. Primary correlograms obtained with various temporal treatment techniques.

Temporal treatment	Measurand	Exposure/ modulation	Type	$M_n(\boldsymbol{x})$	mod$[M_n(\boldsymbol{x})]$	arg$[M_n(\boldsymbol{x})]$
Time averaging	Static	Standard	PM	(4.13)	1	$\phi_o(\boldsymbol{x})-\phi_r$
	Harmonic	Standard	AM	(4.16)	$J_0[\phi_{om}(\boldsymbol{x})]$	$-\phi_r$
		Homodyne	AM	(4.23)	$J_0\{\{\phi_{om}^2(\boldsymbol{x})+\phi_{rm}^2-2\phi_{om}(\boldsymbol{x})\phi_{rm}\times\cos[\varphi_o(\boldsymbol{x})-\varphi_r]\}^{1/2}\}$	$-\phi_{rA}$
	General periodic	Standard	AM	(4.28)	$\prod_{k=1}^{\infty}J_0[\phi_{om,j}(\boldsymbol{x})]$	$-\phi_r$
		Homodyne with jth Harmonic	AM	(4.29)	$J_0\{\{\phi_{om,j}^2(\boldsymbol{x})+\phi_{rm}^2-2\phi_{om,j}(\boldsymbol{x})\phi_{rm}\times\cos[\varphi_{o,j}(\boldsymbol{x})-\varphi_r]\}^{1/2}\}\frac{\prod_{k=1}^{\infty}J_0[\phi_{om,k}(\boldsymbol{x})]}{J_0[\phi_{om,j}(\boldsymbol{x})]}$	$-\phi_{rA}$
	Constant speed	Standard	AM	(4.30)	$\frac{\sin\left(\frac{T_{e,n}}{2}\dot{\phi}_o(\boldsymbol{x})\right)}{\frac{T_{e,n}}{2}\dot{\phi}_o(\boldsymbol{x})}$	$\frac{\phi_o(\boldsymbol{x};t_{1,n})+\phi_o(\boldsymbol{x};t_{2,n})}{2}-\phi_r$
Stroboscopic (pulsed)	General periodic (general)	Single exposure	PM	(4.37)	1	$\phi_o(\boldsymbol{x};t_{p,n})-\phi_r$
		Double Exposure standard	AM	(4.40)	$\cos\left(\frac{\phi_o(\boldsymbol{x};t_{p1,n})-\phi_o(\boldsymbol{x};t_{p2,n})}{2}\right)$	$\frac{\phi_o(\boldsymbol{x};t_{p1,n})-\phi_o(\boldsymbol{x};t_{p2,n})}{2}-\phi_r$
		Homodyne modulation	AM	(4.41)	$\cos\left(\frac{\Delta\phi_{o,n}(\boldsymbol{x})}{2}-\phi_{rS,n}\right)$	$\bar{\phi}_{o,n}(\boldsymbol{x})-\phi_{rA,n}$

5.1. Types of primary correlograms

Two kinds of primary correlograms can be identified by attending to the modulus of the fringe function. We call these two kinds *phase-modulated (PM) correlograms* and *amplitude-modulated (AM) correlograms*.

Phase-modulated correlograms have a constant value for the modulus of their fringe function, typically mod$[M_n(\boldsymbol{x})]=1$. The information related to the measurand is encoded in its argument and appears as local changes of the intensity distribution, which are not normally noticeable, that are revealed only when at least two primary correlograms with a change in the object phase difference $\Delta\phi_o$ are compared. Correlograms of this kind are obtained with the temporal treatment techniques wherein the interferogram does not experience changes during the exposure period (i.e. time-average techniques with static measurands and single-exposure stroboscopic and pulsed techniques).

Amplitude-modulated correlograms have a fringe function whose modulus depends on the changes experienced by the object phase difference during the exposure period: mod$[M_n(\boldsymbol{x})]=f(\Delta\phi_o)$. The variation of mod$[M_n(\boldsymbol{x})]$ yields primary correlation fringes of additive nature, that are present in the primary correlogram as changes in the contrast of speckle that can be seen with the naked eye, albeit with a certain amount of difficulty. AM correlograms result from the application of time-average techniques to measurands that change during the exposure period as well as from double-exposure stroboscopic and pulsed techniques, wherein the interferograms corresponding to different states of the object are incoherently added.

Table 1 summarizes the expressions for the modulus and the argument of the fringe functions corresponding to the main temporal treatment techniques used in TVH, indicating the kind of primary correlograms provided by each of them.

For real-time displaying, primary correlograms have to be electronically processed, either analogically or digitally, to transform the local changes in intensity or contrast of speckle into local variations of the mean brightness with some kind of demodulation process to get secondary correlograms with well contrasted fringes. The secondary-fringe-generation process is very often used also as a first step for automatic evaluation of the object phase difference, although this can also be implemented directly on primary correlograms. Fringe generation may also incorporate techniques to reduce the phase and intensity speckle noise either as a part of the secondary-correlogram-generation process or as a further filtering of the correlograms.

5.2. Basic secondary-fringe-generation techniques

The elementary techniques for the generation of secondary correlograms can be classified into two families: those using a single primary correlogram and those using two of them. In any case, the process comprises two stages. First, the continuous component of the primary correlogram ($g\mathcal{I}_0(\boldsymbol{x})$ in expression (5.3)) is removed and the local changes of intensity are converted into variations of the contrast of speckle. Second, square-law demodulation is applied to transform the local changes in contrast into secondary fringes of mean brightness. For real-time displaying this last stage is often approximated by full-wave rectification (i.e. the calculation of the absolute value), which is easier to implement, whilst for automatic evaluation true square-law demodulation is preferred because of its lower harmonic distortion.

5.2.1. Spatial filtering of a single primary correlogram. This technique is applicable only to AM primary

correlograms, in which contrast fringes are already present. The continuous component is removed by high-pass (HP) spatial filtering. This is usually implemented on the video signal with dedicated analogue circuits.

High-pass filtering is, up to a point, equivalent to subtracting from the primary correlogram its average level $\langle I_n(\boldsymbol{x})\rangle = g\langle \mathcal{I}_0(\boldsymbol{x})\rangle$ and its result [37] can be schematized as follows:

$$\mathrm{HP}[I_n(\boldsymbol{x})] = g\{[\mathcal{I}_0(\boldsymbol{x}) - \langle \mathcal{I}_0(\boldsymbol{x})\rangle] + \mathcal{I}_0(\boldsymbol{x})\mathcal{V}(\boldsymbol{x}) \times \mathrm{mod}[M_n(\boldsymbol{x})]\cos\{\psi_p(\boldsymbol{x}) + \arg[M_n(\boldsymbol{x})]\}\}. \tag{5.4}$$

The secondary correlogram is obtained by square-law demodulation:

$$\tilde{I}_n(\boldsymbol{x}) = \{\mathrm{HP}[I_n(\boldsymbol{x})]\}^2 = g^2\{[\mathcal{I}_0(\boldsymbol{x}) - \langle \mathcal{I}_0(\boldsymbol{x})\rangle]^2 + [\mathcal{I}_0(\boldsymbol{x})\mathcal{V}(\boldsymbol{x})]^2 \,\mathrm{mod}[M_n(\boldsymbol{x})]^2\cos^2\{\psi_p(\boldsymbol{x}) + \arg[M_n(\boldsymbol{x})]\} + 2[\mathcal{I}_0(\boldsymbol{x}) - \langle \mathcal{I}_0(\boldsymbol{x})\rangle]\mathcal{I}_0(\boldsymbol{x})\mathcal{V}(\boldsymbol{x}) \times \mathrm{mod}[M_n(\boldsymbol{x})]\cos\{\psi_p(\boldsymbol{x}) + \arg[M_n(\boldsymbol{x})]\}\} \tag{5.5}$$

and its local mean brightness can be easily found [33]

$$\begin{aligned} B_n(\boldsymbol{x}) &= \langle \tilde{I}_n(\boldsymbol{x})\rangle \\ &= g^2\left(\sigma_0^2 + \frac{1}{2}\langle [\mathcal{I}_0(\boldsymbol{x})\mathcal{V}(\boldsymbol{x})]^2\rangle \,\mathrm{mod}[M_n(\boldsymbol{x})]^2\right) \\ &= g^2\{\sigma_1^2 + \sigma_2^2 + 2\langle I_1(\boldsymbol{x})\rangle\langle I_2(\boldsymbol{x})\rangle \,\mathrm{mod}[M_n(\boldsymbol{x})]^2\} \end{aligned} \tag{5.6}$$

where $\langle\cdot\rangle$ represents the spatial averaging extended to a region where $M_n(\boldsymbol{x})$ has a constant value. Such a region must be much larger than the average size of speckle if one is to get a significant average (i.e. the fringes must be much wider than the speckle). σ_0, σ_1 and σ_2 are the standard deviations of the local average intensity and of the intensities of the interfering beams, respectively. For the second identity it is assumed that I_1 and I_2 are statistically independent.

When secondary correlograms of this kind are displayed on a monitor or when they are low-pass filtered for automatic evaluation, a background level $g^2\,(\sigma_1^2+\sigma_2^2)$ related to the contrast of the original speckle patterns appears superimposed on the changes in mean brightness that are proportional to the modulus of the fringe function. The contrast of the secondary-fringe pattern hence decreases as the contrast of the interfering patterns increases.

This fringe-generation technique requires neither storage nor numerical processing of the correlograms (figure 12) and can be implemented in real time with very simple analogue electronic circuits connected between the video camera and the monitor. It was the first to be used in TVH by Butters and Leendertz [1, 2]. Although it was originally designed for time-average correlograms of vibrating objects [93, 158], it has also been applied to double-exposure stroboscopic [159] and pulsed [153] correlograms.

5.2.2. Subtraction of two primary correlograms. PM correlograms encode information related to the object phase difference ϕ_o corresponding to a single state of the measurand that appears mixed with the phase noise ψ_p. It is necessary to compare at least two such correlograms with a change $\Delta\phi_o$ of the object phase difference in order to get a secondary-fringe pattern. The easiest way to do this and, by far, the most commonly used is to subtract one primary correlogram from another and then apply the square-law demodulation. Subtraction has two effects: on the one hand it yields a random intensity pattern with local contrast related to the argument of the fringe function and, on the other, it removes the continuous component $g\mathcal{I}_0$.

The subtraction technique is also applicable to AM primary correlograms. In this case one has only to remove the continuous component because contrast fringes are already present. The two correlograms one of which is to be subtracted from the other must be different; this is conveniently achieved either by changing the argument of the fringe function by means of the reference phase difference ϕ_r or, much less usually, by comparing AM primary correlograms corresponding to different states of the measurand.

Subtractive secondary-fringe generation admits a general analytical formulation comprising both types of correlograms, AM and PM. Let us take two generic primary correlograms, $I_a(\boldsymbol{x})$ and $I_b(\boldsymbol{x})$, following expression (5.3). Secondary correlograms are obtained by subtraction and square-law demodulation:

$$\tilde{I}_b(\boldsymbol{x}) = [I_b(\boldsymbol{x}) - I_a(\boldsymbol{x})]^2 = g^2[\mathcal{I}_0(\boldsymbol{x})\mathcal{V}(\boldsymbol{x})]^2\{\mathrm{mod}[M_b(\boldsymbol{x})] \times \cos\{\psi_p(\boldsymbol{x}) + \arg[M_b(\boldsymbol{x})]\} - \mathrm{mod}[M_a(\boldsymbol{x})] \times \cos\{\psi_p(\boldsymbol{x}) + \arg[M_a(\boldsymbol{x})]\}\}^2. \tag{5.7}$$

Considering that typically $\mathrm{mod}[M_a(\boldsymbol{x})] = \mathrm{mod}[M_b(\boldsymbol{x})]$ and using simple trigonometric relations [140], we have that

$$\tilde{I}_b(\boldsymbol{x}) = g^2[\mathcal{I}_0(\boldsymbol{x})\mathcal{V}(\boldsymbol{x})]^2\,\mathrm{mod}[M_b(\boldsymbol{x})]^2\{1 - \cos\{\arg[M_b(\boldsymbol{x})] - \arg[M_a(\boldsymbol{x})]\}\} \times \{1 - \cos\{2\psi_p(\boldsymbol{x}) + \arg[M_b(\boldsymbol{x})] + \arg[M_a(\boldsymbol{x})]\}\} \tag{5.8}$$

where the term containing the speckle phase noise ψ_p has zero average and the local mean brightness is

$$B_b(\boldsymbol{x}) = \langle \tilde{I}_b(\boldsymbol{x})\rangle = g^2\langle [\mathcal{I}_0(\boldsymbol{x})\mathcal{V}(\boldsymbol{x})]^2\rangle \,\mathrm{mod}[M_b(\boldsymbol{x})]^2 \times \{1 - \cos\{\arg[M_b(\boldsymbol{x})] - \arg[M_a(\boldsymbol{x})]\}\}. \tag{5.9}$$

Unlike spatial filtering (5.6), this technique does not yield any background brightness and, hence, its secondary fringes are intrinsically more contrasted. There are several variants of the basic technique regarding the choice of the primary correlograms to be subtracted one from another, that will be treated in the following.

5.2.2.1. Sequential acquisition. This is the most usual operating mode. The two correlograms are acquired at different instants, storing the first until the second is available. In the first prototypes using this fringe generation technique the storage of the correlograms was implemented with analogue devices such as magnetic video tapes and discs [4, 5, 93] or scan-converter memories [160]; nowadays, they have been completely replaced by computer-based digital image-processing systems.

Subtraction of a reference correlogram. A reference primary correlogram $I_q(\boldsymbol{x}) = I_{ref}(\boldsymbol{x})$ is acquired with the measurand in a given state and stored. The reference correlogram is then subtracted (figure 13) from the next primary correlograms $I_b(\boldsymbol{x}) = I_n(\boldsymbol{x})$.

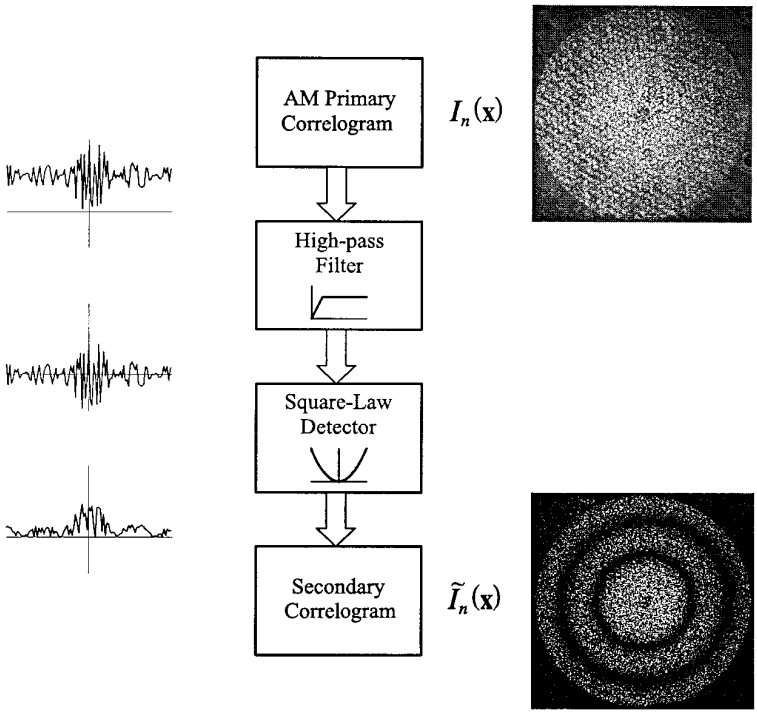

Figure 12. The scheme for secondary-fringe generation by spatial filtering of a single AM primary correlogram. Centre, block diagram; right-hand side, images of real correlograms; and left-hand side, a sketch of the profiles of the central lines of the correlograms.

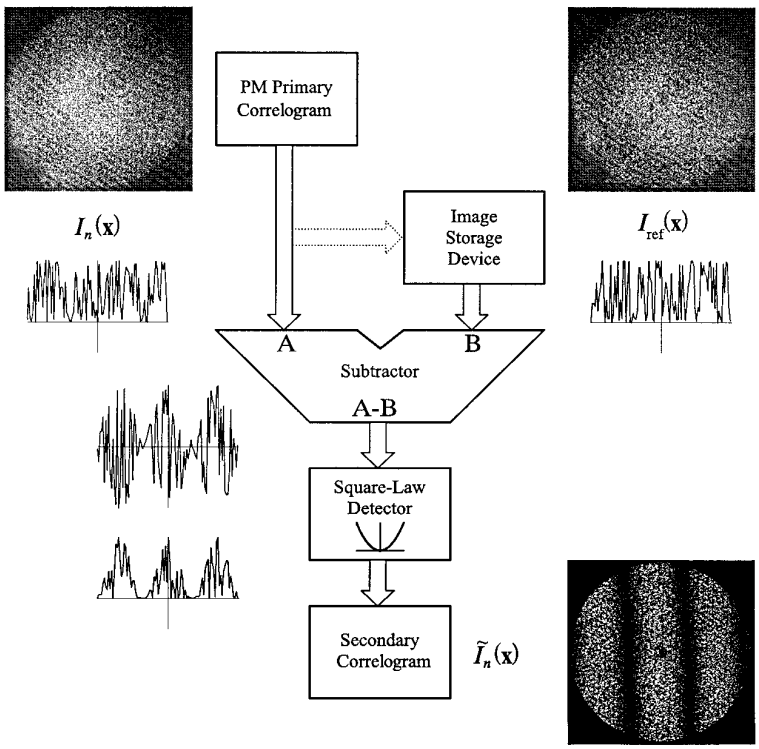

Figure 13. The scheme for secondary-fringe generation by subtraction of a reference applied to PM primary correlograms. Real correlograms and sketched line profiles are shown as in figure 12.

The resulting secondary correlograms reveal the deviation of the measurand from the reference state:

$$\tilde{I}_n(\boldsymbol{x}) = [I_n(\boldsymbol{x}) - I_{ref}(\boldsymbol{x})]^2 \tag{5.10}$$

This technique is typically used with PM correlograms [4, 5], for which $\mathrm{mod}[M_n(\boldsymbol{x})] = 1$ and expression (5.9) becomes

$$B_n(\boldsymbol{x}) = \langle \tilde{I}_n(\boldsymbol{x}) \rangle = g^2 \langle [\mathcal{I}_0(\boldsymbol{x}) \mathcal{V}(\boldsymbol{x})]^2 \rangle \times \{1 - \cos\{\arg[M_n(\boldsymbol{x})] - \arg[M_{ref}(\boldsymbol{x})]\}\}. \tag{5.11}$$

It has been also applied to AM correlograms, taking as reference a correlogram with the measurand at rest, either with time-averaging [79, 161] or with double-exposure stroboscopic illumination [141] and pulsed illumination [162, 163]; it is also practical to acquire the reference with the measurand in other states [151, 164, 165]. Other variants are getting a reference correlogram with the modulus of the fringe function forced to be zero, by sinusoidal [164] or triangular [166] modulation of the reference phase difference during time average, and subtracting the reference beam [155] instead of a correlogram when the state of the measurand is not repeatable.

Sequential subtraction. The last two primary correlograms recorded by the video camera ($I_b(\boldsymbol{x}) = I_n(\boldsymbol{x})$ and $I_a(\boldsymbol{x}) = I_{n-1}(\boldsymbol{x})$) are subtracted one from the other, usually in real time. The first $I_{n-1}(\boldsymbol{x})$ is stored and, once the subtraction has been performed, it is replaced by the next $I_n(\boldsymbol{x})$ until a new correlogram $I_{n+1}(\boldsymbol{x})$ is acquired and subtracted, and so on (figure 14). The resulting secondary correlograms can be expressed as

$$\tilde{I}_n(\boldsymbol{x}) = [I_n(\boldsymbol{x}) - I_{n-1}(\boldsymbol{x})]^2. \tag{5.12}$$

This technique is typically applied to AM correlograms, changing the reference phase difference on going from each video frame to the next to make $|\arg[M_n(\boldsymbol{x})] - \arg[M_{n-1}(\boldsymbol{x})]| = \pi$. Expressions (5.8) and (5.9) then become

$$\tilde{I}_n(\boldsymbol{x}) = 2g^2[\mathcal{I}_0(\boldsymbol{x})\mathcal{V}(\boldsymbol{x})]^2 \operatorname{mod}[M_n(\boldsymbol{x})]^2 \times\{1 + \cos\{2\{\psi_p(\boldsymbol{x}) + \arg[M_n(\boldsymbol{x})]\}\}\} \tag{5.13}$$

$$B_n(\boldsymbol{x}) = \langle\tilde{I}_n(\boldsymbol{x})\rangle = 2g^2\langle[\mathcal{I}_0(\boldsymbol{x})\mathcal{V}(\boldsymbol{x})]^2\rangle \operatorname{mod}[M_n(\boldsymbol{x})]^2. \tag{5.14}$$

Sequential subtraction was originally applied to time-average correlograms [129, 167, 168] and recently extended to double-exposure stroboscopic ones [140, 142, 169, 170].

Some authors have proposed that one could use other values for the increment of the argument of the fringe function among correlograms (e.g. $\pi/2$ [168, 171]), induce random changes in the reference phase difference with a moving diffuser [49], or even rely on air turbulence and mechanical instability [167]. It has been proven [172] that the optimum contrast of the secondary fringes is obtained with a phase increment of π, although any value between 30° and 330° is acceptable.

Sequential subtraction can be also applied to PM correlograms; secondary fringes appear when the object phase difference changes from one frame to the next. It has been used with the single-exposure stroboscopic technique [49], alternating the position of the pulses among frames, and also with single-exposure pulsed illumination [155]; in both approaches, the secondary correlograms map the change of ϕ_o between pulses.

Interval subtraction. This is an extension of sequential subtraction [173] whereby each primary correlogram is subtracted from one acquired d video frames before ($I_b(\boldsymbol{x}) = I_n(\boldsymbol{x})$ and $I_a(\boldsymbol{x}) = I_{n-d}(\boldsymbol{x})$); the secondary correlograms that result are given by

$$\tilde{I}_n(\boldsymbol{x}) = [I_n(\boldsymbol{x}) - I_{n-d}(\boldsymbol{x})]^2. \tag{5.15}$$

It is applied to PM correlograms that change very slowly, compared with the video frame rate. The secondary fringes contour points with the same change in the object phase difference between exposures (i.e. with the same average speed). The sensitivity is controlled by the delay dT_F between the correlograms being compared.

5.2.2.2. Simultaneous acquisition. Wizinowich and Colucci [174, 175] developed a technique for recording two interferograms in the even and odd video fields, respectively, during the same frame period. This technique has been adapted to TVH for double-single-exposure pulsed illumination [156] and also for the time-averaging [26]. It is also possible, by optical means, to obtain simultaneously two or more correlograms each with a different value of the reference phase difference that are recorded by independent cameras [176].

5.3. Secondary-fringe contrast

The contrast of the secondary-fringe patterns is defined as the ratio between the excursion of the local mean brightness and its average value

$$C = \frac{B_{max} - B_{min}}{B_{max} + B_{min}} = \frac{SNR}{2 + SNR}. \tag{5.16}$$

Here B_{max} and B_{min} are the extreme values of the local mean brightness in the correlogram and SNR is the signal-to-noise ratio, considering that the signal is the component of the local mean brightness related to the fringe function.

The mean brightness of the secondary correlograms can be expressed as

$$B = S + N_o + N_e \tag{5.17}$$

S being the signal, N_o the optical noise and N_e the electronic noise. The last term appears at the output of the video camera, combined with the primary correlograms $I_n(\boldsymbol{x})$, and its effect is characterized by its standard deviation σ_e, that is usually approximated [158] by

$$\sigma_e^2 = \sigma_{ed}^2 + k\langle I_n(\boldsymbol{x})\rangle \tag{5.18}$$

where σ_{ed} is the standard deviation of the darkness noise, that is independent of the illumination level, and k is a constant value determined by the construction and the operating characteristics of the sensor, the gain of the amplifiers, etc.

Table 2 summarizes the expressions for the SNR for the main secondary-correlogram-generation techniques that have been derived by Slettemoen [37, 158] for spatial filtering and Joenathan [172] for correlogram subtraction. It is assumed that the intensity distributions of the beams are statistically independent. The effect of the limited resolution of the video camera is taken into account [37] through the *contrast* of the beams (γ_1 and γ_2) and the *degree of resolution* (γ_{12}) of the *fringe carrier* (i.e. of the speckle pattern resulting from their interference). When the speckle pattern is fully resolved by the camera $\gamma_1 = \gamma_2 = \gamma_{12} = 1$; but, if the size of the speckle is similar to or smaller than the dimensions of the pixels, then $\gamma_1 \leqslant 1$, $\gamma_2 \leqslant 1$ and $\gamma_{12} \leqslant 1$.

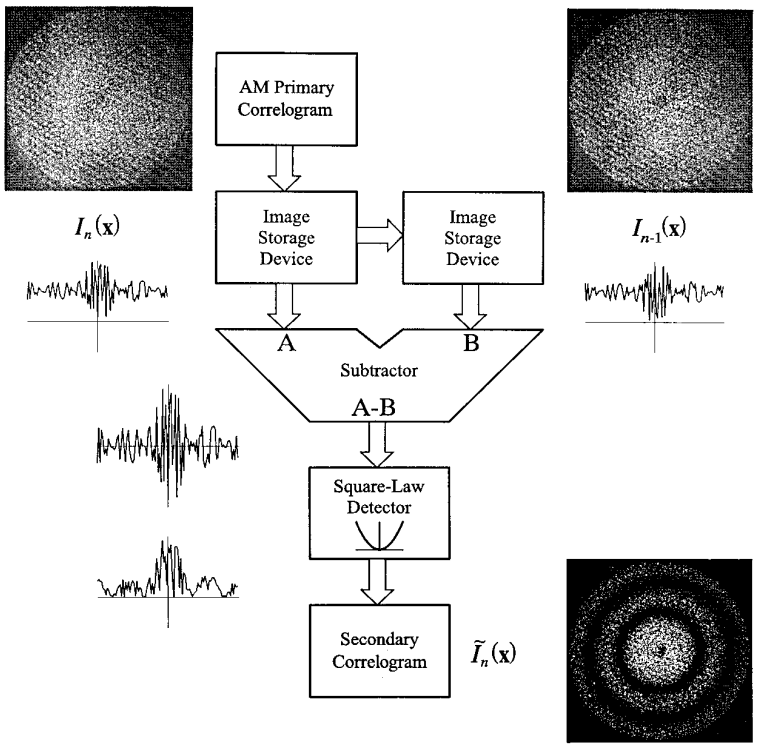

Figure 14. The scheme for secondary-fringe generation by sequential subtraction of AM primary correlograms. Real correlograms and sketched line profiles are shown as in figure 12.

Table 2. Expressions for the signal-to-noise ratio (SNR) for the main fringe-generation techniques.

Primary correlograms	Fringe generation	SNR
PM	Subtraction of reference	$\frac{4g^2\gamma_{12}^2\langle I_1(\boldsymbol{x})\rangle\langle I_2(\boldsymbol{x})\rangle}{\sigma_\varepsilon^2}$
AM	Spatial filtering	$\frac{2g^2\gamma_{12}^2\langle I_1(\boldsymbol{x})\rangle\langle I_2(\boldsymbol{x})\rangle \operatorname{mod}(M_n)_{max}^2}{g^2[\gamma_1^2\langle I_1(\boldsymbol{x})\rangle^2+\gamma_2^2\langle I_2(\boldsymbol{x})\rangle^2]+\sigma_\varepsilon^2}$
	Sequential subtraction	$\frac{4g^2\gamma_{12}^2\langle I_1(\boldsymbol{x})\rangle\langle I_2(\boldsymbol{x})\rangle \operatorname{mod}(M_n)_{max}^2}{\sigma_\varepsilon^2}$

5.3.1. Factors determining the contrast of the secondary fringes. The contrast of the secondary fringes is directly related to the SNR of the secondary correlograms. Every factor that influences the SNR has a similar effect on the fringe contrast. These factors can be classified into those that set the maximum attainable value of the contrast and those determining its actual value under given operating conditions. In any case, their effects can be quantified using the expressions of table 2.

Among the factors that set the maximum attainable contrast, there are many related to the design and the physical implementation of the interferometer, such as the maximum available light power, the sensitivity, electronic SNR, linearity [177], spatial resolution and automatic gain control of the video camera, the quantization noise of the image digitizer if one is present, the degree, relative state of polarization and type (speckled or uniform) of the beams and the shape and alignment of their pupils. Other factors are connected to the operating mode of the TVH system, such as the expression of the fringe function, given by the temporal treatment technique, the secondary-fringe-generation technique, that decides which of the expressions in table 2 gives the SNR, and the de-correlation of the speckle due to the operation mode, which is especially important in contouring [96, 178, 179].

Once the design of the interferometer, the operating mode, the fringe-formation technique and the illumination conditions have been established, the maximum value of the contrast that can be attained is completely determined. However, the actual value of the contrast of the secondary fringes is set by other factors. Some of them that depend on the adjustment of the interferometer can be optimized according to the working conditions; others, related to the object, to the value of the measurand or to environmental factors, cannot be controlled and often lead to a reduction of the contrast.

The optimizable parameters are the intensity balance between the interfering beams, generally represented by the *beam ratio* $\kappa = I_2/I_1$ [36, p 31; 180], and the relative aperture (F number) of the objective; whilst the non-optimizable ones are the reflectivity of the object, the de-polarization of light on certain surfaces, the presence of ambient light, the de-correlation of the speckle due to transversal displacements and tilts of the object induced by the measurand and the density of the secondary fringes [39].

5.3.2. Optimization of the secondary-fringe contrast. Although in practice it is usual to adjust the average intensity of the illumination beam $\langle I_1(\boldsymbol{x})\rangle$ (or $\langle I_2(\boldsymbol{x})\rangle$), the F

number of the objective and the beam ratio κ by 'trial and error', several authors [37, 39, 158, 177, 180] have derived analytically the values of these parameters that maximize the SNR for various types of interferometers under diverse operating conditions.

The first condition for the optimization of contrast is that the dynamic range of the camera must be completely used. For fully developed speckle patterns, the condition

$$\langle I_n(\boldsymbol{x})\rangle + 2\sigma_{I_n} = I_{sat} \tag{5.19}$$

ensures that 95% of the pixels in primary correlograms are under the saturation level, $\langle\cdot\rangle$ being the average extended to a set of macroscopically identical but microscopically different diffusing objects and σ_{I_n} the standard deviation of the intensity of the primary correlograms under the same conditions. Expression (5.19) can be written [33, 180]

$$\langle I_1(\boldsymbol{x})\rangle\{1+\kappa+2[\gamma_1^2+\kappa\gamma_2^2+2\kappa\gamma_{12}^2\,\mathrm{mod}(M_n)^2_{max}]^{1/2}\} = I_{sat} \tag{5.20}$$

that, for a camera with a given saturation intensity I_{sat}, establishes a relation between the values of $\langle I_1(\boldsymbol{x})\rangle$ and κ that is conditioned by the degree of resolution of the fringe carrier and the contrasts of the beams.

To optimize the contrast, in principle, the F number must be set to the minimum value F_{res} that makes $\gamma_{12} = 1$, i.e. provides a fringe carrier coarse enough to be fully resolved by the camera whilst maximizing the irradiance at the sensor. Under these conditions, expression (5.20) can be used to find the value of the beam ratio κ_{max} that maximizes the contrast and then to calculate the corresponding values of the average intensities of the beams $\langle I_1(\boldsymbol{x})\rangle_{max}$ and $\langle I_2(\boldsymbol{x})\rangle_{max}$.

At this stage, two situations may be found in practice: the optimization is performed '*with unlimited power*' if the power of the laser is high enough to reach the intensities $\langle I_1(\boldsymbol{x})\rangle_{max}$ and $\langle I_2(\boldsymbol{x})\rangle_{max}$ at the sensor of the camera with the lens closed to F_{res} and a given object; otherwise the optimization is performed '*with limited power*'.

When one is optimizing with unlimited power the beam ratio is set to κ_{max}, usually by adjusting the intensity of the reference beam (in geometries with double illumination [39] it is always $\kappa_{max} = 1$). Then the illumination intensity must be set according to the characteristics of each object to reach $\langle I_1(\boldsymbol{x})\rangle_{max}$ and $\langle I_2(\boldsymbol{x})\rangle_{max}$.

With limited power, the laser has to be used at full power and the lens must be open to a compromise value $F_{opt} < F_{res}$, whereby the better use of the dynamic range of the camera amply compensates for the loss of degree of carrier resolution. To find such an optimum value of the F number, equation (5.20) must be considered together with the dependences of $\langle I_1(\boldsymbol{x})\rangle_{max}$, $\langle I_2(\boldsymbol{x})\rangle_{max}$ and γ_{12} on the F number. Because this is influenced by the size and reflectivity of the object, the values F_{opt} and κ_{opt} that optimize the contrast are different for each object.

5.4. Speckle-noise-reduction techniques

In the secondary correlograms generated with basic techniques (section 5.2), the fringes appear corrupted by speckle. This is present both as intensity noise, in $\mathcal{I}_0(\boldsymbol{x})\mathcal{V}(\boldsymbol{x})$, and as phase noise, in the term $\cos\{\psi_p(\boldsymbol{x}) + \arg[M_n(\boldsymbol{x})]\}$.

The contrast of these secondary speckle patterns [181] is

$$C = (2+3\tau)^{1/2} \tag{5.21}$$

where τ is a parameter that depends on the type of beams used, the size and relative positions of their pupils and the spatial resolution of the camera. In TVH systems with uniform reference beams $\tau = 0$ and $C = \sqrt{2}$. When two speckle patterns interfere and the camera resolves the interferogram $\tau = 1$ and $C = \sqrt{5}$, but if the resolution is only partial they take intermediate values in the range $0 < \tau < 1$ and $\sqrt{2} < C < \sqrt{5}$.

In any case, the contrast of the speckle noise in the secondary correlograms is even higher than that in fully developed speckle patterns ($C = 1$) so that it is, at the very least, uncomfortable for direct observation of the secondary-fringe patterns and interferes with their automatic analysis. Several techniques to reduce it, either by modifying the process used to generate secondary correlograms or by numerical processing of these, have been developed. Such techniques can be classified as follows.

5.4.1. Speckle-phase-shift-based methods. This type of techniques is characterized by the use of more than two primary correlograms in such a way that a speckle-phase shift between them is introduced through controlled changes of the reference phase difference, ϕ_r or ϕ_{rA} (table 1). The resulting secondary correlograms are almost completely free of phase noise but intensity noise, in general, is still present.

The most popular of these techniques is 'electro-optical holography' (EOH), proposed by Stetson and Brohinsky [15], that implements algorithms related to temporal phase-shift-fringe-pattern-evaluation techniques to eliminate the terms affected by the phase noise. The initial version used four primary correlograms, but variants with three of them have been also proposed [182, 183]. EOH can be applied both to PM and to AM correlograms [184, 185]. For the first case it is necessary to perform a comparison with a reference state. This involves the use of twice the number of primary correlograms, but provides simultaneously two noise-reduced secondary correlograms that depend on the sine and cosine of the object phase difference respectively, thus allowing phase evaluation at no extra cost.

A similar scheme is followed in techniques such as max–min scanning [186], which is also applied to phase evaluation, and the averaging of several secondary correlograms with shifted speckle phase [187, 188] that, although they do not remove phase noise completely, provide very high immunity to environmental disturbance.

The use of a large number of primary correlograms generally leads to incrementation of the SNR, thus improving the contrast of the secondary fringes [172, 189], but intensity noise is still present. To reduce it to some extent, some authors have developed 'normalized' versions of EOH [15, 161, 182, 190] and max–min scanning [186] that involve the division of the secondary correlograms by one without fringes, which is typically obtained with the measurand at rest.

5.4.2. Speckle-de-correlation-based methods. In view of the random character of speckle noise, the average of a given number N of secondary correlograms corresponding to the same state of the measurand but with statistically independent speckle patterns leads to a reduction of the typical deviation of the final intensity distribution and, therefore, of the contrast of the speckle [32] according to the expression

$$C_N = \frac{1}{\sqrt{N}} C = \left(\frac{2 + 3\tau}{N} \right)^{1/2}. \tag{5.22}$$

It is necessary to average a large number of correlograms (typically 10–50) if one is to get a noticeable reduction of the speckle noise, although a similar effect can be achieved with fewer correlograms if the phase noise is removed *a priori* by phase-shift techniques [184, 185] as described in section 5.4.1. Correlogram averaging also helps to reduce electronic noise [191] and, therefore, increases marginally the contrast of the secondary fringes.

Speckle of secondary correlograms must be completely de-correlated if one is to obtain statistically independent patterns. Several methods have been proposed and demonstrated [192], such as tilting the illumination beam (either with a moving mirror [193] or with a rotating plane-parallel window [40, 185]), changing the observation direction by rotation of an eccentric diaphragm [50] and illuminating the object through a moving or rotating diffuser [192]. The averaging may be analogue (e.g. by displaying the secondary correlograms on a high-persistence monitor [50, 192]), although it is usual to apply it numerically in digital computers [194].

The implementation of techniques of this kind is especially simple with AM correlograms; speckle is de-correlated after the generation of each secondary correlogram and just the average has to be stored. For PM correlograms, conversely, it is necessary to acquire and store N speckle-de-correlated primary correlograms with the measurand in a reference state and then N more, correlated one to one to the first ones, with the measurand in a second state; this requires a de-correlating device with very high reproducibility and a huge amount of computer memory.

5.4.3. Spatial filtering of secondary correlograms. Spatial filtering of secondary correlograms, which is often performed numerically, reduces the phase and intensity speckle noise at once, though, in contrast to the techniques that combine a large number of images, the contrast of the correlation fringes is also reduced. As shown in the preceding sections, speckle behaves as a multiplicative noise. Its power spectrum, usually covering the full range of spatial frequencies that the camera can resolve, appears mixed with the correlation fringes' and it is extremely difficult to filter it out. The merit of a filter for speckle removal in TVH is given not only by its ability to reduce the contrast of noise but also by the extent to which the fringe pattern, the edges, the details of the object, etc. remain unaffected.

Linear low-pass convolution filters (mean, Gaussian, etc.) are the most widely used for this purpose because they are very easy to implement and render acceptable results, provided that the spatial frequency of the fringes is low. To avoid the loss of fringe contrast, repeated application of 'smooth' mean filters (i.e. ones with small kernels, typically 3×3 pixels) [127, 195] is often preferred over performing a single step with a larger window. Low-pass filters with recursive formulation [196] and with windows fitted to the shape of the fringes [197] have been proposed with the same aim.

Low-pass filtering can also be applied to the Fourier transform of the correlograms; the shape of the filter may be then tailored for each particular situation [198], although the automation of this process is very difficult. An alternative technique is the 'spectral-subtraction image-restoration' method [163, 199], consisting of the subtraction of the power spectrum of a primary correlogram without fringes from that of a secondary correlogram.

Other frequently used filters are the median [200], truncated median and mode [201] that, for Gaussian noise such as speckle, are even more efficient than are linear ones [202]. These filters can be also used with tailored windows [197] to improve the final contrast of the fringes.

Special filters originally designed for speckle reduction in synthetic-aperture radar have been applied to TVH [203, 204]. These filters are of diverse natures: adaptive [205], based on the local statistical properties of the correlograms such as sigma [206], variance [207] and geometrical [208] filters, based on information theory and statistical mechanics [209], etc. All of them exhibit better noise-rejection and detail-preservation characteristics than do classical filters.

6. Fringe analysis in TVH

Generally speaking, a *fringe pattern* is any distribution of light and dark areas, the fringes. The dependence of the intensity i on the spatial coordinates $\boldsymbol{x}$ in this type of distribution is formalized by the general expression

$$i(\boldsymbol{x}) = i_0(\boldsymbol{x})\{1 + v(\boldsymbol{x}) f[\phi(\boldsymbol{x})]\} \tag{6.1}$$

where $i_0(\boldsymbol{x})$ is the *local average intensity*, $v(\boldsymbol{x})$ the *visibility* or *contrast* of the pattern and f a periodic or quasi-periodic unidimensional function that defines the *profile* of the fringes and whose argument $\phi(\boldsymbol{x})$ is the *phase of the pattern*.

According to this definition, there are three types of fringe patterns in TVH: speckle interferograms and primary and secondary correlograms. Only the correlograms, however, are of practical interest in this context, insofar as they are electronic images susceptible to further processing.

TVH fringe patterns are characterized by the random distribution of $i_0(\boldsymbol{x})$ and $v(\boldsymbol{x})$ due to speckle noise. Their profile is typically sinusoidal for PM correlograms, whereas for AM correlograms it can be sinusoidal, follow a Bessel or sinc function, or even be a combination of them according to the particular expression for the modulus of the fringe function (table 1). The profiles of secondary correlograms may be slightly influenced by the fringe-generation technique, but their essential characteristics are established by those of the corresponding primary correlograms.

The phase of the pattern $\phi(\boldsymbol{x})$ is directly related to the object phase difference $\phi_o(\boldsymbol{x})$ or to its changes $\Delta\phi_o(\boldsymbol{x})$ and,

therefore, to the measurand. It may also depend on the reference phase difference $\phi_r(\boldsymbol{x})$, its variation $\Delta\phi_r(\boldsymbol{x})$ and also the random component of the phase of the speckle, i.e. the phase noise $\psi_p(\boldsymbol{x})$.

6.1. The process of fringe-pattern analysis

Automatic fringe pattern analysis, in its most general conception, comprises four stages [210]

(i) *Phase evaluation*, consisting of the calculation of the spatial distribution of the phase of the pattern from one or more conveniently chosen and sampled fringe patterns $(i_1, i_2, \ldots, i_N)$ all of them corresponding to the same state of the measurand. The resulting array of values $\phi(\boldsymbol{x})$ is the *phase map*.

(ii) *Phase unwrapping*. Most phase-evaluation techniques yield its main value (i.e. modulo 2π), hence, an ambiguity of $\pm 2n\pi$ is present in the resulting phase, n being an integer number called the *fringe order*. This uncertainty has to be resolved by determining the fringe order at each point to build an unwrapped phase map ${}^R\phi(\boldsymbol{x}) = \phi(\boldsymbol{x}) \pm 2n\pi$ free of 2π discontinuities.

Intense interest in the problem of phase unwrapping under the most diverse conditions has arisen during the last few years. The result has been that a great number of techniques, many of them specifically devised for the analysis of speckle-corrupted patterns, has been developed. Several authors such as, for example, Robinson [211], Judge and Bryanston-Cross [212] and Takeda [214] have published excellent compilations on the subject.

(iii) *Removal of additional terms*. Both during the fringe-generation process and during the evaluation stage, terms not related to the measurand (typically constant or linearly dependent on the spatial coordinates) may be added to the phase of the pattern. Their values, that may be known *a priori* or estimated by least-squares fitting [214] or any other process, are subtracted from the phase map at this stage.

(iv) *Re-scaling*. The preceding stages yield a map of the phase as a function of the coordinates of the fringe pattern space. It is often necessary to transform it into a map of the measurand in terms of the coordinates of the object space. The relations between these two sets of parameters are, in general, known for each measurement method used to generate fringe patterns. In our case, TVH, the correspondence between object and fringe-pattern coordinates is given by the object–image transform determined by the objective and the working distance; the relation between the phase of the pattern and the measurand results from the choice of methods used in the three first stages of our approach: the fringe-formation technique (section 5) establishes the relation between the phase of the pattern $\phi(\boldsymbol{x})$ and the fringe function $M_n(\boldsymbol{x})$, the temporal treatment (section 4) fixes the relation between $M_n(\boldsymbol{x})$ and the object optical phase difference $\phi_o(\boldsymbol{x})$ or its changes $\Delta\phi_o(\boldsymbol{x})$ and, finally, the geometry of the speckle interferometer (section 3) determines the relation between $\phi_o(\boldsymbol{x})$ and the measurand.

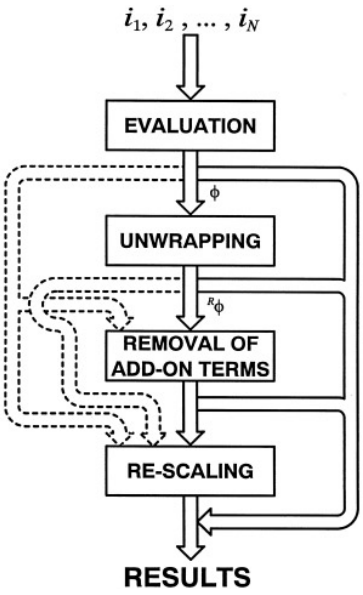

Figure 15. Stages of the process of fringe-pattern analysis.

Figure 15 illustrates this sequence of operations and their possible combinations. Only the first step, phase evaluation, is indispensable; the others are optional and sometimes unnecessary. The use of these steps has to be decided according to the characteristics of each particular case and the way that the final result must be presented.

TVH uses the same phase-evaluation techniques as any other interferometric technique, but the speckled nature of TVH fringes introduces some peculiarities that must be taken into account in their implementation; we will treat these particularities in that which follows. Once the phase map has been calculated, unwrapping, removal of additional terms and re-scaling can be performed with general techniques, not specifically designed for TVH but for noisy phase maps.

6.2. Correlogram to fringe-pattern identification.

Speckle noise appears in TVH correlograms as intensity and phase noise. Intensity noise is present in the random distributions of $\mathcal{I}_0(\boldsymbol{x})$ and $\mathcal{V}(\boldsymbol{x})$; consequently, the average intensity $i_0(\boldsymbol{x})$ and the visibility $v(\boldsymbol{x})$ of such patterns also have random distributions, with the potential of *low-modulation* ($i_0(\boldsymbol{x})v(\boldsymbol{x}) \to 0$) and *saturation* ($i(\boldsymbol{x}) > i_{sat}$) points at which the phase cannot be evaluated, appearing. Phase noise $\psi_p(\boldsymbol{x})$ may appear embedded in the phase of the pattern and also affecting the values of the average intensity and the visibility; this depends on the type of correlogram, the fringe-generation technique and even how the fringe pattern is identified, i.e. which term is considered to represent the fringes.

On the other hand, there are two kinds of fringe patterns: primary and secondary correlograms, and their respective phases can be evaluated. The main benefit of using secondary correlograms is the possibility of reducing speckle noise with techniques as those pointed out in section 5.4 before phase evaluation. This is generally impracticable with primary correlograms because removal of speckle would lead to the suppression of the fringes.

In any case, the measurand is encoded in the changes of the object phase difference $\Delta\phi_o(\boldsymbol{x})$ and this is the first measurement to be extracted from the fringe pattern. At this stage two situations become apparent [34, pp 306–7; 215].

6.2.1. The fringe pattern depends on $\phi_o(\boldsymbol{x})$, but not on $\Delta\phi_o(\boldsymbol{x})$. This is the case of primary PM correlograms, for which, moreover, $\phi_o(\boldsymbol{x})$ appears added to the phase noise $\psi_p(\boldsymbol{x})$. Considering that, in general, $\text{mod}[M_n(\boldsymbol{x})] = 1$, the identification of the terms in the expression for these correlograms (5.3) with a general fringe pattern (6.1) is established as follows:

$$I_n(\boldsymbol{x}) = \underbrace{g\mathcal{I}_0(\boldsymbol{x})}_{i_0(\boldsymbol{x})}\{1 + \underbrace{\mathcal{V}(\boldsymbol{x})}_{v(\boldsymbol{x})}\underbrace{\cos}_{f}\underbrace{\{\psi_p(\boldsymbol{x}) + \arg[M_n(\boldsymbol{x})]\}}_{\phi(\boldsymbol{x})}\} \tag{6.2}$$

where $\arg[M_n(\boldsymbol{x})]$ is proportional to $\phi_o(\boldsymbol{x})$ (table 1).

The most usual method used to obtain $\Delta\phi_o(\boldsymbol{x})$ is to evaluate two primary correlograms corresponding to different states of the measurand, one of them taken as a reference, and then subtract the resulting phase maps. If the speckle pattern does not experience de-correlation for these two states (i.e. $\psi_p(\boldsymbol{x})$ is constant) the difference

$$\Delta\phi(\boldsymbol{x}) = \phi_n(\boldsymbol{x}) - \phi_{ref}(\boldsymbol{x}) = \arg[M_n(\boldsymbol{x})] - \arg[M_{ref}(\boldsymbol{x})] \tag{6.3}$$

is proportional to $\Delta\phi_{o,n}(\boldsymbol{x}) = \phi_{o,n}(\boldsymbol{x}) - \phi_{o,ref}(\boldsymbol{x})$.

It is also feasible to use differential phase-evaluation methods [16, 166, 216, 217], specifically designed for this particular case of TVH, to calculate the increment of the phase $\Delta\phi(\boldsymbol{x})$ from two series of primary correlograms corresponding to two states of the measurand neither by explicitly evaluating their respective phases nor by generating secondary correlograms.

6.2.2. The fringe pattern directly depends on $\Delta\phi_o(\boldsymbol{x})$. This situation corresponds to AM primary correlograms and all the secondary correlograms. For AM primary correlograms (table 1), $\Delta\phi_o(\boldsymbol{x})$ is encoded in the modulus of the fringe function. Thus, identifying the terms of (5.3) with (6.1) results in

$$I_n(\boldsymbol{x}) = \underbrace{g\mathcal{I}_0(\boldsymbol{x})}_{i_0(\boldsymbol{x})}\{1 + \underbrace{\mathcal{V}(\boldsymbol{x})\cos\{\psi_p + \arg[M_n(\boldsymbol{x})]\}}_{v(\boldsymbol{x})} \times \underbrace{\text{mod}[M_n(\boldsymbol{x})]}_{f[\phi(\boldsymbol{x})]}\} \tag{6.4}$$

where $\phi(\boldsymbol{x})$ is normally proportional to $\Delta\phi_{o,n}(\boldsymbol{x})$ and f is a cosine, Bessel or $\sin(x)/x$ function.

As stated in section 5.2.2.1, the most usual method of generating secondary fringes from PM primary correlograms is the subtraction of a reference correlogram. The expression for secondary correlograms of this kind can be obtained by particularizing (5.8) according to (5.10) and the resulting terms can be identified with (6.1) as follows:

$$\tilde{I}_n(\boldsymbol{x}) = \underbrace{g^2[\mathcal{I}_0(\boldsymbol{x})\mathcal{V}(\boldsymbol{x})]^2\{1 - \cos\{2\psi_p(\boldsymbol{x}) + \arg[M_n(\boldsymbol{x})] + \arg[M_{ref}(\boldsymbol{x})]\}\}}_{i_0(\boldsymbol{x})} \times\{1 + \underbrace{(-1)}_{v(\boldsymbol{x})}\underbrace{\cos}_{f}\underbrace{\{\arg[M_n(\boldsymbol{x})] - \arg[M_{ref}(\boldsymbol{x})]\}}_{\phi(\boldsymbol{x})}\} \tag{6.5}$$

therefore, the profile of these patterns is sinusoidal and its phase is proportional to $\Delta\phi_{o,n}(\boldsymbol{x})$.

Sequential subtraction (section 5.2.2.1) is normally used to generate secondary correlograms from AM primary ones. The resulting expression (5.13) is identified with (6.1) in the following terms:

$$\tilde{I}_n(\boldsymbol{x}) = \underbrace{2g^2[\mathcal{I}_0(\boldsymbol{x})\mathcal{V}(\boldsymbol{x})]^2\{1+\cos\{2\{\psi_p(\boldsymbol{x})+\arg[M_n(\boldsymbol{x})]\}\}\}}_{i_0(\boldsymbol{x})} \times \underbrace{\text{mod}[M_n(\boldsymbol{x})]^2}_{1+v(\boldsymbol{x})f[\phi(\boldsymbol{x})]} \tag{6.6}$$

and, therefore, the profile of the pattern and the dependence of its phase $\phi(\boldsymbol{x})$ on $\Delta\phi_{o,n}(\boldsymbol{x})$ are given by the expression for $\text{mod}\,[M_n(\boldsymbol{x})]$, that is characteristic of the temporal treatment technique used to generate the primary correlogram (see section 4 and table 1).

When one is using secondary correlograms, it is possible to apply speckle-noise-reduction techniques before the phase-evaluation process. Speckle-phase-shift-based methods (section 5.4.1) remove only the phase noise and, therefore, the mean intensity of the fringe patterns represented by (6.5) and (6.6) is reduced to

$$i_0(\boldsymbol{x}) = 2g^2[\mathcal{I}_0(\boldsymbol{x})\mathcal{V}(\boldsymbol{x})]^2 \tag{6.7}$$

in which intensity noise is still present in $\mathcal{I}_0(\boldsymbol{x})$ and $\mathcal{V}(\boldsymbol{x})$, whereas with speckle de-correlation (section 5.4.2) and spatial filtering (section 5.4.3) methods one has that

$$i_0(\boldsymbol{x}) \approx 2g^2\langle[\mathcal{I}_0(\boldsymbol{x})\mathcal{V}(\boldsymbol{x})]^2\rangle. \tag{6.8}$$

6.3. Phase evaluation

Phase evaluation of TVH fringe patterns is essentially performed with the same well-known methods as those that are used for other whole-field interferometric techniques. The most relevant particularity is that the presence of speckle noise leads to the appearance of a significant amount of defective points at which it is not possible to calculate the phase with acceptable precision. The percentage of these points in the whole of the phase map depends on the statistical properties of the intensity distribution of the fringe pattern and also on the phase-evaluation technique that is used. Some authors [218, 219] have derived analytical expressions for calculating the expected proportion of valid points, that may be used to optimize the adjustment of the interferometer.

Defective points are usually identified and marked during the phase-evaluation process in order either to bypass them in further stages or to estimate their phase by interpolation [220] or low-pass-filtering techniques. The latter are the most commonly used; their variants are characterized by the type of filtering (convolution [221], median [222], spectral [223], etc.) and by the stage of the analysis process in which they are applied, namely to the unwrapped phase map [222], to the wrapped map [224] or even in the last step of some phase-evaluation methods [43].

6.3.1. Phase-evaluation methods. There are many phase-evaluation methods, most of which were originally designed to be used with smooth sinusoidal fringe patterns such as those generated by classical double-beam interferometry. Nevertheless, they can be applied to other fringe profiles, usually by approximation, and also to speckled patterns such as those obtained in TVH. Many authors have reviewed and classified the phase-evaluation methods according to diverse criteria: local versus global [225], intensity based versus phase based [226, 227], temporal versus spatial [227, 228], electronic versus analytic [229, 230], phase-shifting versus Fourier-transform methods [34, 210], methods with versus without a spatial carrier [231], etc.

In general [231], most of the evaluation methods use some kind of phase modulation whereby an auxiliary phase shift $\alpha_k(\boldsymbol{x})$ is added to the phase of interest to generate the set of fringe patterns $(i_1, i_2, \ldots, i_N)$ necessary for application of the corresponding phase-calculation algorithm. It is usually assumed that the profile of the patterns is sinusoidal and, thence, that they can be written as

$$i_k(\boldsymbol{x}) = i_0(\boldsymbol{x})\{1 + v(\boldsymbol{x})\cos[\phi(\boldsymbol{x}) + \alpha_k(\boldsymbol{x})]\}$$
$$k = 1, 2, \ldots, N. \tag{6.9}$$

It is not within the scope of this review to classify and describe the formulations of the phase-evaluation algorithms. The aforementioned literature constitutes an excellent reference, in particular the review on the subject that our colleagues Dorrío and Fernández [231] recently published in this journal is very well matched to the approach taken here. We shall, however, explain how the auxiliary phase shift is introduced into TVH fringe patterns.

Phase modulation can be applied either in the *temporal* or in the *spatial* domain. In temporal methods the phase shift is usually the same at every point of the pattern but different for each pattern of the evaluation sequence $\alpha_k(\boldsymbol{x}) = \alpha_k$; this is the case of the temporal phase-shift methods (TPSMs) [230, 232] and the temporal Fourier-transform method (TFTM) [233]. On the other hand, in spatial methods the phase shift is different for each point of the pattern $\alpha_k(\boldsymbol{x}) = \alpha(\boldsymbol{x})$ (usually with a linear dependence on the coordinates $\alpha(\boldsymbol{x}) = 2\pi \boldsymbol{f}_c \cdot \boldsymbol{x}$, where $\boldsymbol{f}_c = (f_{cx}, f_{cy})$ can be interpreted as the frequency of a spatial carrier) whilst a single pattern, rather than a set of them, is often enough to perform the evaluation process; the spatial-carrier phase-shift methods (SCPSMs) [234], the spatial synchronous-detection method (SSDM) [235] and the spatial Fourier-transform method (SFTM) [236] are of this type.

In TVH, just like in many other interferometric techniques, the phase shift is introduced by modulation of the reference phase difference $\phi_r(\boldsymbol{x}, t)$ although sometimes it is also possible to add an extra term to the object phase difference $\phi_o(\boldsymbol{x}, t)$. According to the model established for the generation of primary correlograms in section 4, the effects of phase difference modulation appear in the expression for the fringe function, in which the integration of the irradiance both in time (during the exposure interval) and in space (over each pixel) is taken into account. The appropriate identification of the terms $i_0(\boldsymbol{x})$, $v(\boldsymbol{x})$ and $\phi(\boldsymbol{x})$ (section 6.2) allows one to establish the relation between the shape and magnitude of the modulation of the reference phase difference $\phi_r(\boldsymbol{x}, t)$ and the resulting phase shift $\alpha_k(\boldsymbol{x})$. From this point, the corresponding phase-evaluation algorithms can be applied independently of the type of correlograms and fringe-generation methods that had been used.

6.3.2. Temporal phase-shift generation. Temporal modulation of the reference phase difference is implemented in TVH with the same methods as those that are used in other interferometric techniques [34, 229, 231, 232, 237] such as, for example, mirrors and optical fibres attached to piezoelectric devices, translating or rotating wedges and prisms, diffraction gratings, polarizing elements, liquid-crystal devices and current and temperature modulation of laser diodes. Optical phase difference modulation affects both the modulus and the argument of the fringe function, but in different ways according to the temporal treatment technique used to generate the primary correlograms, as shown in table 1. Generally speaking, the part of the reference phase difference that remains constant during the exposure interval T_e modifies the argument of the fringe function $\arg[M_n(\boldsymbol{x})]$, whilst its change during that period appears in $\mathrm{mod}[M_n(\boldsymbol{x})]$.

6.3.2.1. PM correlograms. According to the usual identification of terms (section 6.2), in primary PM correlograms (6.2) as well as in the secondary correlograms obtained from them (6.5), the phase of the pattern is the argument of the fringe function (plus the phase noise $\psi_p(\boldsymbol{x})$ in primary correlogams) that, for the most usual techniques (table 1), is given by

$$\arg[M_n(\boldsymbol{x})] = \phi_o(\boldsymbol{x}) - \phi_r. \tag{6.10}$$

A phase shift is then achieved by modulating the reference phase difference between exposure intervals, i.e. adding to $\arg[M_n(\boldsymbol{x})]$ a value $\Delta\phi_{r,n}$ that is kept constant throughout the exposure interval $T_{e,n}$ of each primary correlogram:

$$\arg[M_n(\boldsymbol{x})] = \phi_o(\boldsymbol{x}) - (\phi_r - \Delta\phi_{r,n}). \tag{6.11}$$

As was pointed out in section 6.2.1, when phase evaluation is performed on primary PM correlograms by standard TPSMs [221, 222], it is necessary to subtract one from the other the phase maps corresponding to two states of the measurand. This implies the acquisition of two sets, one for each state, of N phase-shifted correlograms. However, only N patterns, $N/2$ for each state of the measurand, are needed with differential TPSMs [166, 216] or a sequence of correlograms with slightly different states for the TFTM [238–241].

When secondary correlograms are used (section 6.2.2), on the other hand, it is enough to acquire just one set of N phase-shifted patterns. Three strategies for generating such a set become apparent.

(i) $1 + N$. The same reference primary correlogram is used to generate all the secondary correlograms. N more primary correlograms are then acquired with the measurand in the second state and their phases shifted

by $\Delta\phi_{r,k} = -\alpha_k$ [45]. Using expressions (6.3), (6.5) and (6.11), the resulting set of secondary correlograms is

$$\tilde{I}_k(\boldsymbol{x}) = \underbrace{g^2[\mathcal{I}_0(\boldsymbol{x})\mathcal{V}(\boldsymbol{x})]^2\{1-\cos[2\psi_p(\boldsymbol{x})+\Sigma\phi_{o,k}(\boldsymbol{x}) -2\phi_r+\alpha_k]\}}_{i_{0,k}(\boldsymbol{x})} \times\{1+\underbrace{(-1)}_{v(\boldsymbol{x})}\underbrace{\cos}_{f}[\underbrace{\Delta\phi_{o,k}(\boldsymbol{x})+\alpha_k}_{\phi(\boldsymbol{x})+\alpha_k}]\}. \tag{6.12}$$

(ii) $N+1$. N reference primary correlograms with their phases shifted by $\Delta\phi_{r,k} = \alpha_k$ are acquired. Just one additional primary correlogram with the measurand in the second state is thus needed [242, 243]. The set of secondary correlograms is obtained by subtracting this from each of the first N ones and can be expressed as

$$\tilde{I}_k(\boldsymbol{x}) = \underbrace{g^2[\mathcal{I}_0(\boldsymbol{x})\mathcal{V}(\boldsymbol{x})]^2\{1-\cos[2\psi_p(\boldsymbol{x})+\Sigma\phi_{o,k}(\boldsymbol{x}) +2\phi_r-\alpha_k]\}}_{i_{0,k}(\boldsymbol{x})} \times\{1+\underbrace{(-1)}_{v(\boldsymbol{x})}\underbrace{\cos}_{f}[\underbrace{\Delta\phi_{o,k}(\boldsymbol{x})+\alpha_k}_{\phi(\boldsymbol{x})+\alpha_k}]\}. \tag{6.13}$$

(iii) $N+N$. N primary correlograms are acquired with the measurand in the reference state with one half of the phase shift ($\Delta\phi_{r,k} = \alpha_k/2$) and another N with the remainder ($\Delta\phi_{r,k} = -\alpha_k/2$) are taken in the second state. The secondary-correlogram sequence is generated by subtracting one of these sets from the other:

$$\tilde{I}_k(\boldsymbol{x}) = \underbrace{g^2[\mathcal{I}_0(\boldsymbol{x})\mathcal{V}(\boldsymbol{x})]^2\{1-\cos[2\psi_p(\boldsymbol{x})+\Sigma\phi_{o,k}(\boldsymbol{x}) +2\phi_r]\}}_{i_{0,k}(\boldsymbol{x})} \times\{1+\underbrace{(-1)}_{v(\boldsymbol{x})}\underbrace{\cos}_{f}[\underbrace{\Delta\phi_{o,k}(\boldsymbol{x})+\alpha_k}_{\phi(\boldsymbol{x})+\alpha_k}]\}. \tag{6.14}$$

In these three expressions, $\Sigma\phi_{o,k}(\boldsymbol{x})$ and $\Delta\phi_{o,k}(\boldsymbol{x})$ represent the sum and difference, respectively, of the object phase differences of the two primary PM correlograms used to generate each secondary correlogram $\tilde{I}_k(\boldsymbol{x})$.

When TPSMs are used, $\Delta\phi_{o,k}(\boldsymbol{x})$ must have the same value for the whole set of N correlograms to ensure that the phase-evaluation process is accurate. This implies that only the perturbation of the measurand must be stable for the first of the strategies, whereas only the reference state must be stable for the second (therefore, this option can be applied to transient events) and both reference and perturbed states must be stable for the last.

Moreover, the local average intensity must also be the same for the set of N patterns. This is ensured with the third strategy, but not in the first two, for which $i_{0,k}(\boldsymbol{x})$ is sinusoidally dependent on the phase shift α_k. In this case, the speckle noise must be removed (see section 5.4) before proceeding to evaluate the phase or, alternatively, an algorithm allowing a variable average intensity [215] may be used.

6.3.2.2. AM correlograms. For AM primary (6.4) and the corresponding secondary correlograms (6.6) the value of the phase is related to the modulus of $M_n(\boldsymbol{x})$. Hence the phase shift must be introduced by a modulation of the reference phase difference, somehow synchronized to the changes in the measurand, during the exposure interval. In practice, phase evaluation has been implemented only for secondary AM correlograms of periodic measurands obtained with the time averaging technique or double-exposure stroboscopic illumination and homodyne phase modulation.

In the sinusoidal patterns produced with double-exposure stroboscopic illumination (4.41) the phase shift is controlled by the amplitude of the synchronous reference phase-difference modulation. The primary correlograms can be identified with a general fringe pattern as follows:

$$I_k(\boldsymbol{x}) = \underbrace{g\mathcal{I}_0(\boldsymbol{x})}_{i_0(\boldsymbol{x})}\Bigg[\underbrace{1+\mathcal{V}(\boldsymbol{x})\cos[\psi_p(\boldsymbol{x})+\bar{\phi}_{o,k}(\boldsymbol{x})-\phi_{rA,k}]}_{v(\boldsymbol{x})} \times\underbrace{\cos}_{f}\Bigg(\underbrace{\frac{\Delta\phi_{o,k}(\boldsymbol{x})}{2}}_{\phi(\boldsymbol{x})}\underbrace{-\phi_{rS,k}}_{\alpha_k}\Bigg)\Bigg]. \tag{6.15}$$

For the corresponding secondary correlograms [140, 141]

$$\tilde{I}_k(\boldsymbol{x}) = \underbrace{g^2[\mathcal{I}_0(\boldsymbol{x})\mathcal{V}(\boldsymbol{x})]^2\{1+\cos\{2[\psi_p(\boldsymbol{x})+\bar{\phi}_{o,k}(\boldsymbol{x})]\}\}}_{i_0(\boldsymbol{x})} \times[1+\underbrace{\cos}_{f}(\underbrace{\Delta\phi_{o,k}(\boldsymbol{x})}_{\phi(\boldsymbol{x})}\underbrace{-2\phi_{rS,k})}_{\alpha_k}]. \tag{6.16}$$

On the other hand, the application of time averaging with sinusoidal homodyne reference phase difference modulation to harmonic measurands (section 4.1.2.4) yields non-sinusoidal primary AM correlograms (4.23) and the secondary ones resulting from sequential subtraction (6.6) follow the expression

$$\tilde{I}_n(\boldsymbol{x}) = \underbrace{2g^2[\mathcal{I}_0(\boldsymbol{x})\mathcal{V}(\boldsymbol{x})]^2\{1+\cos\{2[\psi_p(\boldsymbol{x})-\phi_{rA}]\}\}}_{i_0(\boldsymbol{x})} \times\underbrace{J_0^2\{\{\phi_{om}^2(\boldsymbol{x})+\phi_{rm}^2-2\phi_{om}(\boldsymbol{x})\phi_{rm}\cos[\varphi_o(\boldsymbol{x})-\varphi_r]\}^{1/2}\}}_{1+v(\boldsymbol{x})f[\phi(\boldsymbol{x})]}. \tag{6.17}$$

To apply the usual phase-evaluation algorithms, designed for sinusoidal patterns, this expression must be transformed by approximation into one of the type $1+v(\boldsymbol{x})\cos[\phi(\boldsymbol{x})+\alpha_k]$. Two alternative solutions have been proposed.

Pryputniewicz and Stetson [244] take the approximation $J_0(x) \approx \cos(x)$ and apply reference-phase modulation *in phase* with the oscillation of the measurand $\varphi_o(\boldsymbol{x}) = \varphi_r$. Consequently, this technique can be used only when all the points of the object oscillate in phase. Under this condition, the approximate expression for the secondary correlograms is

$$\tilde{I}_k(\boldsymbol{x}) = \underbrace{g^2[\mathcal{I}_0(\boldsymbol{x})\mathcal{V}(\boldsymbol{x})]^2\{1+\cos\{2[\psi_p(\boldsymbol{x})+\phi_{rA}]\}\}}_{i_0(\boldsymbol{x})} \times\{1+\underbrace{\cos}_{f}[\underbrace{2\phi_{om}(\boldsymbol{x})}_{\phi(\boldsymbol{x})}\underbrace{-2\phi_{rm}}_{\alpha_k}\}] \tag{6.18}$$

and the phase shift is controlled by the amplitude ϕ_{rm} of the reference phase difference modulation. In principle, this approximation is valid only for very small values of $\phi_{om}(\boldsymbol{x})-\phi_{rm}$ and, consequently, of the range of amplitudes of oscillation in the object, but, nevertheless, for relatively wide amplitude ranges it is possible to apply correction tables once the erroneous phase has been evaluated and unwrapped.

For very small values of $\phi_{om}(\boldsymbol{x})$, it is possible to shift the working point to the centre of the most linear region of the Bessel function by choosing appropriately the amplitude of the sinusoidal reference phase difference modulation ϕ_{rm} [120, 127]. It is then possible to make the approximation

$$J_0^2\{\{\phi_{om}^2(\boldsymbol{x}) + \phi_{rm}^2 - 2\phi_{om}(\boldsymbol{x})\phi_{rm}\cos[\varphi_o(\boldsymbol{x}) - \varphi_r]\}^{1/2}\} \approx J_0^2(\phi_{rm}) - \frac{\mathrm{d}}{\mathrm{d}\phi_{rm}}[J_0^2(\phi_{rm})]\phi_{om}(\boldsymbol{x})\cos[\varphi_o(\boldsymbol{x}) - \varphi_r]. \tag{6.19}$$

Substitution of this into (6.17) results in

$$\tilde{I}_k(\boldsymbol{x}) \approx \underbrace{2g^2[\mathcal{I}_0(\boldsymbol{x})\mathcal{V}(\boldsymbol{x})]^2\{1+\cos\{2[\psi_p(\boldsymbol{x})-\phi_{rA}]\}\}J_0^2(\phi_{rm})}_{i_0(\boldsymbol{x})} \times\{\{1 \underbrace{-\breve{k}\phi_{om}(\boldsymbol{x})}_{v(\boldsymbol{x})} \underbrace{\cos}_{f} [\underbrace{\varphi_o(\boldsymbol{x})}_{\phi(x)} \underbrace{-\varphi_{r,k}}_{\alpha_k}]\} \tag{6.20}$$

where $\breve{k}$ is a constant that depends solely on ϕ_{rm} and is usually experimentally optimized and measured through a calibration process [127]. The phase shift is controlled by the mechanical phase φ_r of the sinusoidal modulation. The result of the phase-evaluation process is the local phase of oscillation $\varphi_o(\boldsymbol{x})$ of the measurand. To obtain the amplitude of oscillation $\phi_{om}(\boldsymbol{x})$, the visibility of the pattern $v(\boldsymbol{x}) = \breve{k}\phi_{om}(\boldsymbol{x})$ has to be calculated and divided by the scale factor $\breve{k}$.

6.3.3. Spatial carrier generation. Two types of techniques have been proposed in TVH to generate the spatial carrier that methods as SCPSM, SSDM and SFTM require. The most usual is to tilt the reference beam off the optical axis, although a technique based on a degenerated version of contouring has recently been introduced.

6.3.3.1. An off-axis reference beam. This technique is applied in out-of-plane-sensitive interferometers with a, generally uniform, reference beam. When the reference beam is tilted with respect to the object beam, the reference phase difference $\phi_r(\boldsymbol{x})$ becomes different at each point of the interferogram; if the tilt angle is the same for every point, the dependence of $\phi_r(\boldsymbol{x})$ on the coordinates is linear and thence

$$\phi_{r,k}(\boldsymbol{x}) = \phi_r + 2\pi\boldsymbol{f}_c\cdot\boldsymbol{x} = \phi_r + \Delta\phi_{r,k}(\boldsymbol{x}) \tag{6.21}$$

where ϕ_r is a constant.

For the evaluation of primary PM correlograms (that has been implemented with SCPSMs [21, 245] and the SFTM [43, 246]) the tilt of the reference beam is permanent; therefore

$$I_n(\boldsymbol{x}) = \underbrace{g\mathcal{I}_0(\boldsymbol{x})}_{i_0(\boldsymbol{x})}\{1 + \underbrace{\mathcal{V}(\boldsymbol{x})}_{v(\boldsymbol{x})} \underbrace{\cos}_{f} [\underbrace{\psi_p(\boldsymbol{x}) + \phi_o(\boldsymbol{x}) + \phi_r}_{\phi(\boldsymbol{x})} + \underbrace{2\pi\boldsymbol{f}_c\cdot\boldsymbol{x}}_{\alpha(\boldsymbol{x})}]\}. \tag{6.22}$$

When secondary PM correlograms are used [247], the reference beam is tilted on going from the reference to the succeeding primary correlograms. Once again, two strategies are apparent.

(i) *unidirectional tilt.* The reference primary correlogram is acquired with an in-line reference beam ($\Delta\phi_{r,ref} = 0$) and then it is tilted to produce $\Delta\phi_{r,k} = -2\pi\boldsymbol{f}_c\cdot\boldsymbol{x} = -\alpha(\boldsymbol{x})$. By substitution into (6.3) and (6.5), the resulting secondary correlograms are

$$\tilde{I}_k(\boldsymbol{x}) = \underbrace{g^2[\mathcal{I}_0(\boldsymbol{x})\mathcal{V}(\boldsymbol{x})]^2\{1 - \cos[2\psi_p(\boldsymbol{x}) + \Sigma\phi_{o,k}(\boldsymbol{x}) - 2\phi_r + 2\pi\boldsymbol{f}_c\cdot\boldsymbol{x}]\}}_{i_{0,k}(\boldsymbol{x})} \times\{1 + \underbrace{(-1)}_{v(\boldsymbol{x})} \underbrace{\cos}_{f} [\underbrace{\Delta\phi_{o,k}(\boldsymbol{x})}_{\phi(\boldsymbol{x})} + \underbrace{2\pi\boldsymbol{f}_c\cdot\boldsymbol{x}}_{\alpha(\boldsymbol{x})}]\}. \tag{6.23}$$

(ii) *symmetrical tilt.* The reference primary correlogram is acquired with one half of the tilt and, therefore, with a spatial carrier $\Delta\phi_{r,ref} = \pi\boldsymbol{f}_c\cdot\boldsymbol{x} = \alpha(\boldsymbol{x})/2$; the reference beam is then symmetrically tilted in the opposite direction to get $\Delta\phi_{r,k} = -\pi\boldsymbol{f}_c\cdot\boldsymbol{x} = -\alpha(\boldsymbol{x})/2$. The resulting secondary correlograms

$$\tilde{I}_k(\boldsymbol{x}) = \underbrace{g^2[\mathcal{I}_0(\boldsymbol{x})\mathcal{V}(\boldsymbol{x})]^2\{1 - \cos[2\psi_p(\boldsymbol{x}) + \Sigma\phi_{o,k}(\boldsymbol{x}) + 2\phi_r]\}}_{i_{0,k}(\boldsymbol{x})} \times\{1 + \underbrace{(-1)}_{v(\boldsymbol{x})} \underbrace{\cos}_{f} [\underbrace{\Delta\phi_{o,k}(\boldsymbol{x})}_{\phi(\boldsymbol{x})} + \underbrace{2\pi\boldsymbol{f}_c\cdot\boldsymbol{x}}_{\alpha(\boldsymbol{x})}]\} \tag{6.24}$$

are free of carrier noise in their local mean intensity and can be directly evaluated.

Finally, when this technique is applied to AM correlograms the reference beam is tilted during the exposure of each primary correlogram. For example, with double-exposure pulsed illumination [248] the reference beam is tilted between the light pulses.

6.3.3.2. Degenerate contouring In this variant, the carrier is introduced through the changes of the object phase difference $\Delta\phi_o(\boldsymbol{x})$ tilting the illumination beam between exposures; this tilt being symmetrical with respect to the observation direction (section 3.3.3), it is equivalent to a degenerate shape-measurement technique in which the contouring planes are parallel to the observation direction and produce a set of equally spaced parallel fringes that is used as the spatial carrier. The change of the object phase difference among exposures can be expressed as

$$\Delta\phi_{o,k}(\boldsymbol{x}) = \Delta\phi_{oo,k}(\boldsymbol{x}) + \Delta\phi_{oc,k}(\boldsymbol{x}) = \Delta\phi_{oo,k}(\boldsymbol{x}) + 2\pi\boldsymbol{f}_c\cdot\boldsymbol{x} \tag{6.25}$$

where $\Delta\phi_{oo,k}(\boldsymbol{x})$ is the increment due to the changes of the measurand and $\Delta\phi_{oc,k}(\boldsymbol{x})$ is the increment induced by degenerate contouring. This technique has been demonstrated with secondary PM correlograms for contouring [249], shearing [250, 251], out-of-plane [152, 252] and in-plane [253] geometries.

6.3.4. Simultaneous phase shift. Whenever the number N of phase-shifted primary correlograms needed to evaluate the phase with TPSMs is small, they can be generated at once and recorded with individual video cameras (generally three to comply with the input requirements of standard colour video digitizers) to produce phase maps in almost real time. This requires a rigorous alignment of the cameras insofar

as, in general, the speckle size has to be comparable to the size of the pixels in order to maximize the contrast of the fringes. The phase shift among the correlograms is induced either by polarizing elements [176] or by diffraction gratings [228, 254].

7. Concluding remarks

Image-plane TVH is now a well-established branch of this field of optical metrology. Most of its variants have been investigated and, consequently, it can be considered with a global perspective that permits the systematization of its procedures and techniques. The development of the other branch, Fresnel/Fourier TVH, is just beginning and many of its potential methods have not yet been investigated. It would, therefore, be somewhat speculative for the time being to propose a common scheme for both of them.

Our approach to TVH can accommodate the techniques of Fresnel/Fourier TVH that have been reported to date, but this does not mean that all the techniques reported for the first branch have to be applicable to the second; some of then may work and others not.

All the Fresnel/Fourier TVH techniques that have been established use interferometers with a smooth reference beam that provides sensitivity to displacements out of plane (section 3.1.1), in general directions (section 3.1.3) [18, 21, 22], in multiple directions (section 3.1.4) [255] or to the shape (section 3.3.1) [25, 26]. The use of interferometers with two speckle beams such as, for example, double-illumination (section 3.1.2 and 3.3.3.2) and shearing ones (section 3.2) has not been reported.

Apparently, all the temporal treatment techniques that yield PM correlograms can be used in Fresnel/Fourier TVH. Time averaging with a static measurand (section 4.1.1) [22, 23], single-exposure (section 4.3.1) [20, 25] and double-single-exposure (section 4.3.3.1) [21, 24] pulsed illumination have been demonstrated and single-exposure stroboscopic illumination can be used under similar conditions. Nothing has been published about the techniques that yield true AM correlograms but, according to the results obtained by Schnars and Jüptner [23] with synthetic AM correlograms produced by the addition of two PM correlograms, they must be applicable to this branch of TVH too.

The main difference between image-plane and Fresnel/Fourier TVH is that in the latter the analysis of the fringe pattern is always necessary in order to calculate the complex amplitude (i.e. the local average intensity and the phase) of the hologram (the primary correlogram); then the corresponding complex amplitude at the object plane has to be *reconstructed* by simulating the back propagation of light by use of the diffraction integral in Fresnel's or Fourier's (Fraunhofer's) approximation [19, 24, 256, 257]. The phase of the resulting complex amplitude is the phase difference of the interfering beams corresponding to each point of the object and its magnitude can be used to render secondary-fringe patterns.

In most of the Fresnel/Fourier TVH systems that have been reported [18–27] an off-axis reference beam is used to introduce a spatial carrier and the reconstruction is performed directly from the primary correlograms by simulating the optical reconstruction of classical holograms, i.e. the diffraction of the reference beam through the hologram. This procedure is equivalent [258] to calculating the complex amplitude of the primary correlogram using the spatial Fourier-transform method [236] (that involves use of the Fourier transform, filtering and then use of the inverse Fourier transform) and then performing the reconstruction with the diffraction integral, a further Fourier transform with a weighting function [24]. It has been demonstrated that other evaluation methods such as, for example, temporal phase shifting can also be used to calculate that complex amplitude [259], although they cannot be merged with the reconstruction process as they can in the SFTM.

Secondary-fringe-generation techniques can be applied to the reconstructed intensity fields [21], but also to the primary correlograms before the reconstruction [23], in this case omitting the square-law demodulation that is implicitly performed when calculating the intensity of the reconstructed field.

The new Fresnel/Fourier techniques that, beyond the shadow of a doubt, are due to appear in the next years will ultimately determine whether our approach to TVH is fully applicable to both branches or has to be modified to embrace them.

References

[1] Butters J N 1971 Speckle pattern interferometry using video techniques *SPIE J.* **10** 5–9

[2] Butters J N and Leendertz J A 1971 Speckle pattern and holographic techniques in engineering metrology *Opt. Laser Technol.* **3** 26–30

[3] Butters J N and Leendertz J A 1971 Reasons and methods for electronic processing in coherent light systems for engineering measurement *Proc. Technical Program Electro-Optics '71 Int. Conf. (Brighton)* pp 189–93

[4] Butters J N and Leendertz J A 1971 Holographic and video techniques applied to engineering measurement *Trans. Inst. Meas. Control* **4** 349–54

[5] Macovski A, Ramsey S D and Schaefer L F 1971 Time-lapse interferometry and contouring using television systems *Appl. Opt.* **10** 2722–7

[6] Schwomma O 1972 Holographisch-interferometrisches oder moirémetrisches Verfahren *Austrian Patent* 298 830

[7] Köpf U 1972 Meßtechnik **4** 105

[8] Gåsvik K 1980 Vibration analysis of a circular saw blade by means of moiré technique and TV-holography *OSA Technical Digest of the Topical Meeting on Hologram Interferometry and Speckle Metrology (June 1980)* WA6-1

[9] Gåsvik K J 1987 *Optical Metrology* (Chichester: Wiley) pp 108–13

[10] Nakadate S, Yatagai T and Saito H 1980 Electronic speckle pattern interferometry using digital image processing techniques *Appl. Opt.* **19** 1879–83

[11] Nakadate S, Yatagai T and Saito H 1983 Computer-aided speckle pattern interferometry *Appl. Opt.* **22** 237–43

[12] Oreb B F, Sharon B and Hariharan P 1984 Electronic speckle pattern interferometry with a microcomputer *Appl. Opt.* **23** 3940–1

[13] Hirai A, Akatsu T and Horii Y 1985 Dynamic motion measurement using digital TV speckle interferometry *Proc. SPIE* **549** 86–93

[14] Creath K 1984 Digital speckle pattern interferometry (DSPI) using a 100 × 100 imaging array *Proc. SPIE* **501** 292–8

[15] Stetson K A and Brohinsky W R 1985 Electrooptic

holography and its application to hologram interferometry *Appl. Opt.* **24** 3631–7
[16] Stetson K A 1990 Theory and applications of electronic holography *Proc. SEM. Conf. on Hologram Interferometry and Speckle Metrology (Baltimore)* pp 294–300
[17] Malmo J T and Vikhagen E 1988 Vibration analysis of a car body by means of TV holography *Exp. Techn.* **12** 28–30
[18] Schnars U and Jüptner W 1993 Principles of direct holography for interferometry *Fringes '93. Proc. 2nd Int. Workshop on Automatic Processing of Fringe Patterns (Bremen)* (Berlin: Akademie) pp 115–20
[19] Schnars U and Jüptner W 1994 Direct recording of holograms by a CCD target and numerical reconstruction *Appl. Opt.* **33** 179–81
[20] Schnars U, Kreis T M and Jüptner W P O 1996 Digital recording and numerical reconstruction of holograms: reduction of the spatial frequency spectrum *Opt. Engng* **35** 977–82
[21] Pedrini G, Tiziani H J and Zou Y 1997 Digital double pulse-TV-holography *Opt. Lasers Engng* **26** 199–219
[22] Schnars U 1994 Direct phase determination in hologram interferometry with use of digitally recorded holograms *J. Opt. Soc. Am.* A **11** 2011–15
[23] Schnars U and Jüptner W P O 1994 Digital recording and reconstruction of holograms in hologram interferometry and shearography *Appl. Opt.* **33** 4373–7
[24] Pedrini G, Zou Y L and Tiziani H J 1995 Digital double-pulsed holographic interferometry for vibration analysis *J. Mod. Opt.* **42** 367–74
[25] Zou Y-L, Pedrini G and Tiziani H 1996 Two-wavelength contouring with a pulsed ruby laser by employing TV-holography *J. Mod. Opt.* **43** 639–46
[26] Zou Y, Pedrini G and Tiziani H 1996 Surface contouring in a video frame by changing the wavelength of a diode laser *Opt. Engng* **35** 1074–9
[27] Pomarico J, Schnaars U, Hartmann H-J and Jüptner W 1995 Digital recording and numerical reconstruction of holograms: a new method for displaying light in flight *Appl. Opt.* **34** 8095–9
[28] Butters J N, Jones R and Wykes C 1978 Electronic speckle pattern interferometry *Speckle metrology* ed R K Erf (London: Academic) pp 111–58
[29] Løkberg O J 1980 Electronic speckle pattern interferometry *Phys. Technol.* **11** 16–22
[30] Løkberg O J 1984 ESPI—the ultimate holographic tool for vibration analysis? *J. Acoust. Soc. Am.* **75** 1783–91
[31] Løkberg O J 1993 Recent developments in video speckle interferometry *Speckle Metrology* ed R S Sirohi (New York: Marcel Dekker) pp 157–94
[32] Løkberg O J and Slettemoen G Å 1987 Basic electronic speckle pattern interferometry *Applied Optics and Optical Engineering* vol 10 ed R Shannon and J C Wyant (San Diego: Academic) pp 455–504
[33] Jones R and Wykes C 1989 *Holographic and Speckle Interferometry* (Cambridge: Cambridge University Press)
[34] Davies J C and Buckberry C H 1993 Television holography and its applications *Optical Methods in Engineering Metrology* ed D C Williams (London: Chapman & Hall) pp 275–338
[35] Born M and Wolf E 1993 *Principles of Optics* (Oxford: Pergamon) pp 505–8
[36] Goodman J W 1984 Statistical properties of laser speckle patterns *Laser Speckle and Related Phenomena* 2nd edn, ed J C Dainty (Berlin: Springer) pp 9–75
[37] Slettemoen G Å 1979 General analysis of fringe contrast in electronic speckle pattern interferometry *Opt. Acta* **26** 313–27
[38] Butters J N 1976 Electronic speckle pattern interferometry: a general review background to subsequent papers *The Engineering Uses of Coherent Optics* ed E R Robertson (Cambridge: Cambridge University Press) pp 155–69
[39] Jones R and Wykes C 1981 General parameters for the design and optimization of electronic speckle pattern interferometers *Opt. Acta* **28** 949–72
[40] Virdee M S, Williams D C, Banyard J E and Nassar N S 1990 A simplified system for digital speckle interferometry *Opt. Laser Technol.* **22** 311–16
[41] Løkberg O J, Seeberg B E and Vestli K 1997 Microscopic video speckle interferometry *Opt. Lasers Engng* **26** 313–30
[42] Soares O D D, Lage A L V S and Sakowski H 1987 Improvements on electronic speckle pattern interferometry *Optical Metrology* ed O D D Soares (Dordrecht: Martinus Nijhoff) pp 587–605
[43] Saldner H O, Molin N-E and Stetson K A 1996 Fourier-transform evaluation of phase data in spatially phase-biased TV holograms *Appl. Opt.* **35** 332–6
[44] Biedermann K and Ek L 1975 A recording and display system for hologram interferometry with low resolution imaging devices *J. Phys. E: Sci. Instrum.* **8** 571–6
[45] Nakadate S and Saito H 1985 Fringe scanning speckle-pattern interferometry *Appl. Opt.* **24** 2172–80
[46] Peng S, Joenathan C and Khorana B M 1992 Quasi-equal-path electronic speckle pattern interferometric system *Opt. Lett.* **17** 1040–2
[47] Joenathan C and Khorana B M 1993 Quasi-equal-path electronic speckle pattern interferometric system *Appl. Opt.* **32** 5724–6
[48] Schultz B 1994 Electronic speckle-pattern-interferometrie through shearography *Proc. SPIE* **2358** 153–7
[49] Pouet B F and Krishnaswamy S 1993 Additive/subtractive decorrelated electronic speckle pattern interferometry *Opt. Engng* **32** 1360–9
[50] Slettemoen G Å 1980 Electronic speckle pattern interferometric system based on a speckle reference beam *Appl. Opt.* **19** 616–23
[51] Joenathan C and Khorana B M 1991 A simple and modified ESPI system *Optik* **88** 169–71
[52] Joenathan C and Torroba R 1991 Modified electronic speckle pattern interferometer employing an off-axis reference beam *Appl. Opt.* **30** 1169–71
[53] Petrov V and Lau B 1996 Electronic speckle pattern interferometry with a holographically generated reference wave *Opt. Engng* **35** 2363–70
[54] Løkberg O J 1985 Mapping of in-plane vibration modes by electronic speckle pattern interferometry *Opt. Engng* **24** 356–9
[55] Joenathan C, Sohmer A and Bürkle L 1995 Increased sensitivity to in-plane displacements in electronic speckle pattern interferometry *Appl. Opt.* **34** 2880–5
[56] Butters J N and Leendertz J A 1971 A double exposure technique for speckle pattern interferometry *J. Phys. E: Sci. Instrum.* **4** 277–9
[57] Duffy D E 1972 Moiré gauging of in-plane displacement using double aperture imaging *Appl. Opt.* **11** 1178–81
[58] Sirohi R S and Krishna Mohan N 1993 In-plane displacement measurement configuration with twofold sensitivity *Appl. Opt.* **32** 6387–90
[59] Sohmer A and Joenathan C 1996 Twofold increase in sensitivity with a dual-beam illumination arrangement for electronic speckle pattern interferometry *Opt. Engng* **35** 1943–8
[60] Joenathan C, Franze B and Tiziani H J 1994 Oblique incidence and observation electronic speckle-pattern interferometry *Appl. Opt.* **33** 7307–11
[61] Hung Y Y 1978 Displacement and strain measurement *Speckle Metrology* ed R K Erf (London: Academic) pp 51–71
[62] Pedrini G and Tiziani H J 1994 Double-pulse electronic

speckle pattern interferometry for vibration analysis *Appl. Opt.* **33** 7857–63
[63] Mendoza-Santoyo F, Shellabear M C and Tyrer J R 1991 Whole field in-plane vibration analysis using pulsed phase-stepped ESPI *Appl. Opt.* **30** 717–21
[64] Shellabear M C and Tyrer J R 1988 Three-dimensional vibration analysis using electronic speckle pattern interferometry (ESPI) *Proc. SPIE* **952** 251–9
[65] Moore A J and Tyrer J R 1990 An electronic speckle pattern interferometer for complete in-plane displacement measurement *Meas. Sci. Technol.* **1** 1024–30
[66] Shellabear M C and Tyrer J R 1991 Application of ESPI to three-dimensional vibration measurements *Opt. Lasers Engng* **15** 43–56
[67] Winther S 1988 3D strain measurements using ESPI *Opt. Lasers Engng* **8** 45–57
[68] Bhat G K 1995 Measurement of strains in turbine blades vibrating at resonance using electro-optic holography *J. Mod. Opt.* **42** 667–77
[69] Arizaga R, Rabal H and Trivi M 1994 Simultaneous multiple-viewpoint processing in digital speckle pattern interferometry *Appl. Opt.* **33** 4369–72
[70] Wang L-S, Janbunathan K, Dobbins B N and He S-P 1996 Measurement of three-dimensional surface shape and deformations using phase stepping speckle interferometry *Opt. Engng* **35** 2333–40
[71] Ganesan A R, Joenathan C and Sirohi R S 1987 Real-time comparative digital speckle pattern interferometry *Opt. Commun.* **64** 501–6
[72] Ganesan A R, Meinlschmidt P and Hinsch K D 1994 Vibration mode separation using comparative electronic speckle interferometry (ESPI) *Opt. Commun.* **107** 28–34
[73] Saldner H O, Krishna Mohan N and Molin N-E 1995 Comparative TV holography for vibration analysis *Opt. Engng* **34** 486–92
[74] Aebischer H A and Waldner S 1997 Strain distributions made visible with image-shearing speckle pattern interferometry *Opt. Lasers Engng* **26** 407–20
[75] Tyrer J R and Petzing J N 1997 In-plane electronic speckle pattern shearing interferometry *Opt. Lasers Engng* **26** 395–406
[76] Mantravadi M V 1992 Lateral shearing interferometers *Optical Shop Testing* ed D Malacara (New York: Wiley) pp 123–72
[77] Leendertz J A and Butters J N 1973 An image-shearing speckle-pattern interferometer for measuring bending moments *J. Phys. E: Sci. Instrum.* **6** 1107–10
[78] Hung Y Y, Tang S and Hovanesian J D 1994 Real-time shearography for measuring time-dependent displacement derivatives *Exp. Mech.* **34** 89–92
[79] Nakadate S, Yatagai T and Saito H 1980 Digital speckle-pattern shearing interferometry *Appl. Opt.* **19** 4241–6
[80] Rabal H, Henao R and Torroba R 1996 Digital speckle pattern shearing interferometry using diffraction gratings *Opt. Commun.* **126** 191–6
[81] Joenathan C and Bürkle L 1997 Electronic speckle pattern shearing interferometer using holographic gratings *Opt. Engng* **36** 2473–7
[82] Krishna Murthy R, Sirohi R S and Kothiyal M P 1982 Speckle shearing interferometry: a new method *Appl. Opt.* **21** 2865–7
[83] Joenathan C and Torroba R 1990 Simple electronic speckle-shearing-pattern interferometer *Opt. Lett.* **15** 1159–61
[84] Krishna Mohan N, Masalkar P J and Sirohi R S 1992 Electronic speckle pattern interferometry with holo-optical element *Proc. SPIE* **1821** 234–42
[85] Valera J D and Jones J D C 1994 Phase stepping in fiber-based speckle shearing interferometry *Opt. Lett.* **19** 1161–3
[86] Valera J D R, Jones J D C, Towers D P and Buckberry C H 1997 Strain and vibration analysis by fibre based speckle shearing interferometry *Opt. Lasers Engng* **26** 361–76
[87] Krishna Murthy R, Mohanty R K, Sirohi R S and Kothiyal M P 1984 Radial speckle shearing interferometer and its engineering applications *Optik* **67** 85–94
[88] Mohanty R K, Joenathan C and Sirohi R S 1986 High sensitivity tilt measurement by speckle shear interferometry *Appl. Opt.* **25** 1661–4
[89] Ganesan A R, Sharma D K and Kothiyal M P 1988 Universal digital speckle shearing interferometer *Appl. Opt.* **27** 4731–4
[90] Krishna Mohan N, Saldner H and Molin N -E 1993 Electronic speckle pattern interferometry for simultaneous measurement of out-of-plane displacement and slope *Opt. Lett.* **18** 1861–3
[91] del Carreto P and Perlo P 1994 Compact multi-beam shearography for deformation and vibration observation *Proc. SPIE* **2358** 140–4
[92] Denby D, Quintanilla G E and Butters J N 1976 Contouring by electronic speckle pattern interferometry *The Engineering Uses of Coherent Optics* ed E R Robertson (Cambridge: Cambridge University Press) pp 171–97
[93] Butters J N and Leendertz J A 1974 Component inspection using speckle pattern *Proc. Technical Program Electro-Optics '73 Int. Conf.* (Brighton: Kiver Communications) pp 43–50
[94] Jones R and Butters J N 1975 Some observations on the direct comparison of the geometry of two objects using speckle pattern interferometric contouring *J. Phys. E: Sci. Instrum.* **8** 231–4
[95] Jones R and Wykes C 1978 The comparison of complex object geometries using a combination of electronic speckle pattern inteferometric difference contouring and holographic illumination elements *Opt. Acta* **25** 449–72
[96] Wykes C 1977 De-correlation effects in speckle-pattern interferometry. 1. Wavelength change dependent de-correlation with application to contouring and surface roughness measurement *Opt. Acta* **24** 517–32
[97] Tatam R P, Davies J C, Buckberry C H and Jones J D C 1990 Holographic surface contouring using wavelength modulation of laser diodes *Opt. Laser Technol.* **22** 317–21
[98] Peng X, Zou Y L, Diao H Y and Tiziani H J 1992 A simplified multi-wavelength ESPI contouring technique based on a diode laser system *Optik* **91** 81–5
[99] Rastogi P K 1993 Techniques of displacement and deformation measurements in speckle metrology *Speckle Metrology* ed R S Sirohi (New York: Marcel Dekker) pp 41–98
[100] Winther S and Slettemoen G Å 1984 An ESPI contouring technique in strain analysis *Proc. SPIE* **473** 44–7
[101] Rodríguez-Vera R, Kerr D and Mendoza-Santoyo F 1992 Electronic speckle contouring *J. Opt. Soc. Am.* A **9** 2000–8
[102] Rodríguez-Vera R 1997 Optical gauging of diffuse surfaces by electronic speckle contouring *Opt. Lasers Engng* **26** 101–14
[103] Diao H, Zou Y, Peng X, Tiziani H J and Chen L 1992 Calibration of the inclined contour planes formed on ESPI and optimization of ESPI optical system for contouring *Optik* **91** 71–5
[104] Peng X, Diao H Y, Zou Y L and Tiziani H J 1992 Contouring by modified dual-beam ESPI based on tilting illumination beams *Optik* **90** 61–4
[105] Ganesan A R and Sirohi R S 1988 New method of contouring using digital speckle pattern interferometry (DSPI) *Proc. SPIE* **954** 327–32
[106] Joenathan C, Pfister B and Tiziani H J 1990 Contouring by electronic speckle pattern interferometry employing dual beam illumination *Appl. Opt.* **29** 1905–11
[107] Zou Y, Diao H, Peng X and Tiziani H 1992 Geometry for

contouring by electronic speckle pattern interferometry based on shifting illumination beams *Appl. Opt.* **31** 6616–21
[108] Diao H, Zou Y and Tiziani H J 1993 Design considerations of a dual-beam ESPI optical system for contouring *Optik* **93** 45–51
[109] Zou Y, Diao H, Peng X and Tiziani H 1992 Contouring by electronic speckle pattern interferometry with quadruple-beam illumination *Appl. Opt.* **31** 6599–602
[110] Bolognini N, Rabal H and Torroba R 1992 Single-beam digital holographic contouring *Appl. Opt.* **31** 1009–11
[111] Zou Y, Pedrini G and Tiziani H 1994 Contouring by electronic speckle pattern interferometry employing divergent dual beam illumination *J. Mod. Opt.* **41** 1637–52
[112] Arizaga R, Rabal H, Trivi M, Alanís E and Romero G 1994 Single fringe contouring *Opt. Commun.* **108** 209–13
[113] Lu B, Yang X, Abendroth H, Eggers H and Ziolkowski E 1988 Measurement of a three-dimensional temperature field applying ESPI and CT techniques *Opt. Commun.* **69** 6–10
[114] Løkberg O J, Espeland M and Pedersen H M 1995 Tomographic reconstruction of sound fields using TV holography *Appl. Opt.* **34** 1640–5
[115] Løkberg O J, Rustad R and Espeland M 1996 Tomographic reconstruction of sound fields in air using TV-holography *Opt. Lasers Engng* **25** 361–72
[116] Rustad R, Løkberg O J, Pedersen H M, Klepsvik K and Støren T 1996 Full field tomographic reconstruction of acoustic fields using TV-holography theory, developments and possibilities *Proc. SPIE* **2782** 302–12
[117] Løkberg O J 1994 Sound in flight: measurement of sound fields by use of TV holography *Appl. Opt.* **33** 2574–84
[118] Dupont O, Dewandel J L and Legros J C 1995 Use of electronic speckle pattern inteferometry for temperature distribution measurements through liquids *Opt. Lett.* **20** 1824–6
[119] Stetson K A 1969 A rigorous treatment of the fringes of hologram interferometry *Optik* **29** 386–400
[120] Høgmoen K and Pedersen H M 1977 Measurement of small vibrations using electronic speckle pattern interferometry: theory *J. Opt. Soc. Am.* **67** 1578–83
[121] Aleksoff C C 1974 Temporal modulation techniques *Holographic Nondestructive Testing* ed R K Erf (Orlando: Academic) pp 247–63
[122] Løkberg O J 1979 Use of chopped laser light in electronic speckle pattern interferometry *Appl. Opt.* **18** 2377–84
[123] Rosvold G O and Løkberg O J 1993 Effect and use of exposure control in vibration analysis using TV holography *Appl. Opt.* **32** 684–91
[124] Løkberg O J and Høgmoen K 1976 Use of modulated reference wave in electronic speckle pattern interferometry *J. Phys. E: Sci. Instrum.* **9** 847–51
[125] Løkberg O J and Høgmoen K 1976 Vibration phase mapping using electronic speckle pattern interferometry *Appl. Opt.* **15** 2701–4
[126] Løkberg O J and Høgmoen K 1977 Holographic methods made useful by phase modulated ESPI *Proc. SPIE* **136** 222–5
[127] Ellingsrud S and Rosvold G O 1992 Analysis of a data-based TV-holography system used to measure small vibration amplitudes *J. Opt. Soc. Am.* A **9** 237–51
[128] Stetson K A and Brohinsky W R 1988 Fringe-shifting technique for numerical analysis of time-average holograms of vibrating objects *J. Opt. Soc. Am.* A **5** 1472–6
[129] Moran S E, Law R L, Craig P N and Goldberg W M 1987 Optically phase-locked electronic speckle pattern interferometer *Appl. Opt.* **26** 475–91
[130] Valera Robles J D, Harvey D and Jones J D C 1992 Automatic heterodyning in fiber optic speckle pattern interferometry using laser velocimetry *Opt. Engng* **31** 1646–53
[131] Valera J D, Doval A F and Jones J D C 1993 Combined fibre optic laser velocimeter and electronic speckle pattern interferometer with a common reference beam *Meas. Sci. Technol.* **4** 578–82
[132] Moran S E, Luganani R, Craig P N and Law R L 1989 Optically phase-locked electronic speckle pattern interferometer system performance for vibration measurement in random displacement fields *J. Opt. Soc. Am.* A **6** 252–69
[133] Høgmoen K and Løkberg O J 1977 Detection and measurement of small vibrations using electronic speckle pattern interferometry *Appl. Opt.* **16** 1869–75
[134] Pedersen H M, Løkberg O J, Valo H and Wang G 1994 Detection of nonsinusoidal periodic vibrations using phase-modulated TV-holography *Opt. Commun.* **104** 271–6
[135] Løkberg O J, Pedersen H M, Valo H and Wang G 1994 Measurement of higher harmonics in periodic vibrations using phase-modulated TV holography with digital image processing *Appl. Opt.* **33** 4997–5002
[136] Waters J P 1974 Interferometric holography *Holographic Nondestructive Testing* ed R K Erf (Orlando: Academic) pp 87–103
[137] Steinbichler H and Gehring G 1996 TV-holography and holographic interferometry: industrial applications *Opt. Lasers Engng* **24** 111–27
[138] Gaskill J D 1978 *Linear Systems, Fourier Transforms and Optics* (New York: Wiley) pp 60–3
[139] Alén J M, Doval A F, Bugarín J, Dorrío B V, López C, Fernández A, Blanco-García J, Pérez-Amor M and Fernández J L 1997 Phase-shifted double single-pulse additive stroboscopic TV-holography for the measurement of high-frequency vibrations using low-bandwidth phase modulation devices *Proc. SPIE* **3098** 166–75
[140] Doval A F, Fernández J L, Pérez-Amor M, Valera J D and Jones J D C 1994 Phase-stepped additive stroboscopic fibre optic TV holography for vibration analysis *Proc. SPIE* **2248** 229–40
[141] Wang L -S and Krishnaswamy S 1996 Additive-subtractive speckle interferometry: extraction of phase data in noisy environments *Opt. Engng* **35** 794–801
[142] Doval A F, Fernández J L, Pérez-Amor M, Valera J D R and Jones J D C 1996 Contrast enhanced and phase controlled stroboscopic additive fibre optic TV-holography for whole field out-of-plane vibration analysis *Opt. Lasers Engng* **25** 323–42
[143] Chatters T, Pouet B and Krishnaswamy S 1992 ESPI with synchronized pressure stressing *Proc. SPIE* **1821** 38–45
[144] Hughes R G 1976 The determination of vibration patterns using a pulsed laser with holographic and electronic speckle pattern interferometry techniques *The Engineering Uses of Coherent Optics* ed E R Robertson (Cambridge: Cambridge University Press) pp 199–218
[145] Cookson T J, Butters J N and Pollard H C 1978 Pulsed lasers in electronic speckle pattern interferometry *Opt. Laser Technol.* **10** 119–24
[146] Tyrer J R 1985 Application of pulsed holography and double pulsed electronic speckle pattern interferometry to vibrating engineering structures *Proc. SPIE* **599** 181–8
[147] Mendoza-Santoyo F, Tyrer J R, West T C and Kerr D 1989 Vibration analysis using phase stepped pulsed electronic speckle pattern interferometry *Proc. SPIE* **1084** 262–78
[148] Spooren R 1990 TV-holography using a double pulsed single oscillator Nd:YAG laser; restrictions and possibilities *Proc. SEM Conf. on Hologram Interferometry and Speckle Metrology (Baltimore)* ed K A Stetson and R J Pryputniewicz pp 260–7
[149] Spooren R 1992 Double-pulse characteristics of a

single-oscillator Nd:YAG laser affecting its performance in TV holography *Appl. Opt.* **31** 208–16
[150] Shellabear M C, Mendoza Santoyo F and Tyrer J R 1990 Processing of addition and subtraction fringes from pulsed ESPI for the study of vibrations *Proc. SEM Conf. on Hologram Interferometry and Speckle Metrology (Baltimore)* ed K A Stetson and R J Pryputniewicz pp 238–44
[151] Mendoza-Santoyo F, Moore A J, Tyrer J R and Alcalá-Ochoa N 1994 Noise reduction in twin-pulsed addition electronic speckle pattern interferometry fringe patterns *Opt. Engng* **33** 1712–16
[152] Fernández A, Blanco-García J, Doval A F, Bugarín J, Dorrío B V, López C, Alén J M, Pérez-Amor M and Fernández J L 1998 Transient deformation measurement by double-pulsed-subtraction TV holography and the Fourier transform method *Appl. Opt.* **37** 3440–6
[153] Spooren R 1994 Standard charge-coupled device cameras for video speckle interferometry *Opt. Engng* **33** 889–96
[154] Holst G C 1996 *CCD Arrays, Cameras and Displays* (Bellingham, WA: SPIE Optical Engineering Press) pp 55–65
[155] Spooren R 1991 Fringe quality in pulsed TV-holography *Proc. SPIE* **1508** 118–27
[156] Spooren R 1992 Double-pulse subtraction TV holography *Opt. Engng* **31** 1000–7
[157] Pedrini G, Pfister B and Tiziani H 1993 Double pulse-electronic speckle interferometry *J. Mod. Opt.* **40** 89–96
[158] Slettemoen G Å 1977 Optimal signal processing in electronic speckle pattern interferometry *Opt. Commun.* **23** 213–16
[159] Pedersen H M, Løkberg O J and Forre B M 1974 Holographic vibration measurement using a TV speckle interferometer with silicon target vidicon *Opt. Commun.* **12** 421–6
[160] Løkberg O J, Holje O M and Pedersen H M 1976 Scan converter memory used in TV-speckle interferometry *Opt. Laser Technol.* **8** 17–20
[161] Nakadate S 1986 Vibration measurement using phase-shifting speckle-pattern interferometry *Appl. Opt.* **25** 4162–7
[162] Davila A, Kaufmann G H and Kerr D 1993 Digital processing of ESPI addition fringes *Proc. FASIG, 'Fringe '93'* ed W Jüptner and W Osten (Bremen: Akademie) pp 339–46
[163] Davila A, Kerr D and Kaufmann G H 1994 Digital processing of electronic speckle pattern interferometry addition fringes *Appl. Opt.* **33** 5964–9
[164] Creath K and Slettemoen G A 1985 Vibration-observation techniques for digital speckle-pattern interferometry *J. Opt. Soc. Am.* A **2** 1629–36
[165] Kaufmann G H, Kerr D and Halliwell N A 1994 Contrast enhancement of pulsed ESPI addition fringes *Opt. Lasers Engng* **20** 25–34
[166] Facchini M, Albrecht D and Zanetta P 1993 Phase detection algorithm in ESPI fringes with speckle noise reduction by using preliminary time averaging *Proc. FASIG, 'Fringe '93'* ed W Jüptner and W Osten (Bremen: Akademie) pp 45–50
[167] Davies J C, Buckberry C H, Jones J D C and Panell C N 1987 Development and application of a fibre optic electronic speckle pattern interferometer (ESPI) *Proc. SPIE* **863** 194–207
[168] Davies J C, Buckberry C H, Jones J D C and Pannell C N 1988 Developments in electronic speckle pattern interferometry for automotive vibration analysis *Proc. SPIE* **952** 260–74
[169] Pouet B F and Krishnaswamy S 1994 Additive-subtractive phase-modulated electronic speckle interferometry: analysis of fringe visibility *Appl. Opt.* **33** 6609–16
[170] Chatters T C, Pouet B F and Krishnaswamy S 1995 Additive-subtractive phase-modulated shearography with synchronized acoustic stressing *Exp. Mech.* **35** 159–65
[171] Lu B, Yang X, Abendroth H and Eggers H 1989 Time-average subtraction method in electronic speckle pattern interferometry *Opt. Commun.* **70** 177–80
[172] Joenathan C 1991 Vibration fringes by phase stepping on an electronic speckle pattern interferometer: an analysis *Appl. Opt.* **30** 4658–65
[173] Qin Y and Dai J 1994 Real-time interval technique for electronic shearing speckle pattern interferometry *Opt. Lasers Engng* **21** 241–8
[174] Wizinowich P L 1990 Phase shifting interferometry in the presence of vibration: a new algorithm and system *Appl. Opt.* **29** 3271–9
[175] Colucci D and Wizinowich P 1992 Millisecond phase acquisition at video rates *Appl. Opt.* **31** 5919–25
[176] van Haasteren A J P and Frankena H J 1994 Real-time displacement measurement using a multicamera phase-stepping speckle interferometer *Appl. Opt.* **33** 4137–42
[177] Joenathan C 1990 Effect of the nonlinearity of the TV camera in electronic speckle pattern interferometry *Optik* **85** 33–7
[178] Jones R and Wykes C 1977 De-correlation effects in speckle-pattern interferometry. 2. Displacement dependent de-correlation and applications to the observation of machine-induced strain *Opt. Acta* **24** 533–50
[179] Owner-Petersen M 1991 Decorrelation and fringe visibility: on the limiting behaviour of various electronic speckle-pattern correlation interferometers *J. Opt. Soc. Am.* A **8** 1082–9
[180] Wykes C 1987 A theoretical approach to the optimization of electronic speckle pattern interferometry with limited laser power *J. Mod. Opt.* **34** 539–54
[181] Slettemoen G Å 1981 First-order statistics of displayed speckle patterns in electronic speckle pattern interferometry *J. Opt. Soc. Am.* **71** 474–82
[182] Williams D C and Robinson D W 1987 Electro-optic holography *Non-Destructive Testing, Proc. 4th European Conf.* pp 588–96
[183] Pouet B F and Krishnaswamy S 1995 Technique for the removal of speckle phase in electronic speckle interferometry *Opt. Lett.* **20** 318–20
[184] Stetson K A 1989 An electronic system for real-time display and quantitative analysis of hologram interference fringes *Proc. SPIE* **1375** 78–85
[185] Bushman T 1989 Development of a holographic computing system *Proc. SPIE* **1162** 66–77
[186] Vikhagen E 1989 Vibration measurement using phase shifting TV-holography and digital image processing *Opt. Commun.* **69** 214–18
[187] Lu B, Hu Z, Abendroth H, Eggers H and Ziolkowski E 1989 Improvement of time-average subtraction technique applied to the vibration analysis with TV-holography *Opt. Commun.* **78** 217–21
[188] Rosenthal D M, Trolinger J D and Weber D C 1991 The use of double pulsed ESPI for earthquake mitigation of large structures *Proc. SPIE* **1553** 175–84
[189] Joenathan C and Khorana B M 1992 Contrast of the vibration fringes in time-averaged electronic speckle-pattern interferometry: effect of speckle averaging *Appl. Opt.* **31** 1863–70
[190] Johansson S and Predko K G 1989 Performance of a phase-shifting speckle interferometer for measuring deformation and vibration *J. Phys. E: Sci. Instrum.* **22** 289–92
[191] O'Shea M and O'Mongain E 1992 Charge-coupled devices: frame adding as an alternative to long integration times and cooling *Opt. Engng* **31** 522–6
[192] Løkberg O J and Slettemoen G Å 1984 Improved fringe

definition by speckle averaging in ESPI *Proc. ICO-13 Conf. (Sapporo)* pp 116–17
[193] Creath K 1985 Averaging double-exposure speckle interferograms *Opt. Lett.* **10** 582–4
[194] Montgomery P and Bergquist B D 1985 Contrast enhancement of ESPI patterns by specke averaging in a video frame store *Proc. SPIE* **599** 201–6
[195] Towers D P, Judge T R and Bryanston-Cross P J 1991 Automatic interferogram analysis techniques applied to quasi-heterodine holography and ESPI *Opt. Lasers Engng* **14** 239–81
[196] Qin Y, Dai J and Wang J 1994 Recursive filtering technique for electronic speckle fringe patterns *Opt. Engng* **33** 1708–11
[197] Yu E, Cha S S and Joo W 1995 Use of interferometric directionality for noise reduction *Opt. Engng* **34** 173–82
[198] Kerr D, Mendoza-Santoyo F and Tyrer J R 1989 Manipulation of the Fourier components of speckle fringe patterns as part of an interferometric analysis process *J. Mod. Opt.* **36** 195–203
[199] Lim J S 1981 Techniques for speckle noise removal *Opt. Engng* **20** 670–8
[200] González R C and Wintz P 1987 *Digital Image Processing* (Reading, MA: Addison-Wesley) pp 162–3
[201] Davies E R 1990 *Machine Vision: Theory, Algorithms, Practicalities* (London: Academic) pp 47–54
[202] Davies E R 1992 The relative effects of median and mean filters on noisy signals *J. Mod. Opt.* **39** 103–13
[203] Davila A, Kaufmann G H and Kerr D 1995 An evaluation of synthetic aperture radar noise reduction techniques for the smoothing of electronic speckle pattern interferometric fringes *J. Mod. Opt.* **42** 1795–1804
[204] Kaufmann G H, Davila A and Kerr D 1996 Speckle noise reduction in TV holography *Proc. SPIE* **2730** 96–100
[205] Frost V S, Stiles J A, Shanmugan K S and Holtzman J C 1982 A model for radar images and its application to adaptative digital filtering of multiplicative noise *Trans. Pattern Analysis Machine Intelligence* **4** 157–65
[206] Lee J -S 1986 Speckle suppression and analysis for synthetic aperture radar images *Opt. Engng* **25** 636–43
[207] Crennell K M and Bowler I W 1986 The smoothing of electronic speckle pattern interferometric images *Opt. Lasers Engng* **7** 163–73
[208] Crimmins T R 1986 Geometric filter for reducing speckle *Opt. Engng* **25** 651–4
[209] Wong Y F 1993 A nonlinear scale-space filter by physical computation *Proc. IEEE Workshop on Neural Networks for Signal Processing* ed C A Kamm *et al* pp 241–50
[210] Kujawińska M 1993 The architecture of a multipurpose fringe pattern analysis system *Opt. Lasers Engng* **19** 261–8
[211] Robinson D W 1993 Phase unwrapping methods Interferogram analysis *Digital Fringe Pattern Measurement Techniques* ed D W Robinson and G T Reid G T (Bristol: Institute of Physics) pp 194–229
[212] Judge T R and Bryanston-Cross P J 1994 A review of phase unwrapping techniques in fringe analysis *Opt. Lasers Engng* **21** 199–239
[213] Takeda M 1996 Recent progress in phase unwrapping techniques *Proc. SPIE* **2782** 334–43
[214] Gu J and Chen F 1995 Fast Fourier transform, iteration, and least-squares-fit demodulation image processing for analysis of single-carrier fringe pattern *J. Opt. Soc. Am.* A **12** 2159–64
[215] Moore A J, Tyrer J R and Mendoza-Santoyo F 1994 Phase extraction from electronic speckle pattern interferometry addition fringes *Appl. Opt.* **33** 7312–20
[216] Owner-Petersen M 1991 Digital speckle pattern shearing interferometry: limitations and prospects *Appl. Opt.* **30** 2730–8
[217] Pryputniewicz R J 1992 Electro-optic holography *SPIE Critical Reviews of Optical Science and Technology* vol 46, ed J D Trolinger (Bellingham: SPIE) pp 148–74
[218] Slettemoen G Å and Wyant J C 1986 Maximal fraction of acceptable measurements in phase-shifting speckle interferometry: a theoretical study *J. Opt. Soc. Am.* A **3** 210–14
[219] Maack T and Kowarschik R 1996 Camera influence on the phase-measurement accuracy of a phase-shifting speckle interferometer *Appl. Opt.* **35** 3514–24
[220] Hong C K, Ryu H S and Lim H C 1995 Least-squares fitting of the phase map obtained in phase-shifting electronic speckle pattern interferometry *Opt. Lett.* **20** 931–3
[221] Robinson D W and Williams D C 1986 Digital phase stepping speckle interferometry *Opt. Commun.* **57** 26–30
[222] Creath K 1985 Phase-shifting speckle interferometry *Appl. Opt.* **24** 3053–8
[223] Bhat G K 1995 Digital techniques for strain measurement using electro-optic holography *J. Mod. Opt.* **42** 1909–19
[224] Vikhagen E 1990 Nondestructive testing by use of TV holography and deformation phase gradient calculation *Appl. Opt.* **29** 137–44
[225] Kreis T M 1987 Quantitative evaluation of interference patterns *Proc. SPIE* **863** 68–77
[226] Reid G T 1993 Automatic analysis of interference fringes *Optical Methods in Engineering Metrology* ed D C Williams (London: Chapman & Hall) pp 385–413
[227] Robinson D W and Reid G T eds 1993 *Interferogram Analysis. Digital Fringe Pattern Measurement Techniques* (Bristol: Institute of Physics)
[228] Kujawińska M and Wójciak J 1991 Spatial phase-shifting techniques of fringe pattern analysis in photomechanics *Proc. SPIE* **1554B** 503–13
[229] Creath K 1988 Phase-measurement interferometry techniques *Progress in Optics* vol 26, ed E Wolf (Amsterdam: North Holland) pp 350–93
[230] Creath K 1993 Temporal phase measurement methods *Interferogram Analysis. Digital Fringe Pattern Measurement Techniques* ed D W Robinson and G T Reid (Bristol: Institute of Physics) pp 94–140
[231] Dorrío B V and Fernández J L 1999 Phase-evaluation methods in whole-field optical measurement techniques. *Meas. Sci. Technol.* **10** R33–55
[232] Greivenkamp J E and Bruning J H 1992 Phase shifting interferometry *Optical Shop Testing* ed D Malacara (New York: Wiley) pp 501–98
[233] Morimoto Y and Fujisawa M 1994 Fringe pattern analysis by a phase-shifting method using Fourier transform *Opt. Engng* **33** 3709–14
[234] Kujawińska M 1993 Spatial phase measurement methods *Interferogram Analysis. Digital Fringe Pattern Measurement Techniques* ed D W Robinson and G T Reid (Bristol: Institute of Physics) pp 141–93
[235] Womack K H 1984 Interferometric phase measurement using spatial synchronous detection *Opt. Engng* **23** 391–5
[236] Takeda M, Ina H and Kobayashi S 1982 Fourier-transform method of fringe-pattern analysis for computer-based topography and interferometry *J. Opt. Soc. Am.* **72** 156–60
[237] Schwider J 1988 Advanced evaluation techniques in interferometry *Progress in Optics* vol 26, ed E Wolf (Amsterdam: North Holland) pp 272–359
[238] Joenathan C, Franze B, Haible P and Tiziani H J 1998 Speckle interferometry with temporal phase evaluation for measuring large-object deformation *Appl. Opt.* **37** 2608–14
[239] Joenathan C, Franze B, Haible P and Tiziani H J 1998 Large in-plane displacement measurement in dual-beam speckle interferometry using temporal phase measurement *J. Mod. Opt.* **45** 1975–84
[240] Joenathan C, Franze B, Haible P and Tiziani H J 1998

Novel temporal Fourier transform speckle pattern shearing interferometer *Opt. Engng* **37** 1790–5
[241] Joenathan C, Franze B, Haible P and Tiziani H J 1998 Shape measurement by use of temporal Fourier transformation in dual-beam illumination speckle interferometry *Appl. Opt.* **37** 3385–90
[242] Kujawińska M, Spik A and Robinson D W 1989 Analysis of ESPI interferograms by phase-stepping techniques *Proc. 4th Int. Conf. on Fringe Analysis (FASIG '89) (Loughborough University)*
[243] Buckberry C H and Davies J C 1990 The application of TV holography to engineering problems in the automotive industry *Proc. SEM Conf. on Hologram Interferometry and Speckle Metrology (Baltimore)* ed A Stetson and R J Pryputniewicz pp 268–78
[244] Pryputniewicz R J and Stetson K A 1989 Measurement of vibration patterns using electro-optic holography *Proc. SPIE* **1162** 456–67
[245] Pedrini G, Zou Y-L and Tiziani H J 1996 Quantitative evaluation of digital shearing interferogram using the spatial carrier method *Pure Appl. Opt.* **5** 313–21
[246] Schedin S and Gren P 1997 Phase evaluation and speckle averaging in pulsed television holography *Appl. Opt.* **36** 3941–7
[247] Petzing J N and Tyrer J R 1996 The effect of metallographic structure on clamped plate vibration characteristics *Exp. Mech.* **36** 127–34
[248] Farrant D I, Kaufmann G H, Petzing J N, Tyrer J R, Oreb B F and Kerr D 1997 Transient deformation measurement using dual-pulse addition ESPI *Proc. SPIE* **3173A** 132–40
[249] Paoletti D and Schirripa Spagnolo G 1994 Fast Fourier transformed electronic speckle contouring for diffuse surfaces profilometry *Opt. Lasers Engng* **20** 87–96
[250] Davila A, Kauffman G H and Pérez-López C 1998 Transient deformation analysis by a carrier method of pulsed electronic speckle-shearing pattern interferometry *Appl. Opt.* **37** 4116–22
[251] Fernández A, Doval A F, Dávila A, Blanco-García J, Pérez-López C and Fernández J L 1998 Double-pulsed carrier speckle-shearing pattern interferometry for transient deformation analysis *Proc. SPIE* **3478** 352–8
[252] Fernández A, Doval A F, Bugarín J, Dorrío B V, López C, Alén J M, Blanco-García J, Pérez-Amor M and Fernández J L 1997 Transient bending waves analysis by Fourier evaluation of single pulsed TV-holography fringe patterns *Proc. SPIE* **3098** 575–81
[253] Preater R W T and Swain R 1994 Fourier transform fringe analysis of electronic speckle pattern interferometry fringes from high-speed rotating components *Opt. Engng* **33** 1271–9
[254] Kujawińska M, Spik A and Robinson D W 1989 Quantitative analysis of transient events by ESPI *Proc. SPIE* **1121** 416–22
[255] Pedrini G, Zou Y-L and Tiziani H J 1997 Simultaneous quantitative evaluation of in-plane and out-of-plane deformations by use of a multidirectional spatial carrier *Appl. Opt.* **36** 786–92
[256] Kreis T M, Adams M and Jüptner W P O 1997 Methods of digital holography: a comparison *Proc. SPIE* **3098** 224–33
[257] Kreis T M and Jüptner W P O 1997 Principles of digital holography *Fringe'97. Proc. 3rd International Workshop on Automatic Processing of Fringe Patterns* ed W Jüptner and W Osten (Berlin: Akademie) pp 353–63
[258] Pedrini G, Tiziani H J and Zou Y 1996 Speckle size of digitally reconstructed wavefronts of diffusely scattering objects *J. Mod. Opt.* **43** 395–407
[259] Yamaguchi I and Zhang T 1997 Phase-shifting digital holography *Opt. Lett.* **22** 1268–70